The stochastic movements of individual streambed grains

by

J. Kevin Pierce

B.S. Physics, West Virginia University 2013

M.Sc. Physics, University of British Columbia 2016

A THESIS SUBMITTED IN PARTIAL FULFILLMENT
OF THE REQUIREMENTS FOR THE DEGREE OF

Doctor of Philosophy

in

THE FACULTY OF ARTS
(Department of Geography)

The University of British Columbia
(Vancouver)

June 2021

The following individuals certify that they have read, and recommend to the Faculty of Graduate and Postdoctoral Studies for acceptance, the thesis entitled:

The stochastic movements of individual streambed grains

submitted by **J. Kevin Pierce** in partial fulfillment of the requirements for the degree of **Doctor of Philosophy** in **Department of Geography**.

Examining Committee:

Marwan Hassan, Geography
Supervisor

Brett Eaton, Geography
Supervisory Committee Member

Rui Ferreira, University of Lisbon
Civil Engineering

Magnus Monolith, Other Department
External Examiner

Additional Supervisory Committee Members:

Person1
Supervisory Committee Member

Person 2
Supervisory Committee Member

Abstract

Bedload transport is the movement of coarse sediment grains in a river channel by rolling, sliding, and bouncing. Motivated by the need to predict river morphodynamics, a central problem in river science is to calculate the downstream flux of grains moving as bedload. This problem is usually formulated in terms of continuum mechanics, but this approach is questionable considering that bedload grains are coarse, they rarely reach densities approximating a continuum. This thesis contains four projects that abandon the continuum hypothesis to interpret sediment transport in terms of individual grains. First, I develop a new theory to calculate the sediment flux from the trajectories of individual grains as they alternate between motion and rest. This leads to a sediment flux probability distribution which predicts mean sediment fluxes that depend on the timescale over which they are observed, explaining why measurements of the bedload flux can give such poor results. Second, I evaluate the interplay between bed elevation changes and sediment transport rates, finding that because aggradation and degradation oppose changes in the sediment flux, bed elevation changes buffer sediment transport fluctuations. Third, I incorporate the process of sediment burial into a model of downstream sediment trajectories, demonstrating that burial eventually halts downstream transport. This has implications for the transport of contaminants in river channels. Finally, using concepts borrowed from the theory of granular gases, I develop a stochastic model of individual particles moving downstream in the turbulent flow through a sequence of collisions with the bed surface. This indicates that the velocity characteristics of sediment particles are tuned by the amount of dissipation particles

experience when colliding with the sedimentary bed. This research has implications across river science, where there is increasing acknowledgement of the shortcomings of the continuum hypothesis for predicting dynamics in mountain streams. This work extends a wide body of work on individual particle motions which originates from the 1930s, and unifies it with more recent approaches to calculate the bulk bedload flux which have not, until now, been related to the movement characteristics of individual grains.

Lay Summary

The lay or public summary explains the key goals and contributions of the research/scholarly work in terms that can be understood by the general public. It must not exceed 150 words in length.

Preface

This thesis is entirely the original research of Kevin Pierce, including all figures, writing, and calculations. The supervisory committee and especially the research supervisor Marwan Hassan provided guidance in the research. The thesis includes two published works, Chapters 3 and **??**, available in *Journal of Geophysical Research: Earth Surface* and **?** respectively, with Marwan Hassan as coauthor (*Pierce and Hassan*, 2020; **?**). Chapters 2 and 5 will be submitted for publication subsequent to the thesis submission.

This thesis deals with the transport of coarse sediment in flowing water from the perspective it fundamentally results from the movements of individual grains. The research has been motivated by the belief that geomorphology as a science will benefit from mechanistic, process-based, mathematical models of sediment transport processes.

Geomorphology has long been characterized by observation, description, and the building of conceptual models, not mathematical ones. Only relatively recently has the science turned toward quantitative methods, with researchers working to frame observations in terms of underlying processes and to describe them with methods adapted from physics.

Given the complexity of geomorphology problems, a complete reduction of geomorphology to physics would be narrow-minded, but we can nonetheless borrow ways of thinking. An extremely successful approach in physics has been to construct idealized models with little intention of direct realism, study them deeply to obtain complete understanding, and then, decades or centuries later, to embellish these models with more sophisticated features to describe real-world phenomena. An example is the block on the spring, the simple harmonic oscillator, which starts as a toy model studied by every first year physics student, but somehow shows up in the deepest inquiries of theoretical physics, from quantum matter to cosmological inflation. This thesis applies this "simple harmonic oscillator approach" to some problems in Earth science. The objective is to build up simple archetypes which can be embellished later, not to build **the model** of fluvial geomorphology. That's for later! (And not for me.) CHEERS.

Contents

List of Tables

List of Figures

List of Notation

Symbol	Meaning
α	first letter of the alphabet
β	second!

Acknowledgments

Attending university long enough to earn a PhD is an unbelievable privilege, and I only got here with an incredible amount of guidance and support.

Most of all, to mom Calisa Pierce, dad Jim Pierce, my sisters Kelsey and Kim, and my grandmother Wilma Steele (Gugs), you've formed all of the best parts of my personality and continually guided me toward this point, and it's impossible to explain how thankful I am for that.

Mom, during my childhood, you worked full time, taught piano lessons, earned Master and Doctoral degrees, played organ every Sunday, consoled us through every difficulty, and engaged us in as many extracurricular activities as we were willing to take on. I cannot imagine a better role model of work ethic, open-mindedness, and devotion. I hope I picked a few things up.

Dad, I've watched you solve an insane diversity of problems without hesitation, from easy ones, like worn out brake pads or blown engines, to hard ones, like burnt eyes and broken arms. By age 10 I must have helped with copper plumbing, woodwork, car repair, home wiring, and tree felling. I had unintentional lessons in water currents, fish habits, electrons, engines, wings, hellgrammites, heat transfer, and radio waves. Canoeing the South Branch together taught me more science than school ever did. The overarching message is that phenomena can be understood, and most any problems can be solved, at least with the right tools. It's incredibly useful in a PhD! Thanks for this and so much more.

Kelsey and Kim, my earliest memories are sitting in your bedroom floor struggling through your books, asking for help every couple of paragraphs. You made me good at reading and taught me to enjoy it, and this is the basis of everything. Kim, you were my first role model, and I think of you all the time. Kelsey, I know it goes without saying, but thanks for a lifetime of guidance. You're now, as always, five steps ahead and far more successful. On the one hand, I'm deeply proud at your progress through life, with a stable career and now two beautiful kids, but on the other, I'm flatly shocked by it. I'll be playing catch up forever!

Gugs, your approach to life is clean and selfless, and you've been so exceptionally reliable and invested in my development, more like a second mother than a typical grandmother. I'll never be able to thank you enough! It's always my goal to take up your 4am wakeups and completely measured responses to all of life's challenges. I'm making a bit of progress. Let's hope I can get there!

Finally with regard to family, I'd like to thank my great aunt Alice. Thanks so much for paying my undergrad education! We hardly met before you passed, but we're family, and that was enough. It really means a lot.

Next comes education. Thanks to my early teachers and mentors who put in the extra care to keep me on track and shield me from harm, Jonathan Ramey, Linda Afzhalirhad, Brandon Willard, Linda Mendez, Marty Ojeda, Phyllis Adkins, and Red Hamlin among many others. Thanks also to the later ones at Southern WV Community College (SWVCC) and West Virginia University (WVU) whose lessons fostered my way of thinking and provided me with many of the tools I used for the research in this thesis. At SWVCC, I'd like to thank especially Mindy Saunders, Tex Wood, Anne Klein, Charles Wood, Don Saunders, and George Trimble. Mindy in particular transformed my view of the world into one based on mathematics with her incredibly effective teaching, Anne dismantled it into chemistry, and Tex reconstructed it into artistic interpretation, which will always transcend science. Everyone encouraged me to continue my education. You all made SWVCC a transformation and an unbelievable privilege.

At WVU, I'd like to thank Alan Bristow, Tudor Stanescu, and Leo Golubovic. Alan and Tudor, thanks you for providing my first opportunities in research. (Sorry I was bad at it!) Leo, you are the key person in my development as a researcher. You inspired me to learn mechanics, statistical physics, and mathematical physics at a high level, and I can't thank you enough. Thanks to you, I read Mathews, Landau, and Goldstein, and I saw that mechanics was really what I wanted to do. Every time I solve a challenging problem with some Bessel functions or contour integrals, I think "Dr. Golubovic would like this one." I wish I had taken more advantage of the opportunity to speak to you outside of classes. I'll feel deeply successful if I can one day become as inspiring an educator as you are. I hope we can chat in Morgantown sometime!

To my extended cohort at WVU physics, Payne, Megat, Collins, Scott, Dustin, Rice, Wolfe, Samet, Craig, April, Evan, Larry, Robert, Stephen, Rick, Matt, Caleb, John, and all of you others, thanks for the collaboration and the hilarious times. I'll never forget Scott's quaternions and borderline quantum consciousness beliefs, Samet's olympiad problems, or Megat's power tower magic (which still blows my mind). I have yet to experience teamwork and shared exploration like we had in the undergrad lounge. I hope the lounge is still happening, that its residents by some miracle still have 24 hour access into the building, that some barefoot Megat-like character is still gaming in the corner, and that they have some Andrew Rice imitator to flip some cars for em (mike jones). May that live on forever. Because of you all, WVU was magic for me.

Now we come to Marwan Hassan. About five years ago now I wandered into Marwan's office saying I liked rivers and wanted to describe sediment transport with statistical physics. I realize now when I said "statistical physics" Marwan's eyes lit up with thoughts of Einstein, Nakagawa, Yano, Hubbell, Crickmore, and so many other names I now know well. I was lucky to use the right trigger words. Marwan, thanks for taking the risk and taking me on from outside the field, for all of the guidance, for loaning me so many papers and books, giving me freedom to explore ideas, and most of all for showing me that it's ok to be human in science. At this point I also want to thank Yusuf for trying your patience to its limits over a long enough period so that things didn't seem so bad once I came along for this short time together.

My friends in geography have also been great. Thanks to the whole extended research family: Shawn, Matteo, Conor, Nisreen, Yinlue, Alex, Kyle, Leo, Dave, Tobias, Katie, Maria, Elli, David, Jiamei, Xingyu, Niannian, and Emma, plus the outsiders, Will, Dave, Rose, and Anya. In particular, thanks to Shawn for all of the shared speculations, and Matteo and Conor – friendships forged through suffering! We'll have to keep in touch and transform our shared venting sessions into well-rounded friendships and productive research collaborations.

Thank you Rui Ferreira and Brett Eaton! Rui, you welcomed me to Portugal, offered me guidance in the laboratory, and educated me on turbulence and hydraulics. Your kindness, deep fluid and granular physics knowledge, and wide-ranging interests beyond physical science are inspiring. Thanks for the thoughtful comments and advice on my PhD. I'm not forgetting what I owe you! But I am impressed at your concise way of speaking and unbounded kindness. Brett, you were the first person to welcome me to UBC, and I'll always appreciate your effort to teach me how to write, interpret flume experiments, and understand modelling in light of the real world and its complexity. Although I'm not sure if I understood your lessons as well as you would have liked, I still have a list of your favorite books on my computer, and they're a first task for as soon as I can read something besides articles! Maybe they'll bring me closer to your way of thinking.

I'd be amiss not to mention David Furbish. Before I started my PhD, when I was still exclusively a physics kid, I attended Furbish's colloquium in Geography at Marwan's invitation. At the end I asked a vague question about whether Langevin equations might be useful for describing sediment transport, and the answer was "absolutely yes". Now I have a thesis on it. Later on, David recruited me into a lovely series of meetings where we discussed gases with adhesion, moon craters, entropy, soft matter, martian hillslopes, the social repercussions of disinformation, and a whole range of questions in natural philosophy, pondering implications of stochastic landscape evolution, comparing probability to mass, momentum, and energy, and evaluating fringe ideas in cosmology. These are my people! David, Rachel, Sarah W, Sarah Z, Nakul, Tyler, Erika, and Shawn, thanks sincerely for letting me on board the spacecraft.

Among UBC Geographers, thanks especially to Nina Hewitt! It was always a pleasure and sometimes a sigh of relief to TA your courses, which are so uniquely organized and student-focused. UBC Geography is a much greater department with you in it. I'm so thankful to have been a part of your process to transform undergrads into capable scientists. I'll be happy if I can teach like you one day!

Finally, Mary! My PhD has not been great in terms of work-life balance. Thanks for sticking it out, putting up with my late bedtimes, my early wakeups, and all of those social events I skipped. It's time! I'm done. The pandemic also seems to be winding down. We can finally get to Aus! I'm ready for an extensive tour of the gap and some beautiful Queensland beaches with your family, featuring SPF110 and an incredibly giant umbrella. After that, we're a step closer to settling once and for all whether our cat will be white or orange. I'm leaning toward white again.

Completing a PhD looks like a personal achievement, but it's really not. It's an expression of 30 years of influence and guidance from other people at every stage, my parents, sisters, grandmother, and a huge network of teachers and mentors. I'm kinda tired because it's the end, so it's natural to drift into daydreams of Watoga and Williams River with my family, reading encyclopedias in Gugs' living room, lining up just left of center with my dad and bracing on the paddle for the hit, calm discussions with Johnathan Ramey about my education, the glowing fireflies under my great grandpa's tree, "cross-up, cross-up, squeeze" in Mindy's class, or laughing about a broken watermelon at Kumbrabow with my sisters. It's easy too to shift years later, flipping on the light in the physics lounge at 3am and surprising Megat who was asleep on the couch, or finishing a problem set with Payne and snapping the book shut, discussing Tsujimoto with Marwan, or roaming through Kitsilano with Mary at the edge of dark. The PhD is all of it! Thank you all for every part of it. University is finished.

Chapter 1

Sediment transport and landscape evolution

Landscapes evolve when water, wind, and ice, driven by gravity, erodes down slopes uplifted by tectonics. Channels initiate along faults and depressions wherever climatic conditions are suitable, incising networks in the landscape and transferring sediments from uplands to lowlands, grinding boulders to sand in a machine of abrasion. Earth's biota colonize these networks which form conduits for migration, transmitting water, genetic information, and organic material alike, while biota and chemical decomposition convert sediments to soils, staging the joint evolution of life and landscapes which has occurred across geological time. Human impacts on these old patterns have become severe, in what has been characterized as an environmental and social crisis (**?**). Geologic records display unprecedented recent shifts in ancient climatic, denundational, and biotic patterns, requiring effective aquatic habitat restoration, contaminant management, and engineering strategies more than ever before.

In this context river geomorphology as a scientific discipline has shifted toward more quantitative methods that enable concrete predictions about the natural world (**?**). Sediment transport in river channels is especially amenable to this quantitative approach since it is mechanistically the result of fluid and granular physics. Sediment moves in different modes depending on the relative importance of the fluid forces against the weight of grains (*Bagnold*, 1956). When particles are coarse, as in gravel-bed rivers, the fluid forces are relatively weak and particles move as "bedload", by bouncing, rolling, and sliding along the bed surface (*Kalinske*, 1947). In bedload transport conditions, fluid turbulence and the irregular bed surface adopt particular control over the sediment dynamics (*Frey and Church*, 2011; **?**).

Bedload transport exerts unique influence over channel morphology and stability (*Church*, 2006; *Recking et al.*, 2016), in part because the coarsest grains in a river provide a partially-immobile skeleton upon which sedimentary deposits can develop (*Hassan et al.*, 2007; **?**). A longstanding problem in river science is therefore to determine the bedload flux, or the rate of coarse sediment movement. Unfortunately, existing approaches to compute the bedload flux are inadequate, and predictions often deviate from measured values by orders of magnitude (*Barry et al.*, 2004; *Bathurst*, 2007; *Gomez and Church*, 1989; *Recking et al.*, 2012). Given that this problem has been researched intensively for over a century now (**?**), it is clear that new research strategies are needed (*Ancey*, 2020; *Ancey and Pascal*, 2020).

Predicting bedload fluxes is challenging because transport is not always well correlated to average characteristics of the flow and bed material. Local fluxes can range through orders of magnitude as details of turbulent fluctuations and bed organization vary, while average characterizations of flow and sediment remain constant (*Charru et al.*, 2004; *Hassan et al.*, 2007; *Sumer et al.*, 2003; *Venditti et al.*, 2017). The same turbulence and sediment organization details which correlate with the bedload flux are also modified by it. Turbulent impulses drive sediment motion (*Amir et al.*, 2014; *Celik et al.*, 2014; *Shih et al.*, 2017; *Valyrakis et al.*, 2010), but moving sediment affects turbulent flow characteristics (*Liu et al.*, 2016; *Santos et al.*, 2014; *Singh et al.*, 2010). The surface arrangement and consolidation of grains (*Dwivedi et al.*, 2012; *MILLER and BYRNE*, 1966; *Paintal*, 1971) affects sediment mobility, but transport rearranges grains and consolidates the bed (*Allen and Kudrolli*, 2018; *Charru et al.*, 2004; *KIRCHNER et al.*, 1990). Bedload fluxes are in cyclical feedback with their controls (*Jerolmack and Mohrig*, 2005), and this challenges us to step beyond descriptions based on averaged values.

The approach taken in this thesis is to consider bedload transport as an aggregate result of many individual transported grains whose movements have probabilistic characteristics. This departs from the traditional strategy of correlating transport rates to the average flow and sedimentary characteristics (*Meyer-Peter and Müller*, 1948; *Wilcock*, 2001; **?**). Because the trajectories of individual grains are governed by Newtonian mechanics, this approach brings reliable tools to the problem, but it is nonetheless complicated because the forces driving and resisting sediment motion vary through space and time due to fluid turbulence and the erratic interactions of moving particles with the bed.

To address these complications, I develop in this thesis a handful of new bedload transport models using methods adopted from statistical physics and the body of earlier literature which inspired my approach. To provide context and motivation, the thesis begins by reviewing this literature, rephrasing earlier work as necessary to indicate common themes and show continuity with my own developments which follow in subsequent chapters.

1.1 Theories of individual particle movement

A basic problem in sediment transport theory is to predict the downstream movement of an individual particle. At first glance, this seems an elementary problem in general physics, but numerous challenges appear. Particles moving as bedload are driven downstream by a turbulent fluid flow (), but the exact relationships between the fluid flow and the applied forces are not exactly known (**?**). Downstream movement is resisted by frictional encounters (skidding, pivoting, colliding) between moving particles and the bed, but since the bed is a granular surface, its geometry is difficult to characterize (*Gordon et al.*, 1972), and the outcomes of these encounters are variable (*Sekine and Kikkawa*, 1992).

Entrainment and deposition provide an additional layer of complexity. Moving particles that encounter the bed with sufficiently low velocities can settle into pockets which protect them from the flow (*MILLER and BYRNE*,

1966) and cause their deposition (*Charru et al.*, 2004). These pockets are not permanent shelter because rearrangement of the surrounding bed by entrainment of neighboring particles or subsurface creep (*Frey*, 2014; *Houssais et al.*, 2016) can re-expose particles to the flow, and sufficiently strong turbulent fluctuations (*Cameron et al.*, 2020) can overcome shelter even if its geometry is not disturbed (*Celik et al.*, 2014; **?**). As a result, particles generally alternate through sequences of entrainment and deposition, but determining precisely when these events occur is impractical.

Particles at rest on the bed surface can also become covered by other transported particles (**?**), These buried particles cannot move again until those burying them have been transported away (**?**), generating long periods of immobility (*Ferguson and Hoey*, 2002; **?**).

Individual trajectories of particles therefore involve a number of contributing processes which occur over different characteristic timescales, from seconds to years, and each of these processes eludes precise description.

Nikora et al. (2001a, 2002) provided a conceptual framework which helps to organize this complexity. Nikora et al divided the downstream tractories of individual particles into three timescales, or "ranges", termed local, intermediate, and global. The local range refers to the period of motion between subsequent interactions with the bed, when the particles accelerate downstream within the turbulent flow. The intermediate range reflects particle motions through sequences of bed encounters, when particles alternately accelerate and decellerate. The global range refers to particle trajectories through sequential entrainment and deposition events as they cycle between motion and rest. *Hassan and Bradley* (2017) added an additional range, referred to as "geomorphic", to reflect the even longer period over which particles become buried within the subsurface or embedded among sedimentary deposits (*Bradley*, 2017; **?**). This set of timescales – local, intermediate, global, and geomorphic – are used below to organize the literature describing trajectories of individual grains.

1.1.1 Motivation: tracers and basic understanding

An early motivation to understand individual particle motions was to predict the efficiency of sediment transport measurements (*Ettema and Mutel*, 2004), and this motivation still drives a great deal of research into individual particle motions today (*Hassan and Bradley*, 2017; **?**). A common technique to estimate sediment transport is to seed a stream with tracer stones and track their progress downstream (*Einstein*, 1937; **?**; **?**). In principle, tracers provide a proxy for the population of grains in a stream, so one can estimate tracer velocities of tracers, then multiply by an estimate of the number of grains available for motion to calculate the overall sediment flux (*Ferguson and Hoey*, 2002; **?**). In practice, challenges arise due to the distinct behavior of tracers over the local, intermediate, global, and geomorphic timescales. Apparently, tracer particle velocities depend on the observation time, in a phenomenon which has been called "advective slowdown" (*Ferguson and Hoey*, 2002; **?**). This obscures the mapping between measured tracer velocities and actual sediment fluxes, exposing a need for further research into how exactly individual particle motions depend on observation scale.

1.1.2 Einstein 1937

Einstein was probably the first to focus on the movements of individual particles through streams (*Einstein*, 1937). Watching painted tracers move through a flume, Einstein came to the conclusion that the movement characteristics of any one particle could not be predicted, so he turned to probabilistic methods to characterize their transport. Einstein's key insight was to represent particle motions as an alternating sequence of movements and rests having random characteristics. As his interest was on the global range of particle motion, and the duration of particle motions is usually short compared to rests, Einstein made the approximation that individual motions (between entrainment and deposition) are mathematically instantaneous. With this configuration, the downstream movement of sediment becomes an alternate cycle of instantaneous steps of random length, separated by rests of random duration. Implicitly, this picture of sediment trajectories assumes that movement velocities are infinite. Einstein's experiments indicated that both step lengths and resting times were well-described by exponential distributions, and the focus of his PhD was to find the probability density $P(x, t)$ that a particle had travelled a net distance x after a time t has elapsed. In the process, Einstein formulated an example of what is now called the continuous time random walk, but this was not was not formalized until much later (*Montroll*, 1964).

Einstein's assumptions mean that if the position of a single sediment particle at a given time is $x(t)$, the assumptions of infinite movement velocity, random resting durations, and random movement distances between entrainment and depositon (step lengths) can be written

$$\dot{x}(t) = \mu(t), \tag{1.1}$$

where $\dot{x} = dx/dt$, and $\mu(t)$ is a white shot noise (*Van Den Broeck*, 1983), which is essentially a sequence of pulses having random heights with mean height ℓ (the mean step length), and random locations in time with mean separation $1/k_E$ (the mean resting time, interpreted as the reciprocal of the entrainment rate k_E). A particular realization of this pulsed noise can be written

$$\mu(t) = \sum_{i=1}^{N(t)} s_i \delta(t - t_i), \tag{1.2}$$

where $N(t)$ is the number of particle entrainments in time t, distributed as a Poisson distribution $P(N) = e^{-k_E t}(k_E t)^N/N!$, the t_i are distributed according to $P(t) = k_E \exp(-k_E t)$, and the s_i are step lengths distributed according to $P(s) = \ell^{-1} \exp(-s\ell^{-1})$. Figure 1.1 panel (a) sketches this noise, and panel (b) sketches the resulting global range trajectory as a sequence of steps and rests. Equation 1.1 is a kind of dynamical equation representing how the position of a sediment grain evolves through time (**?**), similar in spirit to Newtonian mechanics (**?**), but with random driving term (equation 1.2).

The governing equation of the distribution $P(x, t)$ to find the particle at x can be calculated as an ensemble average of $\delta(x - x(t))$ over all possible

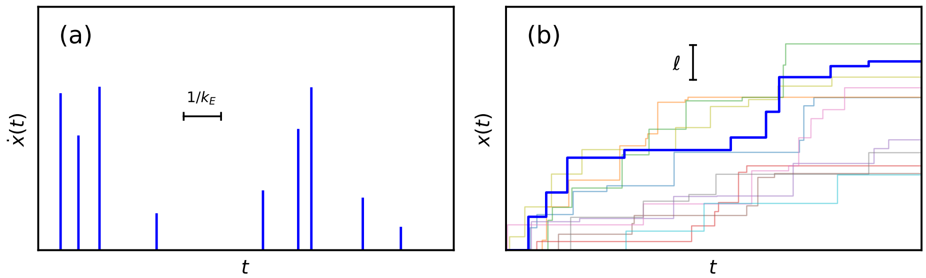

Figure 1.1: Panel (a) indicates the representation of Einstein's model as an idealized "white shot noise", as indicated in eq. 1.2, while panel (b) shows the "stairstep" trajectories of sediment particles moving downstream through cycles of steps (which are instantaneous) and rests (which have mean duration $1/k_E$).

realizations of the noise (*Moss and Peter Vaughan Elsmere*, 1989; **?**). Different methods exist to compute such averages (*Balakrishnan*, 1993; *Hanggi*, 1978; *Hänggi*, 1985; *Van Den Broeck*, 1983), but whatever the approach, the governing equation for the distribution comes out as

$$\big(\ell\partial_x\partial_t + k_E\ell\partial_x + \partial_t\big)P(x,t) = 0. \tag{1.3}$$

This equation can be solved by standard methods (series solutions or transform calculus) (*Arfken*, 1985; *Prudnikov et al.*, 1986) to reproduce the original result of *Einstein* (1937) for the probability distribution of position of a sediment particle:

$$P(x,t) = \delta(x)e^{-k_Et} + e^{-k_Et-x/\ell}\theta(x)\sqrt{\frac{k_Et}{\ell x}}\mathcal{I}_1\Big(2\sqrt{\frac{k_Ext}{\ell}}\Big) \tag{1.4}$$

Here, $\mathcal{I}$ is a modified Bessel function. The probability distribution eq. **??** fully characterizes the dynamics of an individual particle alternating through steps and rests.

This distribution displays both advective and diffusive characteristics. One can calculate all moments of the position by multiplying eq. 1.3 by x^n

and integrating over space. This gives the mean position of the particle

$$\langle x \rangle(t) = k_E \ell t, \tag{1.5}$$

so in Einstein's view, sediment grains move with effective velocity $V_{\text{eff}} = k_E \ell$, given by the entrainment rate times the mean step length. The rate at which one particle spreads out from another due to differences in their trajectories can be represented by the variance, $\sigma_x^2 = \langle x^2 \rangle - \langle x \rangle^2$. This gives

$$\sigma_x^2(t) = 2 k_E \ell^2 t, \tag{1.6}$$

so particles in Einstein's model spread apart as a normal diffusion process $\sigma_x^2 = 2 D_{\text{eff}} t$ (**?**), with an effective diffusivity $D_{\text{eff}} = k_E \ell^2$.

1.1.3 Inclusion of the movement duration

Einstein's model provides an adequate description of global range particle transport when the period of interest is much larger than the timescales of individual particle movements (local and intermediate ranges) and much smaller than the timescales over which particles become embedded in sedimentary deposits (geomorphic range). The advent of high speed camera experiments of bed load transport produced new insight into the local and intermediate ranges of particle motion (*Drake et al.*, 1988; **?**; **?**) which *Einstein* (1937) never intended for his model to describe. In the local range, particles move with a fluctuating velocity due to the variable drag of the turbulent flow (*Fathel et al.*, 2015; *Lajeunesse et al.*, 2010) and changes in the particle's height within the flow profile (*van Rijn*, 1984; *Wiberg and Smith*, 1985). In the intermediate range, particle-bed collisions impart additional variability to sediment velocities (*Gordon et al.*, 1972; *Martin*, 2013). Einstein's infinite movement velocity assumption excludes the timescales over which these processes occur.

Studies by *Gordon et al.* (1972), *Lisle et al.* (1998), and *Lajeunesse et al.* (2018) generalized the Einstein theory to include these timescales. They approximated particle velocities as constant (neglecting fluctuations), and assumed that the movement times are also (along with rests) exponentially distributed random variables, this time characterized by a deposition rate k_D, whose reciprocal is the average period of time a particle spends in motion (between entrainment and deposition). The analogue of Einstein's model equation 1.1 with a finite movement velocity V can be written

$$\dot{x} = V\eta(t), \tag{1.7}$$

where the noise is now a "dichotomous Markov noise" (*Bena*, 2006), which is essentially a random switch or telegraph-type signal that alternates between "on" ($\eta(t) = 1$, meaning the particle is moving) and "off" ($\eta(t) = 0$, meaning the particle is resting) (*Horsthemke and Lefever*, 1984; *Masoliver and Weiss*, 1991; *Masoliver et al.*, 1996; **?**) as displayed in figure 1.4 panel (a). Some particle trajectories solving equation **??** are displayed in 1.4 panel (b).

The governing equation of the position probability distribution $P(x,t) = \langle \delta(x - \int_0^t V\eta(t')dt') \rangle$ becomes (*Balakrishnan*, 1993)

$$\big(\partial_t^2 + V\partial_x\partial_t + k_E V\partial_x + k\partial_t\big)P(x,t) = 0, \tag{1.8}$$

where k_E and k_D are the entrainment and deposition rates, V is the particle velocity during the motion phase, and $k = k_E + k_D$. This partial differential equation is called an asymmetric telegrapher's equation (*Rossetto*, 2018), and although the symmetric analogue of this equation is well-studied (*Masoliver and Lindenberg*, 2017; *Weiss*, 2002b), the asymmetric problem is not often encountered.

For the intitial condition that particles have a probability k_E/k to start in motion, the solution of equation **??** is (*Lisle et al.*, 1998)

$$\tag{1.9}$$

Incorporating the duration of sediment motion, the mean position of the sediment grain remains linear in time: $\langle x\rangle(t) = k_E Vt/k$, representing movement at effective velocity $V_{\text{eff}} = k_E V/k$, which is the fraction of time spent in motion multiplied by the velocity during the motion phase. The variance,

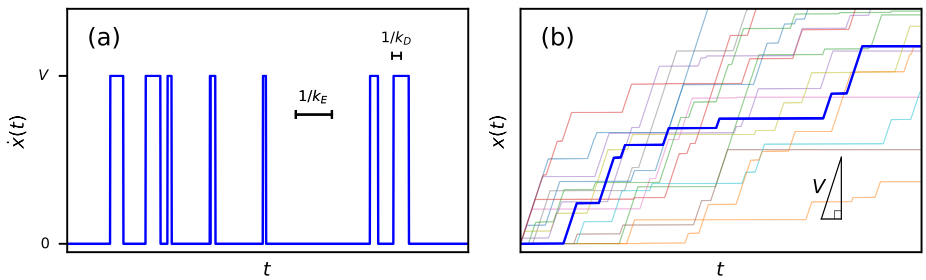

Figure 1.2: Panel (a) indicates the generalization of Einstein's model to include the interval of sediment motion between entrainment and deposition, now represented with dichotomous noise eq. **??**, while panel (b) shows the tilted stair-step trajectories of sediment particles moving downstream in cycles of motion at velocity V (with mean duration $1/k_D$) and rest (with mean duration $1/k_E$).

however, is different. Computing σ_x^2 provides

$$\sigma_x^2(t) =, \tag{1.10}$$

which is a non-trivial result. At short times, for $t \ll 1/k$, equation **??** shows diffusion $\sigma_x^2 \sim t^2$, which is a faster "ballistic" rate of spreading than the Einstein model predicts (**?**). At long times ($t \gg 1/k$), the diffusion becomes normal again ($\sigma_x^2 = 2D_{\text{eff}}t$), with an effective diffusion constant $D_{\text{eff}} = k_E k_D V^2/k^3$. In this model, both intermediate and global ranges are adequately represented, but local and geomorphic are not, since fluctuations of the velocity between entrainment and deposition have been neglected.

1.1.4 The Newtonian approach

Some authors have attempted to model local and intermediate ranges of individual particle trajectories by writing approximate Newtonian equations for the dynamics of individual particles and integrating them numerically. Early efforts impart particles with time-averaged fluid forces, typically linked to a logarithmic flow velocity profile (*van Rijn*, 1984), and some include simplified collision forces that modify particle velocities upon bed contact according to a set of simplified rules (*Sekine and Kikkawa*, 1992; *Wiberg and Smith*, 1985). Later on, researchers began to include granular interactions among particles to model collisions using the discrete element method (*Jiang and Haff*, 1993; **?**). The early works utilizing this approach used a two dimensional domain with a highly simplified flow model (**?**), while later works have included synthetic turbulence to drive particles (*Maurin et al.*, 2015; *McEwan and Heald*, 2001; *Schmeeckle and Nelson*, 2003) or clever reduced-complexity representations of the flow (*Clark et al.*, 2015, 2017). The state of the art within this category of sediment transport models is to include two-way coupling between particles and the fluid flow. The latter is modelled either by large eddy simulation or direct numerical simulation of the Navier-Stokes equations, using particles as the boundary condition for the fluid (*Elghannay and Tafti*, 2018; *González et al.*, 2017; *Ji et al.*, 2013; *Schmeeckle*, 2014; *Youse et al.*, 2020; **?**). A next step in this inquiry is to include non-spherical particles, and the foundation for this inquiry is now built (*Azéma and Radjaï*, 2012; *Wachs*, 2019; **?**). These computational physics models produce impressive insight into the underlying granular and fluid physics mechanisms producing bed load transport (*Frey and Church*, 2011), but analytical models are desired for further insight into the problem.

1.1.5 Mechanistic-stochastic models for the sediment velocity distribution

Some models have been developed to describe particle velocities in the local and intermediate ranges when velocities fluctuate due to turbulence and particle-bed collisions. Experimental studies on bedload velocities have provided two dominant conclusions. One subset of observations indicates that bedload velocities follow exponential distributions (*Fathel et al.*, 2015; *Furbish et al.*, 2012a; *Lajeunesse et al.*, 2010), and another subset indicates Gaussian distributions (*Ancey and Heyman*, 2014; *Heyman et al.*, 2016; *Martin et al.*, 2012).

Fan et al. (2014) set out to describe exponenential-distributed bedload particle velocities with a mechanistic model including a noisy driving term to represent fluid turbulence. They wrote, for the streamwise particle velocity u, a Langevin equation

$$\dot{u}(t) = -\Delta \mathrm{sgn}(u) + F + \sqrt{2D}\xi(t). \tag{1.11}$$

This equation drives the particle velocity by a fluid drag $F+\sqrt{2D}\xi(t)$, where F is a constant, D is a diffusivity that characterizes the magnitude of particle velocity fluctuations, and $\xi(t)$ is a Gaussian white noise with unit variance and vanishing mean (*Gardiner*, 1983). The fluid drag is resisted by a heuristic particle friction term $-\Delta \mathrm{sgn}(u)$, introduced as a proxy for particle-bed collisions. The "Fokker-Planck equation" governing the probability distribution $P(u,t)$ of the particle velocity can be derived from equation 1.11 as (*Van Kampen*, 2007; **?**)

$$\frac{\partial}{\partial t}P(u,t) = -\Delta\frac{\partial}{\partial u}\Big[\mathrm{sgn}(u)P\Big] + D\frac{\partial^2 P}{\partial u^2}, \tag{1.12}$$

implying that the steady-state velocity distribution ($\partial_t P(x,t) = 0$) provided by equation 1.11 is

$$P(u) = \frac{\Delta^2 - F^2}{2\Delta D}\exp\Big(-\frac{-\Delta|u| + Fu}{D}\Big). \tag{1.13}$$

This is the (two-sided) exponential distribution observed in one subset of experiments.

Ancey and Heyman (2014) formulated a Langevin equation to describe the Gaussian velocity distributions observed in the other subset of experiments. They wrote for the streamwise velocity

$$t_r\dot{u}(t) = -(U-u) + \sqrt{2D}\xi(t), \tag{1.14}$$

where U is the mean velocity of particles, D characterizes the magnitude of velocity fluctuations, and $\xi(t)$ is again a Gaussian white noise with vanishing mean and unit variance. The timescale t_r is a relaxation time over which velocity fluctuations decay. This time, the Fokker-Planck equation is

$$\frac{\partial}{\partial t}P(u,t) = -\frac{\partial}{\partial u}\Big[\frac{U-u}{t_r}P\Big] + \frac{D}{t_r^2}\frac{\partial^2 P}{\partial u^2}, \tag{1.15}$$

and the steady state solution becomes

$$P(u) = \sqrt{\frac{t_r}{2\pi D}}\exp\Big(-\frac{t_r(u-U)^2}{2D}\Big), \tag{1.16}$$

which is the Gaussian velocity distribution from the other subset of the experiments.

These two models of bedload velocity distributions are summarized in figure 1.3.

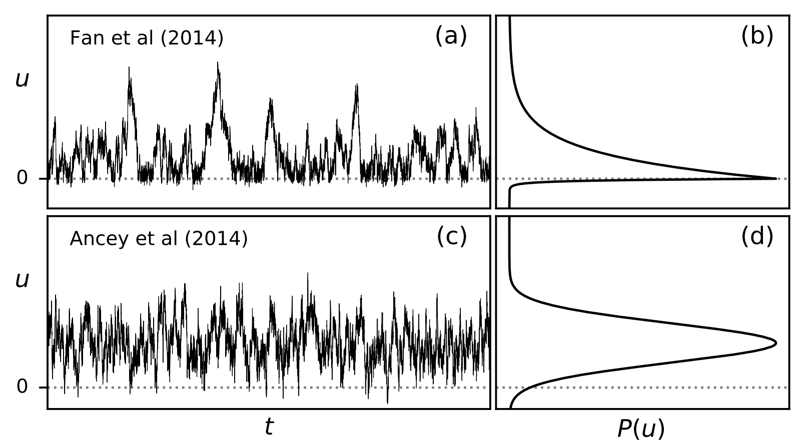

Figure 1.3: Panel (a) demonstrates the trajectory of a particle within the Fan et al model, where Coulomb friction impedes turbulent drag. Panel (b) shows the resulting exponential particle velocity distribution, having relatively large fluctuations with mode at $u = 0$. Panel (c) shows the analogous trajectory from the Ancey et al model, where turbulent Stokes drag generates the Gaussian velocity distribution seen in (d). The latter has relatively narrow and symmetric fluctuations, with the mode well above $u = 0$.

1.1.6 The definition of the flux

Perhaps a surprising summary of bedload transport research is that no one definition of the sediment flux has even been agreed upon despite over a century of research (*Ballio et al.*, 2018). Today, there are two main competing (or complementary) approaches to define the bedload flux. The first definition is reminiscent of continuum mechanics and formulates the flux as a kind of current of sediment across a control surface $\mathcal{S}$ (*Ballio et al.*, 2014; *Furbish et al.*, 2012a; *Heyman et al.*, 2016):

$$q = \int_{\mathcal{S}} c(\mathbf{x}, t)\mathbf{u} \cdot d\mathbf{S}. \tag{1.17}$$

This definition involves the concentration c of particles in space and their velocites at the instant they cross the control surface, which is a somewhat elusive quantity since bedload particles are not a continuous field (*Heyman et al.*, 2016). The second definition formulates the downstream flux in terms of the number of particles moving within a control volume $\mathcal{V}$:

$$q = \frac{1}{L} \sum_{i \in \mathcal{V}} u_i. \tag{1.18}$$

Here, the flux is evaluated as a sum over all downstream velocities of particles within the volume (of which there are a fluctuating number), and the division by the downstream length of the control volume is incorporated to count only that proportion of particles near the downstream boundary of the volume.

1.1.7 The scaling arguments of Bagnold

One of the most influential formulations of the bedload flux is due to Bagnold (*Bagnold*, 1956, 1966), who derived a formula for the mean sediment flux using an energy balance approach. Bagnold understood sediment transport as a process which converts flow energy to heat via the effective friction (*Bagnold*, 1954) of grains against the bed as they move downstream through a succession of collisions (*Bagnold*, 1973). He assumed that the flow power P_f available to move sediment scales as $P_f \propto \tau - \tau_c$, where τ is the average bed shear stress and τ_c is the threshold shear stress at which particles first begin to move. Considering that the average downstream flux of particles is q, and particles move with mean velocity proportional to the fluid velocity near the bed, Bagnold hypothesized that the power P_g required to sustain particle motion scales as $P_g \propto q/\tau^{1/2}$. Balancing flow energy against frictional dissipation ($P_f = P_g$) then provides Bagnold's sediment transport formula

$$q = k(\tau - \tau_c)\tau^{1/2}, \tag{1.19}$$

which has shown good correspondence with laboratory data at large transport rates, given careful calibration of the constant factors k and τ_c.

The large shear stress limit $q \sim \tau^{3/2}$ of Bagnold's formula is shared in common with many other empirical formulas describing the mean downstream flux of bedload (e.g. *Meyer-Peter and Müller*, 1948; *Wilcock and Crowe*, 2003; *Yalin*, 1972; **?**). The distinguishing feature of Bagnold's formula is its derivation from mechanical principles, although many of the details have since turned out to be incorrect. Bagnold's assumption that the power available to move sediment scaled with the excess shear stress leads to unphysical results over arbitrarily sloping beds (*Seminara et al.*, 2002), and the flow power dissipated by sediment transport shows only a weak correlation the sediment flux (*Ancey et al.*, 2008), while Bagnold assumed they were directly proportional. These issues have been hinted when calibrating Bagnold's formula to data, where the parameters k and τ_c take on unphysical values at low transport rates (*Niño and Garcia*, 1996). More generally, Bagnold's formulation faces the notorious challenge of defining the critical shear stress τ_c for the initiation of sediment transport (*Allen and Kudrolli*, 2018; *Clark et al.*, 2017; *Houssais et al.*, 2015; *KIRCHNER et al.*, 1990; *Paintal*, 1971), which is a topic for another thesis. The difficulties with Bagnold's approach led to many revisions of his theory which kept Bagnold's sharp physical insights, but included new experimental conclusions on the energetics of sediment transport as they became available (*Engelund and Fredsoe*, 1976; *Greenbaum et al.*, 2000; *Luque and van Beek*, 1976; *Niño and García*, 1998).

1.1.8 Einstein's probabilistic approach

Among these revisions of Bagnold, one category shows a return to the probabilistic ideas of Einstein (*Ancey et al.*, 2006; *Parker et al.*, 2003). Einstein formulated his original model of individual grains in transport (*Einstein*, 1937) in terms of particle entrainment and deposition using the conceptual picture of grains moving downstream through a sequence of instantaneous steps. Later, *Einstein* (1950); *Zee and Zee* (2017) calculated the bulk sediment flux with these same probabilistic ideas, providing an alternative to the Bagnold scaling approach. The conceptual picture that Einstein considered is depicted in figure **??**.

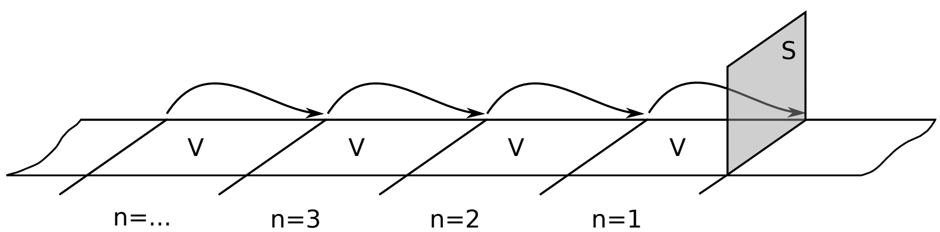

Figure 1.4: Einstein's conceptual picture (modified from *Yalin* (1972)). Particles move in discrete jumps of length ℓ from left to right through an array of adjacent control volumes. The bedload flux is the rate of bedload particles crossing the surface $\mathcal{S}$ per unit width and time, collected from all upstream control volumes.

He partitioned the channel into a sequence of identical control volumes V, and calculated the average rate at which particles cross a control surface by aggregating the contributions from each upstream control volume. Each control volume has downstream length ℓ which is also the average particle step length. Denoting by P_n the probability that an individual grain undergoes at least n jumps of length ℓ in a time interval T, meaning it travels at least a distance $n\ell$, and considering that there is a density ρ of particles at rest on the bed, it follows that on average $\rho\ell P_n$ particles will displace a distance $n\ell$ or more from within each control volume during the time interval

T. As a result, since grains crossing $\mathcal{S}$ in a time T could have come from any upstream location, the number of grains crossing $\mathcal{S}$ in T is a sum over all control volumes: $\sum_{n=1}^{\infty} \rho \ell P_n$. Dividing by the time T to get the average rate of grains crossing $\mathcal{S}$ provides the mean flux:

$$q = \frac{\rho \ell}{T} \sum_{n=1}^{\infty} P_n. \tag{1.20}$$

The final quantity to evaluate is P_n, the probability a particle entrains *at least* n times in a time T.

Einstein originally constructed this probability by assuming that each particle had n independent entrainment opportunities in the period T, each with probability p, so that $P_n = p^n$, giving $q \propto p/(1-p)$, but this approach has been revised by *Yalin* (1972) and others (*Armanini*, 2017; *Armanini et al.*, 2015; *Cheng*, 2004; *Paintal*, 1971). Some of these authors have argued that instead, one should calculate P_n as an exceedance probability. If the entrainment rate of an individual grain is k_E (probability per unit time), then the probability that it entrains *exactly* n times in time T, denoted by p_n (distinct from P_n!) is a Poisson distribution (**?**):

$$p_n = \frac{(k_E T)^n}{n!} e^{-k_E T}. \tag{1.21}$$

This implies that the probability that it entrains *at least* n times is $P_n = \sum_{i=n}^{\infty} \frac{(k_E T)^n}{n!} e^{-k_E T}$, so Einstein's mean sediment flux (eq. 1.20) becomes

$$q = \frac{\rho \ell}{T} \sum_{n=1}^{\infty} \sum_{l=n}^{\infty} = \frac{\rho \ell}{T} \sum_{n=1}^{\infty} n \frac{(k_E T)^n}{n!} e^{-k_E T} = \rho k_E \ell. \tag{1.22}$$

Noticing that ρk_E is the entrainment rate of a single grain multiplied by the density of grains available for entrainment on the bed, we can summarize the Einstein theory as

$$q = E \ell, \tag{1.23}$$

where the quantity $E = \rho k_E$ is the "areal entrainment rate", representing the number of grains entrained per unit bed area (*Furbish et al.*, 2012a; **?**).

Alongside this central result $q = E\ell$ for the mean flux, one of Einstein's most influential and enduring ideas was his formulation of the entrainment rate k_E of the individual particle in terms of the force balance on the stationary particle. The original approach considers that entrainment is driven by the fluctuating lift force imparted by the turbulent flow, and it is resisted by the submerged weight the grain. The entrainment rate is calculated from the exceedance probability of the turbulent lift over the weight, providing an alternative to the critical shear stress concept which explicitly incorporates turbulent fluctuations in the fluid flow. This formulation of entrainment probability in terms of the exceedance of random driving quantities over (possibly random) resisting quantities (*Grass*, 1970) is a key part of Einstein's legacy. *Paintal* (1971) made a significant extension by including the random supporting geometry of bed particles into the force balance. More recently, *Tregnaghi et al.* (2012) ammended the theory to include both force magnitude and duration (*Celik et al.*, 2014; *Diplas et al.*, 2008; **?**). Refined theories of the single-particle entrainment rate, all fundamentally similar to the original ideas of *Einstein* (1950), have been carefully reviewed by *Dey and Ali* (2018) and are a topic under active development.

1.1.9 Fusing Einstein and Bagnold: The erosion-deposition model

Although Einstein worked to relate the single-particle entrainment rate k_E to the flow, other parameters of Einstein's model (ρ, ℓ) retain a heuristic character and are not clearly linked to any underlying fluid-granular physics. The erosion-deposition model originally developed by *Charru* (2006); *Charru et al.* (2004); **?** modifies the Einstein model and relates its parameters to properties of the flow using scaling relations obtained from experiments (*Charru*, 2006; *Charru et al.*, 2004; *Lajeunesse et al.*, 2010, 2017; *Seizilles et al.*, 2014). This can be characterized as a mixture of the Einstein and Bagnold strategies.

The erosion-deposition model is

$$\partial_t \gamma + \partial_x V \gamma = E - D. \tag{1.24}$$

This is derived by evaluating a mass balance within a control volume. In this equation, γ is the "particle activity", which is the number of moving particles per unit area (*Furbish et al.*, 2012a), V is the ensemble averaged movement velocity of sediment grains (which in unsteady conditions may depend on space and time), E is the areal entrainment rate (the number of particles transitioning to motion per unit area and time), and D is the areal deposition rate (the number of particles coming to rest on the bed per unit area and time).

Scaling arguments provide relations for E, D, and V in terms of the fluid shear stress τ, particle size d, particle settling velocity V_s, and critical shear stress τ_c:

$$E = a\frac{\tau - \tau_c}{d^3 V_s}, \tag{1.25}$$

$$D = b\frac{\gamma V_s}{d}, \tag{1.26}$$

$$V = c + d(\sqrt{\tau} - \sqrt{\tau_c}). \tag{1.27}$$

The constant coefficients a, b, c, and d are determined experimentally.

Equation 1.24 indicates that the mean flux in steady transport conditions is the implicit solution to the equation $E = D$. Using the scaling relations 1.25 and 1.27 provides the mean particle activity

$$\gamma \propto \frac{\tau - \tau_c}{d^2 V_s^2}. \tag{1.28}$$

Expressing the mean flux as $q = \gamma V$, the relationship between flux and bed shear stress becomes

$$q = \frac{A}{d^2 V_s^2}\left(\tau - \tau_c\right)\left[c + d(\sqrt{\tau} - \sqrt{\tau_c})\right]. \tag{1.29}$$

This recovers the Bagnold scaling $q \propto \tau^{3/2}$ at large bed shear stresses.

1.1.10 The nonlocal formulation

Einstein's model of the bulk bedload flux is inherently nonlocal in that it aggregates particle motions from all upstream locations (*Schumer et al.*, 2009; **?**). *Nakagawa and Tsujimoto 9 Kyoto* (1977) and later *Parker et al.* (2002) formalized this by writing the sediment flux in an explicitly nonlocal form:

$$q(x,t) = \int_0^\infty dx' F(x-x',t)E(x',t). \tag{1.30}$$

In this equation, motions are instantaneous, and $F(x,t)$ is the probability that a just-entrained particle steps a distance l before deposition. In general, this approach can handle non-uniform conditions by including space and time dependence in E and F.

Furbish et al. (2012a) generalized the Parker model to include a finite duration of motion. They wrote

$$q(x,t) = \int_0^\infty dx' \int_0^\infty dt' F(x',t')E(x-x',t-t'), \tag{1.31}$$

where $F(x,t)$ represents the probability density that particles move *at least* a distance x in time t (right after entrainment). For a simple example of the Furbish et al formalism, consider that particles move with a constant velocity V and have a deposition rate k_D. Then the probability density that a particle moves *exactly* a distance x in time t is $f(x,t) = \delta(x-Vt)k_D \exp(-k_D t)$, so the probability that it moves *at least* a distance x in t is

$$F(x,t) = \int_0^t \delta(x-Vt)k_D \exp(-k_D t) = \theta(Vt-x)k_D \exp(-k_D t). \tag{1.32}$$

Considering uniform conditions with a density ρ of particles available for motion on the bed surface, each having entrainment rate k_E, the bulk entrainment rate can be expressed as $E = \rho k_E$, and equation 1.31 provides a mean flux

$$q = \rho k_E \int_0^\infty dx' \int_0^\infty dt' \theta(Vt-x)k_D \exp(-k_D t) = \rho k_E V/k_D. \tag{1.33}$$

Since $1/k_D$ is the average time spent in motion, V/k_D is the average step length ℓ. Equation 1.33 therefore provides another perspective on Einstein's result $q = E\ell$.

1.1.11 Landscape evolution

Exner was probably the first to write the mathematical relationship between sediment transport and topographic change (**?**). He wrote

$$(1-\phi)\frac{\partial z}{\partial t}(\mathbf{x},t) = -\nabla q(\mathbf{x},t). \tag{1.34}$$

This equation links the temporal evolution of the land elevation z at a location $\mathbf{x} = (x, y)$ to spatial gradients in the sediment flux q. The parameter ϕ is the bed porosity.

Within the Exner equation, the elevation z and sediment flux q are represented as continuum fields. This representation can be interpreted as a spatial average over the detailed positions of individual grains, and it is expected to be valid whenever the scales of interest are large compared to the size of the averaging window, which is must be taken much larger than the largest grains in the modelling domain (*Coleman and Nikora*, 2009). Yet there are many Earth surface processes where the scale of interest is not much larger than the largest grains involved in the system. We can wonder, for example, how large boulders in mountain channels control the formation of steps (*Church and Zimmermann*, 2007; *Saletti and Hassan*, 2020; **?**), or other bed structures having sizes comparable to channel widths, like ribs or stone cells (*Hassan et al.*, 2007; *Venditti et al.*, 2017). In these cases, individual grains are comparable to the scales of interest, and the continuum description provided by the Exner equation is not applicable.

? and *Tsujimoto* (1978) developed an alternative statement of the Exner equation based upon Einstein's concepts of entrainment and deposition rates. According to their formulation, spatial gradients in the sediment flux arise due to local discrepancies in entrainment and deposition:

$$\partial_x q(x,t) = E - D. \tag{1.35}$$

Owing to 1.34, this expression of the sediment flux immediately implies the "entrainment form of the exner equation" (*Fathel et al.*, 2015; *Furbish et al.*, 2012a, 2017; *Parker et al.*, 2002) by which topographic evolution can be described in an Einstein-like framework:

$$(1 - \phi)pxz(x, t) = D - E. \tag{1.36}$$

In a nonlocal framework, as in equation 1.31, sediment deposition can be interpreted as the result of entrainment at all upstream locations, giving

$$(1 - \phi)pxz(x, t) = \int_0^\infty dx' int_0^\infty dt' E(x', t')F(x', t') - E(x, t). \tag{1.37}$$

This "entrainment form of the Exner equation" (*Furbish et al.*, 2017) phrases topographic change from a stochastic interpretation of sediment transport.

1.1.12 Fluctuations and scale dependence

The sediment flux . . . .. has fluctuations and scale dependence. An early approach to calculate the sediment flux distribution is due to **?**, who evaluated the sediment flux as the result of migrating bedforms. This approach has been extended to include bedforms with a range of sizes (*Guala et al.*, 2014; **?**).

1.1.13 Birth death models for bedload flucuations

The prevalence of large bedload fluctuations motivated *Ancey et al.* (2006, 2008) to revisit Einstein's assumptions to develop a model of the bedload flux as a random variable. They derived the probability distribution of this variable by counting the number of moving particles in a control volume. This number changes through time as a result of entrainment and deposition. To obtain realistically-wide fluctuations in particle activity, they introduced a positive feedback called "collective entrainment", whereby the entrainment rate of grains increases in proportion to the number of moving grains in the volume (*Ancey et al.*, 2008; *Heyman et al.*, 2013).

Their governing equations are completely analogous to a stochastic population model (*Pielou*, 2008; **?**) where entrainment is "birth" and deposition is "death". They formulated the probability mass function $P(n, t)$ of the number of moving grains in the control volume at time t as

$$\partial_t P(n,t) = \big[\lambda + (n-1)\mu\big]P(n-1,t) - [n+1]\sigma P(n+1,t) - \big[\lambda + n(\sigma+\mu)\big], \tag{1.38}$$

whose terms describe entrainment at rate λ, collective entrainment at rate μ, and deposition at rate σ. The final term encodes the possibility that n does not change at a given instant. These coupled equations (one for each $n = 0, 1, \dots$) can be solved by generating functions (*Ancey et al.*, 2008; **?**), providing the steady-state distribution

$$P(n) = \frac{\Gamma(r+n)}{\Gamma(r)n!}p^r(1-p)^n, \tag{1.39}$$

where $r = \lambda/\mu$ and $p = 1 - \mu/\sigma$. This is a negative binomial distribution, which is a wide-tailed generalization of the Poisson distribution.

From eq. 1.39, the mean number of moving particles is $\langle n\rangle = \lambda/(\sigma-\mu)$, and the variance is

$$\sigma_n^2 = \frac{\lambda\sigma}{(\sigma-\mu)^2}. \tag{1.40}$$

Owing to the collective entrainment process, particle activity fluctuations can be arbitrarily wide: $\sigma_n/\langle n\rangle = \sqrt{\sigma/\lambda}$, whereas in the absence of collective entrainment ($\mu = 0$), the strength of fluctuations is always pinned to 1, as the distribution 1.39 limits to a Poisson distribution (*Ancey et al.*, 2006).

The probability distribution of the bedload flux can be computed by the control volume form, eq. 1.18 given, in addition, the probability distribution of particle velocites, which can be determined experimentally (*Fathel et al.*, 2015; *Heyman et al.*, 2016; **?**) or calculated using the Langevin models described in section 1.1.5. Assuming that the particle activity in the control volume and the velocities of moving particles are completely independent, which may be a good assumption for a large enough control volume, the probability distribution $Q(q)$ of the flux is (*Ancey*, 2020; *Ancey and Heyman*, 2014; *Ancey et al.*, 2008)

$$Q(q) = L\sum_{k=1}^{\infty} P(k)G(U), \tag{1.41}$$

where $P(n)$ comes from eq. 1.39 and $G(U)$ is the probability that the sum of k particle velocities at some instant is equal to U.

1.1.14 Renewal theories for scale dependence

The final approach to summarize that of calculating the sediment flux probability distribution from an "arrival time distribution" representing the distribution of times between subsequent arrivals of particles to a control surface (*Ancey*, 2020; *Turowski*, 2010). This distribution changes depending on the observation time T used to calculate the averaged flux. This is the phenomenon of scale dependence. The statistics machinery of counting arrivals is called renewal theory (**?**).

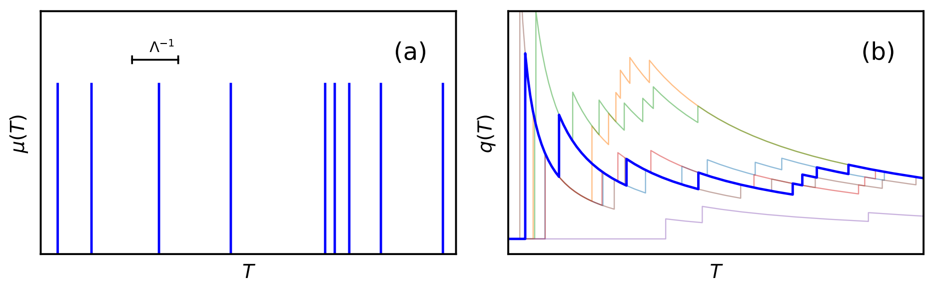

Figure 1.5: The scale-dependent sediment flux is described as a renewal process. Panel (a) indicates the arrivals of particles at rate Λ, while panel (b) shows an ensemble of realizations of the sediment flux versus the observation time T. Note that different realizations of the flux converge toward the same value at large observation times, whereas at small observation times, uncertainty in the flux is large. This is observation-scale dependence. The nature of this convergence depends on the particle dynamics in an as yet unspecified way.

Earlier studies have considered two different arrival time distributions to calculate the probability distribution of the time-averaged sediment flux, but only one of these is reviewed here. This is an exponential distribution: $P(t) = \Lambda \exp(-\Lambda t)$, so the mean time between particle arrivals is $1/\Lambda$. In this case, the flux averaged over a period T can be represented with a Poisson pulse noise, similar to the particle position in the Einstein model of section **??**:

$$q(T) = \frac{1}{T}\int_0^T dt'\mu(t'). \tag{1.42}$$

Here, the noise is

$$\mu(t) = \sum_{i=1}^{N(t)} \delta(t - t_i), \tag{1.43}$$

as indicated in figure 1.5 panel (a). In this equation, $N(t)$ is Poisson distributed with rate Λt. The flux in eq. 1.42 is a random variable as indicated in 1.5 panel (b). Its probability distribution which is contingent on the observation time T can be derived by evaluating $P(q|T) = \langle \delta(q - \int_0^T \mu(t')dt'/T)\rangle$. This equation entails an average over all possible realizations of the noise in eq. 1.43, producing (*Van Kampen*, 2007)

$$P(q|T) = \sum_{l=0}^{\infty} \frac{\left(\Lambda T\right)^l}{l!} e^{-\Lambda T}\delta(q - \frac{l}{T}), \tag{1.44}$$

which is a Poisson distribution.

The mean flux derived from this scheme ($\langle q\rangle(T) = \int_0^\infty dqP(q|T)$ is

$$\langle q\rangle = \Lambda, \tag{1.45}$$

which is independent of observation scale, while the magnitude of bedload transport fluctuations scales with $1/T$:

$$\sigma_q^2 = \frac{\Lambda^2}{T}. \tag{1.46}$$

Even this simple model gives a non-trivial conclusion that the relative uncertainty in a measurement of bedload transport depends on observation time: $\sigma_Q/\langle q\rangle \propto T^{-1/2}$. The limitation of these approaches is that they do not obviously relate to the dynamics of individual particles. In renewal models, the distribution of arrival times is heuristic.

1.2 Summary

This literature review has indicated that successful bedload transport descriptions have been developed to describe individual particles and bulk bedload fluxes. All of the works reviewed so far are either mean field models that do not include fluctuations, or stochastic models that calculate probability distributions for the quantities of interest. The common thread of all of these models is that they take advantage of various devices to side-step the complex interplay of turbulence and granular physics which control bedload transport. In the case of mean field models, the devices are heuristic scaling arguments and semi-empirical formulas, while in the case of stochastic models, they are simplified dynamical equations driven by idealized noises, like sequences of pulses, alternating switches, and erratic fluctuations.

1.3 Outline of the thesis

1.3.1 Problem 1: The scale-dependent flux from individual particle dynamics

The original model by *Einstein* (1937) describing particle trajectories when the movement velocity is infinite was subsequently improved to include a finite yet constant velocity (*Gordon et al.*, 1972; *Lisle et al.*, 1998; **?**). Particle velocities fluctuate during movements between entrainment and deposition, so this should also be accounted for in bedload trajectory models. In addition, the scale-dependence of the sediment flux has been calculated from renewal models (*Ancey*, 2020; *Turowski*, 2010), but these overlook the details of individual particle motions, so it remains unclear how the sediment flux distribution and its scale dependence originate from individual particle trajectories.

Chapter 2 introduces a new model of individual bedload trajectories which includes velocity fluctuations in the motion phase, then demonstrates how these trajectories can be used to calculate scale-dependent probability distribution of the bedload flux, building on all of these earlier studies.

1.3.2 Problem 2: Feedbacks between sediment transport fluctuations and bed elevation change

Birth-death models calculate the flux probability distribution assuming that entrainment and deposition do not change the local bed elevation (*Ancey and Heyman*, 2014; *Ancey et al.*, 2008; *Heyman et al.*, 2013), which violates conservation of mass and the Exner equation (**??**), and precludes the possibility that sediment can become buried in the subsurface of the bed. Although sediment burial is known to affect tracer particle motions at geomorphic timescales (*Hassan and Bradley*, 2017; **?**), our understanding of how long sediment can remain buried is limited.

Chapter **??** generalizes the model of *Ancey et al.* (2008) to include bed elevation changes in order to evaluate the effect of bed elevation variability on bedload transport fluctuations and to study how the timescales of sediment burial relate to the movements characteristics of grains.

1.3.3 Problem 3: The effect of sediment burial on downstream transport of sediment tracers

The model of sediment transport as an alterating sequence of motion and rest intervals implicitly assumes that particles are either moving or resting on the bed surface, and it provides a useful description of bedload transport on the intermediate and global timescales of *Nikora et al.* (2001a, 2002). Tracers become buried, and this affects their motion characteristics at global and geomorphic timescales (*Hassan and Bradley*, 2017). These phenomena are not yet included in Einstein-type models that treat individual sediment trajectories as a random walk (e.g. *Lisle et al.*, 1998).

Chapter **??** generalizes the model of *Lisle et al.* (1998) and **?** to include sediment motion, rest, and burial to develop a description of sediment trajectories over intermediate, global, and geomorphic timescales.

1.3.4 Problem 4: The control of particle-bed collisions over bedload particle velocity distributions

Finally, the Langevin models of *Fan et al.* (2014) and *Ancey and Heyman* (2014) describe the velocity distributions of sediment moving downstream in the local and intermediate ranges in between entrainment and deposition. These models describe two different end-member distributions from among the experimental record on bedload velocities. One develops exponential velocities, and the other develops Gaussian velocities. Since the forces included in these models are phenomenological, we can assume the issue is that particle-bed collisions are not adequately represented.

Chapter 5 presents a stochastic Langevin model including episodic particle-bed collisions formulated by analogy with the theory of granular gases (**?**). This produces a satisfying description of all different bedload velocity distributions which have been reported in experimental studies.

Chapter 2

From particle dynamics to the sediment flux

2.1 Introduction

A relativity weak flow shearing a bed of sediment entrains individual particles into a state of motion controlled by turbulent forcing and intermittent collisions with other grains at rest on the bed, generating wide fluctuations in the sediment velocity (*Fathel et al.*, 2015; *Heyman et al.*, 2016). Bed load particles move downstream until they are disentrained when they happen to encounter sufficiently sheltered pockets on the bed surface to interrupt their motions (*Charru et al.*, 2004; *Gordon et al.*, 1972). Eventually, the bed around them rearranges and destroys this shelter, or turbulent fluctuations overcome the shelter (**??**), particles are once again entrained, and the cycle repeats. Bed load transport is thus a kind of itinerant motion, characterized by alternation between fluctuating movements and rest. This process is difficult to describe mathematically given the technicality of the stochastic physics involved (*Ancey*, 2020; *Furbish et al.*, 2017).

To date, descriptions of bed load transport have therefore simplified the problem in various ways to enable progress. The foundational work is due to Einstein, who considering bed load motions as instantaneous so he could describe bed load transport as an alternating sequence of "steps" and rests having random length and duration (*Einstein*, 1937), in a pioneering application of the continuous time random walk (*Montroll*, 1964). Einstein concluded that particles move downstream with a mean velocity $\langle u \rangle = k_E l$, where k_E is the rate at which an individual bed particle entrains into motion, and l is the mean length of each downstream step. Later, Einstein applied these ideas to calculate the mean downstream flux due to the movements of many such particles (*Einstein*, 1950). Einstein reasoned that if the density of resting particles on the bed is ρ_b, the overall areal entrainment rate of particles can be written $E = \rho_b k_E$, giving a mean sediment flux $\langle q_s \rangle = \rho_b \langle u \rangle = El$.

Many researchers have since refined Einstein's approach to provide more realistic descriptions of individual particle motions than Einstein's instantaneous step model. One set of efforts has neglected particle deposition process to calculate the downstream velocity distributions of moving particles after entrainment using mechanistic equations with terms representing turbulent fluid forces and particle-bed collisions (*Ancey and Heyman*, 2014; *Fan et al.*, 2014). Another set of efforts has described particles alternating between motion and rest, considering that motions occur with a constant velocity (*Lajeunesse et al.*, 2018; *Lisle et al.*, 1998; *Pierce and Hassan*, 2020). No models have yet been formulated which describe particles alternating between motion and rest, while motions have a realistic fluctuating velocity.

A set of studies has developed stochastic formulations of the sediment flux which improve on the mean field description provided by Einstein (*Furbish et al.*, 2012a). Sediment fluxes generally exhibit wide fluctuations due to variations in the number of moving particles and their velocities (*Ancey and Heyman*, 2014; *Ancey et al.*, 2008), the migration of bedforms and sediment waves (*Guala et al.*, 2014; *Hoey*, 1992; *Recking et al.*, 2012; **?**), and a host of other processes (*Dhont and Ancey*, 2018). Because these fluctuations occur over disparate timescales, measurements of mean sediment fluxes depend on the timescale over which they are collected, a phenomenon called scale-dependence (*Ancey*, 2020; *Singh et al.*, 2009; *Turowski*, 2010; **?**; **?**). To date, very few models have calculated the probability distribution of the bed load sediment flux due to individual particle motions (*Ancey and Hey-*

man, 2014; *Ancey et al.*, 2008), and among these, even fewer have described any observation-scale dependence of the flux (*Ancey*, 2020; *Turowski*, 2010). Among those that do, none have yet formulated the sediment flux in terms of the downstream trajectories of individual grains.

This survey provides context for the two problems addressed in this chapter. First, we do not yet have the capability to describe individual sediment trajectories through motion and rest including velocity fluctuations in the motion state; and second, we need more understanding of how to connect individual particle trajectories through motion and rest to the overall downstream sediment flux, including its probability distribution, and the dependence of its statistical moments on the observation time. Here, we develop a new statistical physics-based formalism which addresses both of these problems by describing individual particle trajectories with a Langevin-type dynamical equation which combines earlier approaches (*Ancey and Heyman*, 2014; *Fan et al.*, 2014; *Lajeunesse et al.*, 2018; *Lisle et al.*, 1998) This stochastic equation includes alternation between motion and rest at random intervals while particles in motion have velocity that fluctuate around a mean value. Using the probability distribution of particle position generated by this model, we construct a formalism to derive analytically the probability distribution of the sediment flux. This distribution exhibits observation-scale dependence as a result of velocity fluctuations among moving sediment. Below, we develop the new formalism in sec. 2.2, solve it in sec. 2.4, and we discuss the implications of our results and future research ideas in secs. 2.5 and 2.6.

2.2 Description of motion-rest alternation with velocity fluctuations

We consider an infinite one-dimensional domain populated with sediment particles on the surface of a sedimentary bed. We consider that the flow is weak enough that interactions among moving grains are very rare, although interactions between moving particles and the bed may be common. The flow is in constrast strong enough so that particles move. We label the downstream coordinate as x, so that the downstream velocity of a moving particle is $\dot{x}$, and we describe all sediment particles as independent from one another but governed by the same underlying dynamical equations, meaning we neglect any influence of sediment size or shape or spatial variations in the overlying fluid flow.

2.2.1 Dynamical equation for grain-scale sediment transport

From these assumptions, our first target is to write an equation of motion for the individual sediment particle encompassing two features. First, particles should alternate between motion and rest. The transition rate from rest to motion is called entrainment and occurs with probability per unit time (or rate) k_E, while the transition from motion to rest is called deposition and occurs with rate k_D. Second, particles in motion should move with mean velocity V and some fluctuations around this velocity. The simplest equation of motion including these features is

$$\dot{x}(t) = [V + \sqrt{2D}\xi(t)]\eta(t). \tag{2.1}$$

Here $\xi(t)$ is a Gaussian white noise having zero mean and unit variance representing velocity fluctuations among moving particles, and $\eta(t)$ is a dichotomous noise which takes on values $\eta = 1$, representing motion (with mean duration $1/k_D$), and $\eta = 0$, representing rest (with mean duration $1/k_E$). Here, V is the mean particle velocity, and D is a diffusivity [units L^2/T] describing velocity fluctuations among moving particles. The transition rate from $\eta = 0$ to $\eta = 1$ is k_E, and the transition rate from $\eta = 1$ to $\eta = 0$ is k_D. We write $k = k_E + k_D$ as a shorthand.

2.2.2 Derivation of the master equation for the sediment position distribution $P(x,t)$

The solution of equation 5.3 for a given realization of the two noises $\eta(t)$ and $\xi(t)$ gives the trajectory of one particle. Averaging over the ensemble of all such trajectories from different realizations of the noises will obtain the probability distribution $P(x, t)$ that a particle which started at position $x = 0$ at time $t = 0$ has travelled to position x by time t. This distribution, by construction, will generalize earlier models of bedload alternation between motion and rest which did not include velocity fluctuations among moving particles (*Lajeunesse et al.*, 2018; *Lisle et al.*, 1998).

We form the desired probability distribution of position as $P(y, t) = \left\langle \delta(y - x(t)) \right\rangle_{\eta,\xi}$, where $x(t)$ is the formal solution of eq. 5.3 and the average is over both noises, but this symbolic equation is not yet useful as taking averages over both noises directly is a challenging mathematical problem (*Hanggi*, 1978). A simpler approach is to conduct the averages in Fourier space. Integrating eq. 1, using its solution in the probability distribution, then Fourier transforming gives

$$\tilde{P}(g, t) = \left\langle \left\langle \exp\left[-ig \int_0^t du[V + \sqrt{2D}\xi(u)]\eta(u) \right] \right\rangle_\eta \right\rangle_\xi. \tag{2.2}$$

Taking time derivatives and conducting the averages using known characteristics of averages of exponentials of Gaussian white noise (*Gardiner*, 1983; **?**) and the Furutsu-Norikov procedure for time derivatives of averages involving dichotomous noise (**?**) in a method similar to (*Balakrishnan*, 1993) provides the Fourier-space master equation

$$\partial_t^2 \tilde{P}(g, t) = (igV - g^2 D - k)\partial_t \tilde{P} + k_E(igV - g^2 D)\tilde{P}, \tag{2.3}$$

and inverse Fourier transforming provides the desired real-space master equation

$$(\partial_t^2 + V\partial_x\partial_t + k_E V\partial_x + k\partial_t - D\partial_x^2\partial_t - k_E D\partial_x^2)P(x, t) = 0. \tag{2.4}$$

This is a diffusion-like equation governing the probability distribution of position for individual particles as they transport downstream through a sequence of motions and rests, with the movement velocity being a fluctuating quantity. One can see in particular that taking an the entrainment rate k_E very large, meaning that all particles are generally moving, implies an advection-diffusion equation $(\partial_t + V\partial_x - D\partial_x^2)P = 0$ for the position, characteristic of a particle moving downstream with Gaussian velocity fluctuations (*Ancey and Heyman*, 2014). Otherwise, with k_E of similar order as k_D, there is a finite probability that the particle is at rest, and the advection-diffusion process is often interrupted by deposition, giving rise to the additional terms in eq. 5.4 reminiscient of earlier motion-rest models with constant velocity (*Lajeunesse et al.*, 2018; *Lisle et al.*, 1998).

2.3 Formalism for the downstream sediment flux

The probability distribution of the sediment flux is calculated using the probability distribution of particle position $P(x,t)$ provided as the solution of equation 5.4. This method is modified from the approach recently developed by Banerjee and coworkers in physics (*Banerjee et al.*, 2020). The basic idea, as depicted in Figure 1, is that particles are initially distributed in all states of motion along a domain at random locations to the left of $x = 0$. The flux is calculated using the number of particles that end up to the right of $x = 0$ during the sampling time T.

The rate of particles crossing the surface in an observation time T is

$$Q(T) = \frac{1}{T}\sum_{i=1}^{N}\mathcal{I}_i(T). \tag{2.5}$$

In this equation, $\mathcal{I}_i(T)$ is an indicator function which is 1 whenever the ith particle has passed our control surface and 0 otherwise. All particles which have not crossed the control surface (or which have crossed and then crossed back) contribute nothing to the flux. The probability distribution of the flux is then

$$P(Q|T) = \Big\langle \delta\Big(Q - \frac{1}{T}\sum_{i=1}^{N}\mathcal{I}_i(T)\Big)\Big\rangle. \tag{2.6}$$

The average is over the initial conditions of each particle and the ensemble of trajectories for each particle. Taking the Laplace transform over Q (i.e.

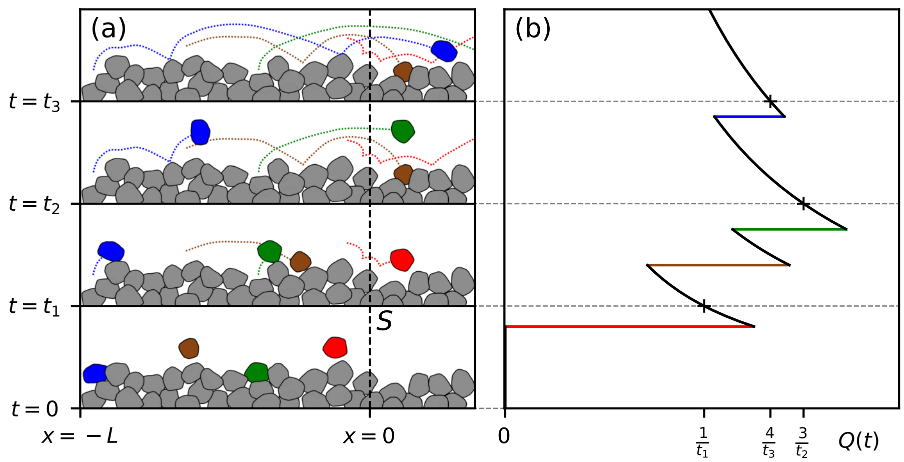

Figure 2.1: The left panel indicates the configuration for the flux. The particle trajectories within are calculated from equation 5.3, demonstrating alternation between rest and motion with fluctuating velocity. Particles begin their transport with positions $-L \leq x \leq 0$ at $t = 0$, and as depicted in the right panel, the flux is calculated as the number of particles $N_>(t)$ which lie to the right of $x = 0$ at the observation time t, divided by t: $Q(t) = t^{-1}N_>(t)$. We calculate the probability distribution of Q over all realizations of the trajectories and initial positions as $L \to \infty$

forming the characteristic function) obtains

$$\tilde{P}(s|T) = \left\langle \int_0^\infty dQ e^{-sQ} \delta\Big(Q - \frac{1}{T}\sum_{i=1}^{N} \mathcal{I}_i(T)\Big) \right\rangle \tag{2.7}$$

$$= \Big\langle \exp\Big(\frac{s}{T}\sum_{i=1}^{N} \mathcal{I}_i(T)\Big)\Big\rangle \tag{2.8}$$

$$= \prod_{i=1}^{N} \Big\langle \exp\Big(-\frac{s}{T}\mathcal{I}_i(T)\Big)\Big\rangle \tag{2.9}$$

$$= \prod_{i=1}^{N} \Big[1 - \big(1 - e^{-s/T}\big)\langle \mathcal{I}_i(T)\rangle\Big] \tag{2.10}$$

This progression relies on the independence of averages for each particle (so the average of a product is the product of averages) and the fact that $\mathcal{I}_i(T)$ is either 1 or 0, so that $e^{ax} = 1 - (1 - e^a)x$. The average over initial conditions and possible trajectories for the ith particle can be written

$$\langle \mathcal{I}_i(t) \rangle = \frac{1}{L} \int_L^0 dx' \int_0^\infty dx \mathcal{P}(x, t|x') = \frac{1}{L} \int_0^L dx' \int_0^\infty dx \mathcal{P}(x, t|-x'), \tag{2.11}$$

where $\mathcal{P}(x, t|x')$ is the probability density that the particle is found at position x at time t given it was initially at x' at time 0. This is the part of the flux that depends on the particle dynamics (ie instantenous velocities and entrainment/deposition characteristics).

Inserting (7) into (6) and taking the limit as $L \to \infty$ and $N \to \infty$ while the density of particles $\rho = N/L$ remains constant provides

$$\tilde{P}(s|T) = \lim_{N\to\infty} \Big(1 - \frac{1}{N}\big(1 - e^{-s/T}\big)\mu(T)\Big)^N = \exp\Big[-\big(1 - e^{-s/T}\big)\mu(T)\Big]. \tag{2.12}$$

where $\mu(T) = \rho \int_0^\infty dx \int_0^\infty dx' \mathcal{P}(x, T|x')$ is a rate constant which encodes the particle dynamics. This expression is the characteristic function of a Poisson distribution (**?**). Expanding in $e^{-s/T}$ and inverting the Laplace transform provides the probability distribution of the flux, contingent on the sampling time T:

$$P(Q|T) = \sum_{k=0}^{\infty} \frac{\mu(T)^k}{k!} e^{-\mu(T)} \delta(Q - \frac{k}{T}). \tag{2.13}$$

This equation implies that the mean flux is $\langle Q \rangle(T) = \int_0^\infty dQ Q P(Q|T) = \mu(T)/T$, and similarly the variance is $\sigma_Q^2(T) = \mu(T)/T^2$. The conclusion is that if the flux is considered as a time averaged number of particles crossing a control surface, the mean flux is always Poissonian, no matter how particles move, provided the particles are independent and do not interact.

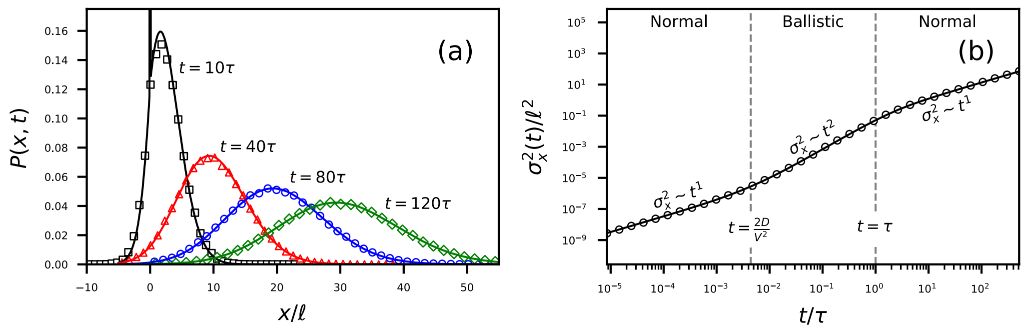

Figure 2.2: Panel (a) indicates the probability distribution of particle position as it evolves through time. From the initial mixture of motion and rest states, particles advect downstream as they diffuse due to differences in their fluctuating velocities and exchange between motion and rest. Panel (b) shows the resulting particle diffusion. At timescales $t \ll 2D/V^2$, the diffusion is normal since the movement is approximately a standard diffusion process (as advection is irrelevant on these timescales). For larger timescales, $2D/V^2 \ll t \ll \tau$, particles undergo ballistic diffusion similar to *Lisle et al.* (1998) as a result of some particles being stationary as others advect. Finally longer than the timescale $\tau = 1/k$ associated with entrainment and deposition, diffusion is again normal, exemplified by exchange between motion and rest. All results are scaled by the mean hop length $l = V/k_D$ and the autocorrelation time $\tau = 1/k$ of the motion/rest alternation.

2.4 Results

2.4.1 The position probability distribution and its moments

The master equation 5.4 describes the evolution of the probability distribution of position through time. Loosely speaking the solution of this equation is expected to be some combination of the *Einstein* (1937) theory for particle transport with the Gaussian propagator of the advection-diffusion equation (**?**).

Because the master equation is second order in time, it requires initial conditions for P and $\partial_t P$. Considering that particles start at rest in a mixture of motion and rest states, with a fraction k_E/k starting in motion and a fraction k_D/k starting in rest, these conditions derive from the state

$$P(x,0) = \lim_{t \to 0} \frac{k_E}{k} \sqrt{\frac{1}{4\pi D t}} \exp\Big[- \frac{(x - Vt)^2}{4Dt} \Big] + \frac{k_D}{k} \delta(x) \tag{2.14}$$

which gives $P(x,0) = \delta(x)$ and $\partial_t P(x,0) = \frac{k_E}{k} \big[D\delta''(x) - V\delta'(x) \big]$ (*Weiss*, 2002a).

The master equation 5.4 is solved by transform calculus in the appendix, providing

$$P(x,t) = \big[- \varphi D \partial_x^2 + V\varphi \partial_x + k + \partial_t \big] \int_0^t \mathcal{I}_0\Big(2\sqrt{k_E k_D u(t-u)} \Big) e^{-k_E(t-u)} \times \sqrt{\frac{1}{4\pi D u}} \exp\Big[- k_D u - \frac{(x - Vu)^2}{4Du} \Big] du. \tag{2.15}$$

This integral term encodes the earlier expectation of Einstein model-like behavior mixed with a Gaussian propagator. The integral term convolves the probability that the particle has been in motion for a period u out of a time t with the probability density that a particle has travelled a distance x in time u. The prefactor involving partial derivatives can be understood as adapting this distribution to the initial conditions.

The moments of position from this distribution could be calculated by integrating equation 2.15, but this is challenging. Instead, we calculate the governing equation of the moments directly from the master equation 5.4. Multipling this equation by x^l and integrating over all x provides

$$\partial_t^2 m_l - Vl\partial_t m_{l-1} - k_E V l m_{l-1} + k\partial_t m_l - Dl(l-1)\partial_t m_{l-2} - k_E D l(l-1) m_{l-2} = 0, \tag{2.16}$$

where $\langle x^l \rangle = m_l$. For $l = 1$, this equation generates the mean position $\langle x \rangle(t) = k_E V t/k$, which is unaffected by diffusion (since Gaussian velocity fluctuations are symmetric). The case $l = 2$ provides the second moment, which provides the variance of position

$$\sigma_x^2 = \frac{2k_E k_D V^2}{k^3}\left(t + \frac{1}{k}e^{-kt} - \frac{1}{k}\right) + 2\frac{k_E D}{k}t. \tag{2.17}$$

At short times $t \ll k^{-1}$, this becomes

$$\sigma_x^2 \sim \frac{k_E k_D V^2}{k^2}t^2 + \frac{2k_E D}{k}t, \tag{2.18}$$

so it scales as $\sigma_x^2 \sim t^2$ when $t \gg \frac{2Dk}{V^2 k_D}$ and $\sigma_x^2 \sim t$ when $t \ll \frac{2Dk}{V^2 k_D}$. Similarly at long times $t \gg k^{-1}$,

$$\sigma_x^2 \sim \frac{2k_E k_D V^2}{k^3}t, \tag{2.19}$$

so we have a non-trivial multi-scale diffusion phenomenon. Provided that $2D/V^2 \ll k_D/k^2$, we therefore have

$$\sigma_x^2 \sim \begin{cases} t, & t \ll \frac{2Dk}{V^2 k_D}, \\ t^2, & \frac{2Dk}{V^2 k_D} \ll t \ll \frac{1}{k}, \\ t, & t \gg \frac{1}{k}. \end{cases} \tag{2.20}$$

Note in the physical condition when $k \approx k_D$, the condition for the existence of three ranges becomes $Pe \ll 1$, where $Pe = 2Dk_D/V^2$. The small Peclet limit, when three diffusion ranges are obtained, is characteristic of bedload sediment transport where velocity fluctuations are typically small compared to mean downstream movement velocites.

2.4.2 Calculation of the sediment flux

From the formalism in section xxxx, the central parameter of the sediment flux distribution is

$$\mu(t) = \rho \int_0^\infty dx_i \int_0^\infty dx P(x + x_i, t). \tag{2.21}$$

This represents the rate of particles crossing $x = 0$ at the observation time T given they started somewhere to left of $x = 0$ at $T = 0$.

It is convenient to calculate this quantity in Laplace space. Taking the Laplace transform,

$$\tilde{\mu}(s) = \rho \int_0^\infty dx_i \int_0^\infty dx \tilde{P}(x + x_i, s), \tag{2.22}$$

then performing both integrals provides

$$\tilde{\mu}(s) = -\frac{\phi D}{VR(s + k_E)} + \frac{2D\phi}{VR(1-R)(s + k_E)} + \frac{4D^2(s + k)}{V^3 R(1-R)^2(s + k_E)}. \tag{2.23}$$

$\mu(t)$ derives as the inverse Laplace transform of this equation. This calculation is performed in the appendix, providing

$$\mu(t) = \int_0^t \mathcal{I}_0\Big(2\sqrt{k_E k_D u(t-u)}\Big) e^{-k_E(t-u) - k_D u}$$
$$\times \left[\sqrt{\frac{D}{\pi u}}\Big([\overleftarrow{\partial}_t + k]u - \frac{k_D}{2k}\Big) e^{-V^2 u/4D} + \frac{V}{2}\Big([\overleftarrow{\partial}_t + k]u - \frac{k_D}{k}\Big) \operatorname{erfc}\left(-\sqrt{\frac{V^2 u}{4D}}\right)\right] du. \tag{2.24}$$

In this equation, the notation $\overleftarrow{\partial}$ means that the derivative acts from the left of all terms in which it is involved, as in $f(t)\overleftarrow{partial}_t g(t) = \partial_t f(t) g(t)$.

This is a complicated result for the rate constant in the sediment flux **??**, but this complexity is not surprising given that equation 5.3 involves two interacting diffusion processes. As displayed in 5.3, as a result of eq. 2.24 the mean flux takes on a non-trivial scale-dependence, characterized by a decay toward the Einstein prediction $Q_0 = El$ as the observation time becomes much larger than $1/(k_D Pe)$.

The convergence time of the flux thus scales with the inverse Peclet number. When particle velocity fluctuations during motions are larger compared to advection, the flux becomes slow to converge, in general.

2.4.3 Reduction to earlier work

The mathematical form of our results is complicated, although the ideas are conceptually clear. Particles alternate through motion and rest, and

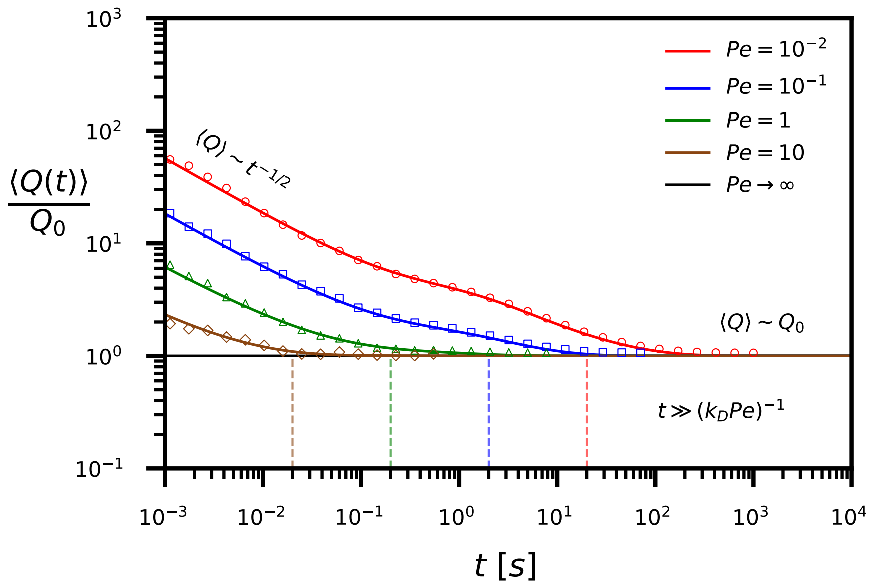

Figure 2.3

particle motions have a fluctuating velocity, not a deterministic velocity. Nevertheless, turning off velocity fluctuations by setting $D = 0$ re-derives the results of *Lisle et al.* (1998), who formulated sediment transport as a random walk between motion and rest states. Further taking the velocity infinite as the time spent in motion vanishes, while their product $V/k_D = \ell$, the mean step distance, rederives the central result of *Einstein* (1937), given originally in **??**.

In either of these limit cases, the mean sediment flux becomes $\langle q\rangle = E\ell$, with no dependence on observation scale. This indicates that scale dependence in the sediment flux is a consequence of velocity fluctuations among moving particles, at least when observation timescales are relatively short.

2.5 Discussion

This chapter has generalized the earlier descriptions of individual sediment trajectories (e.g. *Lisle et al.*, 1998; **?**) to include velocity fluctuations in the motion state. Using results from this generalized model as an example, I demonstrated how to calculate the sediment flux probability distribution, phrasing earlier renewal theory approaches more directly in terms of the underlying particle dynamics (e.g. *Ancey*, 2020; *Turowski*, 2010). Calculated in this way, the sediment flux distribution is observation-scale dependent, describing how sediment fluxes depend on the period over which they are measured.

2.5.1 Fluctuations and collective motions

The sediment flux probability distribution in equation **??** represents a Poisson distribution with an observation-scale dependent rate. Poisson distributions have a relatively thin tail, meaning fluctuations are typically small (*Ancey et al.*, 2006). In reality, sediment flux distributions are only Poissonian at high transport rates, whereas in other conditions they have wide tails representing the possibility of extremely large transport fluctuations (*Ancey et al.*, 2008; *Turowski*, 2010; **?**; **?**) which appear as bursts (e.g. *Goh and Barabási*, 2008) in the sediment flux timeseries (*Heyman et al.*, 2013; *Singh et al.*, 2009; **?**). This exposes a need to generalize a mechanistic theory of the sediment flux I developed here to produce wider fluctuations.

Descriptions of sediment transport based on population dynamics in a control volume have realistically-wide fluctuations by incorporating a positive feedback between the number of moving particles and the particle entrainment rate called collective entrainment (*Ancey and Heyman*, 2014; *Ancey et al.*, 2008). This feedback generates spatially-correlated waves of moving particles (*Ancey and Heyman*, 2014; *Heyman et al.*, 2015) and produces non-exponential interarrival time distributions (*Heyman et al.*, 2013) which imply wide-tailed flux distributions when incorporated in renewal theory (*Ancey*, 2020; *Turowski*, 2010). Collective entrainment has been attributed to particle-particle interactions, such as small granular avalanches and collision-induced entrainment, and to fluid-particle interactions, such as large eddies entraining particles as they sweep downstream (*Ancey and Heyman*, 2014; *Lee and Jerolmack*, 2018; **?**).

We can imagine generalizing the description in equation **??** to include such fluid-particle interactions by including time dependence in the movement velocity (V), diffusivity (D), or entrainment and deposition rates (k_E and k_D) as necessary, although the resulting equations would likely require numerical solutions. Particle-particle interactions would be more challenging to include. The dynamical equation 5.3 would generalize to $\dot{x}_i(t) = F_i(x_i,t) + \sum_{i\neq j} G_{ij}(\{x_j\},t)$, where the F_i are the driving terms unique to each particle, while the G_{ij} are some (generally stochastic) terms representing interactions between the ith and jth particles (**?**). The resulting joint distribution of particle positions and velocities ($P(x_1, v_1, \ldots, x_{N(t)}, v_{N(t)}, t)$) might be formulated by analogy to the theory of reaction diffusion systems (**?**), non-ideal gases (**??**), or other interacting particle models available in physics literature (*Escaff et al.*, 2018; **?**). By analogy to collective entrainment, interacting models which generalize the approach established in this chapter should be capable of producing wide sediment transport fluctuations.

2.5.2 Measurement protocol for the sediment flux

2.5.3 Stochasticity in landscape evolution

? originally phrased channel morphodynamics in terms of spatial gradients in the sediment flux (sec. 1.34), writing

$$(1-\phi)\partial_t h(x,t) = -\partial_x q(x,t).\mathbf{??} \tag{2.25}$$

In this one-dimensional equation, $h(x,t)$ is a continuous field representing the longitudinal channel profile. Traditionally, the Exner equation is evaluated considering the flux as a deterministic quantity (*An et al.*, 2017; *Parker et al.*, 2007; **?**), which provides a solitary trajectory of the profile through time.

Considering the flux in the Exner equation as a stochastic quantity requires us to reinterpret channel dynamics in a way which few researchers have explored (*Jerolmack and Mohrig*, 2005; **?**). In contrast to the traditional analysis, a stochastic Exner equation with fluctuating $q(x,t)$ generates an ensemble of possibilities for the channel profile $z(x)$ at each instant. This set of possibilities is characterized by a probability distribution $P(\{z(x)\},t)$ for each possible profile. Mathematically, since the channel profile is a field, evaluating such a probability distribution of channel profiles would require statistical field theory (**?**). A starting point on this analysis might be $P(\{z(x)\},t) = \langle \delta[z(x,t) - h(x,t)] \rangle$, where $h(x,t)$ involves the stochastic flux $q(x,t)$ from equation **??**. In this equation, $\delta[f(x)]$ is a Dirac delta functional, which generalizes the delta function $\delta(x)$ from a single-valued parameter x to a continuous field $f(x)$. Such ideas are commonly applied to understand polymers and membranes (**??**), but they have not been introduced in geomorphology.

Introducing such a description with the stochastic Exner equation would lend new mathematical language to the old unsolved problem in geomorphology: how does variability affect landscape evolution? The classic works all acknowledge variability (**?**), although one of their main efforts was to construct strategies to describe landscapes without explicitly accounting for it, producing ideas like competent flows to summarize climatic variability (**?**), characteristic grain sizes to overcome sorting processes (*Parker and Klingeman*, 1982), or average flow energies to avoid turbulence (*Bagnold*, 1954). Progress in stochastic approaches to river science (e.g. **??**) invites us to step beyond averaged descriptions, propagate noises through the governing equations of landscape evolution, and ask again with these classic works to what extent fluctuations shape Earth's surface.

2.6 Summary and Conclusion

This chapter introduced a two-noise stochastic dynamical equation to describe individual bedload trajectories for particles alternating between motions and rests. The motion phase was enriched to include velocity fluctuations, forming the first physical model of this type. The probability distribution of the bedload sediment flux was calculated from these particle dynamics, and the resulting flux distribution was demonstrated to adopt scale-dependence from the underlying trajectories of individual particles. The measurement timescales over which sediment flux observations converge were expressed in terms of the mean particle movement velocity and the typical magnitude of its fluctuations in terms of a Peclet number.

These results generalize the bedload trajectory models of *Einstein* (1937), *Lisle et al.* (1998), and **?** to include fluctuating movement velocities, and they reframe earlier renewal models of the sediment flux probability distribution (*Ancey*, 2020; **?**) to explicitly include the transport dynamics of individual sediment grains. They further quantify the dependence of the sediment flux on the observation scale, and provide guidance as to the measurement times required to resolve sediment transport without ambiguity, at least in simplified configurations when bedforms are absent. Next steps are to include interactions between particles to produce wider sediment transport fluctuations, and to evaluate the effects of sediment transport fluctuations on channel morphodynamics.

Chapter 3

Analysis of bed elevation change and sediment transport fluctuations

The transport characteristics of coarse grains moving under a turbulent flow ultimately control a wide set processes within rivers, including the export of contaminants (*Macklin et al.*, 2006; *Malmon et al.*, 2005), the success of ecological restoration efforts (*Gaeuman et al.*, 2017), and the response of channel morphology to disturbances (*Hassan and Bradley*, 2017). Although the displacements of individual grains are certainly a mechanical consequence of forces imparted from the flow, bed, and other grains (*González et al.*, 2017; *Vowinckel et al.*, 2014; *Wiberg and Smith*, 1985), accurately characterizing these forces within natural channels is practically impossible, especially considering the intense variability these forces display (*Celik et al.*, 2010; *Dwivedi et al.*, 2011; *Schmeeckle et al.*, 2007). In response, investigators have developed a stochastic concept of bedload transport (*Einstein*, 1937), whereby the erosion and deposition of individual grains are modeled as the random results of undetermined forces (*Ancey et al.*, 2006; *Einstein*, 1950; *Paintal*, 1971).

Essentially two types of bedload transport model have been developed from this concept. The first type provides the probabilistic dynamics of a small population of tracer grains as they transport downstream (*Einstein*, 1937; *Hubbell and Sayre*, 1964; *Lajeunesse et al.*, 2018; *Martin et al.*, 2012; *Nakagawa and Tsujimoto 9 Kyoto*, 1977; *Wu et al.*, 2019a), while the second provides the statistics of the number of moving grains ("the particle activity") within a control volume (*Ancey et al.*, 2006, 2008; *Einstein*, 1950; *Furbish et al.*, 2012b). In the first type, individual displacements are considered to result from alternate step-rest sequences, where step lengths and resting times are random variables following statistical distributions (*Einstein*, 1937). Differences between the random-walk motions of one grain and the next imply a spreading apart of tracer grains as they transport downstream: bedload tracers undergo diffusion.

Resting time distributions have been carefully studied in relation to these models because the predicted diffusion characteristics are critically dependent on whether the distribution has a light or heavy tail (*Bradley*, 2017; *Martin et al.*, 2012; *Weeks and Swinney*, 1998). Resting times have puzzled researchers because early experiments show exponential distributions (*Einstein*, 1937; *Hubbell and Sayre*, 1964; *Nakagawa and Tsujimoto 9 Kyoto*, 1977; *Yano*, 1969), while later experiments show heavy-tailed power-law distributions (*Bradley*, 2017; *Liu et al.*, 2019; *Martin et al.*, 2012; *Olinde and Johnson*, 2015; *Voepel et al.*, 2013; **?**). A predominant hypothesis is that power-law distributed resting times originate from buried grains (*Martin et al.*, 2014; *Voepel et al.*, 2013); this hypothesis permits surface grains to retain exponential resting times. Conceptually, when grains rest on the surface, material transported from upstream can deposit on top of them, preventing entrainment until its removal, driving up resting times and imparting a heavy tail to the distribution. To our knowledge, *Martin et al.* (2014) have provided the only direct support for this hypothesis by tracking grains through complete cycles of burial and exhumation using a narrow flume with glass walls. They observed heavy-tailed resting times of buried grains and described their results with a mathematical model similar to an earlier effort by *Voepel et al.* (2013). Both of these models treat bed elevation changes as a random walk and interpret resting times as return periods from above in the bed elevation time-series (*Redner and Dorfman*, 2002). Each describes resting time distributions from different experiments, but they rely on different random walk models, and their treatment of bed elevations as a process independent of sediment transport is questionable at first glance, since bedload transport is the source of bed elevation changes (*Wong et al.*, 2007), and neither model explicitly includes bedload transport. Models of sedimentary bed evolution incorporating sediment transport processes might enhance understanding of sediment resting times.

The second type of stochastic model prescribes rates (probabilities per unit time) to the erosion and deposition events of individual grains within a control volume to calculate the particle activity (*Einstein*, 1950). These approaches aim at a complete statistical characterization of the bedload flux (*Fathel et al.*, 2015; *Furbish et al.*, 2012b, 2017; *Heyman et al.*, 2016), including probability distributions (*Ancey et al.*, 2006, 2008), spatial and temporal characteristics of its fluctuations (*Ancey et al.*, 2008; *Dhont and Ancey*, 2018; *Heyman*, 2014; *Roseberry et al.*, 2012), and the dependence of these statistical characteristics on the length and time scales over which they are measured or calculated (*Ma et al.*, 2014; *Singh et al.*, 2009, 2012; **?**). A recent surge in research activity has generated rapid progress and spawned many new inquiries in this subject. For example, *Ancey et al.* (2006) demonstrated that a constant erosion rate as originally proposed by *Einstein* (1950) was insufficient to develop realistically large particle activity fluctuations, so they added a positive feedback between the particle activity and erosion rate they called "collective entrainment" (*Ancey et al.*, 2008; *Heyman et al.*, 2013, 2014; *Lee and Jerolmack*, 2018; *Ma et al.*, 2014). While they deemed this feedback necessary to model realistic activity fluctuations, the implications of this collective entrainment term on bed topography and particle activity changes has not been fully explored.

In this work, we present the first stochastic model coupling the erosion and deposition of individual bedload grains to local bed elevation changes. Our model extends the *Ancey et al.* (2008) model to describe the interplay between bedload flux and bed elevation fluctuations in a control volume. This development permits a systematic study of the repercussions of collective entrainment, and it frames bed elevation changes as a direct consequence of the sediment transport process. Our model has two key assumptions: (1) bedload erosion and deposition can be characterized by probabilities per unit time, or rates (*Ancey et al.*, 2008; *Einstein*, 1950); and (2) these rates are contingent on the local bed elevation, encoding the property that erosion of sediment is emphasized from regions of exposure, while deposition is emphasized in regions of shelter (*Wong et al.*, 2007; **?**). We study statistical characteristics of bedload transport, bed elevation, and resting times of sediment undergoing burial using a mixture of numerical simulations and analytical approximations. We introduce the stochastic model in section 5.2, and we solve it in section 5.3.1 with a mixture of numerical and analytical techniques. We discern several new features of particle activity and bed elevation statistics that result from feedbacks between the erosion and deposition rates and the local bed elevation. We present these features in section 5.3. We conclude with the implications of our results and speculate on topics for future research in sections 5.4 and 5.5.

3.1 Stochastic model of bedload transport and bed elevations

We prescribe a volume of downstream length L containing some number n of moving particles in the flow and some number m of stationary particles composing the bed at time t, as depicted in figure 3.1. We define m relative to the mean number of grains within the control volume, so that it can be either positive or negative. n is always a positive integer including 0. For simplicity, we consider all particles as approximately spherical with the same diameter $2a$, so their mobility and packing characteristics are consistent. Following *Ancey et al.* (2008), we prescribe four events that can occur at any instant to modify the populations n and m, and we characterize these events using probabilities per unit time (rates). These events are (1) migration of a moving particle into the volume from upstream ($n \to n+1$), (2) the entrainment (erosion) of a stationary particle into motion within the volume ($m \to m-1$ and $n \to n+1$), (3) the deposition of a moving particle to rest within the volume ($m \to m+1$ and $n \to n-1$), and (4) the migration of a moving particle out of the volume to downstream ($n \to n-1$). The four events are depicted as arrows in figure 3.1. As the events occur at random intervals, they set up a joint stochastic evolution of the populations n and m characterized by a joint probability distribution $P(n, m, t)$ for the number of particles in motion and rest in the volume at t. The populations

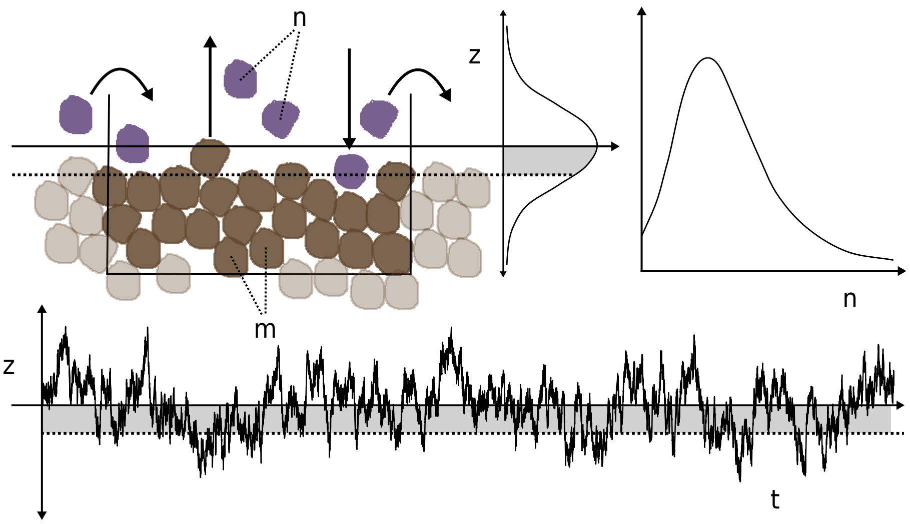

Figure 3.1: Definition sketch of a control volume containing n moving grains and m resting grains. Migration, entrainment, and deposition are represented by arrows, and the instantaneous bed elevation is depicted by dotted lines. The bed is displayed in a degraded state, where $m < 0$. The marginal distributions of n and m are indicated in the upper right panel, while the bottom panel is a realized time-series of bed elevations computed from m using (3.1).

n and m provide the bulk bedload flux q_s and the local bed elevation z. The mean bedload transport rate is given by $q_s = u_s\langle n\rangle/L$, where u_s is the characteristic velocity of moving bedload and $\langle n\rangle = \sum_{n,m} nP(n,m)$ is the mean number of grains in motion (*Ancey et al.*, 2008; *Charru et al.*, 2004; *Furbish et al.*, 2012b). The bed elevation is related to m through the packing geometry of the bed. To quantify this, we introduce a packing fraction ϕ

of grains in the bed (*Bennett*, 1972), and for simplicity we consider the bed as two-dimensional (*Einstein*, 1950; *Paintal*, 1971). The deviation from the mean bed elevation is then

$$z(m) = \frac{\pi a^2}{\phi L} m = z_1 m. \tag{3.1}$$

The constant $z_1 = \pi a^2/(\phi L)$ is an important scale of the problem. z_1 is the magnitude of bed elevation change in an average sense across the control volume associated with the addition or removal of a single grain.

Bed elevation changes modify the likelihood of entrainment and deposition in a negative feedback (*Wong et al.*, 2007; **?**); that is, aggradation increases the likelihood of entrainment, while degradation increases the likelihood of deposition. *Wong et al.* (2007) concluded that bed elevation changes induce an exponential variation in entrainment and deposition probabilities, while **?** concluded that the variation is linear. For simplicity, we incorporate the scaling of **?** and note its equivalence to the *Wong et al.* (2007) scaling when bed elevation changes are small. Because experimental distributions of bed elevations are often symmetrical, (*Martin et al.*, 2014; *Pender et al.*, 2001; *Wong et al.*, 2007; **?**), we expect the erosion and deposition feedbacks to have the same strength. That is, as bed elevation changes drive up (down) erosion rates, so they drive down (up) deposition rates to the same degree. Merging these ideas with those of *Ancey et al.* (2008), we write the four possible transitions with local bed elevation-dependent entrainment and deposition rates as

$$R_{MI}(n+1|n) = \nu \qquad \text{migration in,} \tag{3.2}$$

$$R_E(n+1, m-1|n, m) = (\lambda + \mu n)[1 + \kappa m], \qquad \text{entrainment,} \tag{3.3}$$

$$R_D(n-1, m+1|n, m) = \sigma n[1 - \kappa m], \qquad \text{deposition.} \tag{3.4}$$

$$R_{MO}(n-1|n) = \gamma n \qquad \text{migration out.} \tag{3.5}$$

In equations (3.3) and (3.4), κ is a coupling constant between bed elevations and the entrainment and deposition rates. ν is the rate of migration into the control volume, λ is the conventional entrainment rate, μ is the collective entrainment rate, σ is the deposition rate, and γ is the rate of migration out of the control volume. At $m = 0$, these equations reduce to those of the *Ancey et al.* (2008) model. Away from this elevation, entrainment and deposition are alternatively suppressed and enhanced depending on the sign of m, constituting a feedback between bed elevation changes and erosion and deposition. We refer to κ as a coupling constant since it controls the strength of this feedback. We later demonstrate the relationship

$$\kappa \approx \left(\frac{z_1}{2l}\right)^2 \tag{3.6}$$

where l is a characteristic length scale of bed elevation change that we interpret as the active layer depth (*Correa et al.*, 2017; *Wong et al.*, 2007). All four rates are independent of the past history of the populations and depend only on the current populations (n, m). As a result, the model is Markovian (**??**), meaning time intervals between any two subsequent transitions are exponentially distributed (*Gillespie*, 2007).

We write the master equation for the probability flow using the forward Kolmogorov equation $\partial P(n,m;t)/\partial t = \sum_{n',m'}[R(n,m|n',m')P(n',m';t) - R(n',m'|n,m)P(n,m;t)]$ (*Ancey et al.*, 2008; **?**; **?**) as

$$\begin{aligned}\frac{\partial P}{\partial t}(n,m;t) &= \nu P(n-1,m;t)+[\lambda(m+1)+\mu(n-1)][1+\kappa(m+1)]P(n-1,m+1;t)\\ &+ \sigma(n+1)[1-\kappa(m-1)]P(n+1,m-1;t)+\gamma(n+1)P(n+1,m;t)\\ &- \{\nu+\lambda+\mu n(1+\kappa m)+\sigma n(1-\kappa m)+\gamma n\}P(n,m;t). \end{aligned}\tag{3.7}$$

The joint probability distribution $P(n, m; t)$ solving this equation fully characterizes the statistics of n and m – proxies for the bedload flux and local bed elevation. The average entrainment and deposition rates E and D over all bed elevations are $E = \lambda + \mu\langle n\rangle$ and $D = \sigma\langle n\rangle$. We anticipate that solutions of (5.4) will adjust from the initial conditions to a steady-state distribution $P_s(n, m)$ – independent of time – if the constant factors in the transition rates are representative of equilibrium conditions. Equilibrium requires $E = D$, meaning there is no net change in elevation, and $\nu = \gamma\langle n\rangle$, meaning mass is conserved in the control volume (inflow = outflow). This

Master equation describes a two-species stochastic birth-death model (**?**) of a type well-known in population ecology (*Pielou*, 2008; *Swift*, 2002) and chemical physics (*Gardiner*, 1983). In our context, the two populations are the moving and stationary grains in the volume.

3.2 Model solutions

Unfortunately, equation (5.4) does not appear to admit an analytical solution unless $\kappa = 0$ (but see *Swift* (2002) for the generating function method which fails in this case). The difficulty originates from the product terms between n and m representing the bed elevation dependence of collective entrainment and deposition rates. In response to this difficulty, we resort to numerical methods and analytical approximations, simulating equation (5.4) with the Gillespie algorithm (*Gillespie*, 1977, 2007; **?**) and solving it approximately with mean field and Fokker-Planck approaches (*Gardiner*, 1983; **?**). The simulation algorithm is described in 3.2.1, and analytical approximations are described in 3.2.2.

3.2.1 Numerical study of the joint model

The Gillespie algorithm leverages the defining property of a Markov process: when transition rates are independent of history, time intervals between transitions are exponentially distributed (**?**). As a result, to step the Markov process through a single transition, one can draw a first random value from the exponential distribution of transition intervals to determine the time of the next transition, then draw a second random value to choose the type of transition that occurs using relative probabilities formed from equations (3.2-3.5). The tran-

Table 3.1: Migration, entrainment, and deposition rates at $z(m) = 0$ from *Ancey et al.* (2008). Units are s^{-1} (probability/-time). In our model, bed elevation changes modulate these rates in accord with (3.2-3.5).

flow	ν	λ	μ	σ	γ
(a)	5.45	6.59	3.74	4.67	0.77
(g)	7.74	8.42	4.34	4.95	0.56
(i)	15.56	22.07	3.56	4.52	0.68
(l)	15.52	14.64	4.32	4.77	0.48

sition is enacted by shifting t, n and m by the appropriate values to the type of transition (that is, entrainment is $m \to m-1$ and $n \to n+1$, and so on). This procedure can be iterated to form an exact realization of the stochastic process (*Gillespie*, 2007). We provide additional background on the stochastic simulation method in the supplementary material and refer the reader to *Gillespie* (2007) for more detail.

Using this method, we simulated 4 transport conditions with 13 different values of l taken across a range from $l = a$ (a single radius) to $l = 10a$ (10 radii). These values include the range exhibited by the available experimental data on bed elevation timeseries (*Martin et al.*, 2014; *Singh et al.*, 2009; *Wong et al.*, 2007). For the migration, entrainment, and deposition parameters representing bedload transport at each flow condition $(\nu, \lambda, \mu, \sigma, \gamma)$, we used the values measured by *Ancey et al.* (2008) in a series of flume experiments: these are summarized in table 3.1. Flow conditions are labeled (a), (g), (i), and (l), roughly in order of increasing bedload flux (see *Ancey et al.* (2008) for more details). In all simulations, we take the packing fraction $\phi = 0.6$ – a typical value for a pile of spheres (e.g., *Bennett*, 1972), and we set $L = 22.5$cm and $a = 0.3$cm in accord with the *Ancey et al.* (2008) experiments. Each simulation was run for 250 hours of virtual time, a period selected to ensure neat convergence of particle activity and bed elevation statistics.

3.2.2 Approximate solutions of the joint model

We approximately decouple the n and m dynamics in equation (5.4) using the inequality $l \gg z_1$ (equivalently $\kappa \ll 1$) which holds for large values of the active layer depth l. These inequalites mean many entrainment or deposition events are required for an appreciable change in the entrainment or deposition rates. We concentrate on steady state conditions $\partial P/\partial t = 0$ and introduce the exact decomposition $P(n, m) = A(n|m)M(m)$ to equation (5.4), with the new distributions normalized as $\sum_m M(m) = 1$ and $\sum_n A(n|m) = 1$. This provides the steady state equation

$$0 = \nu A(n-1|m)M(m) + [\lambda+\mu(n-1)][1+\kappa(m+1)]A(n-1|m+1)M(m+1) + \sigma(n+1)[1-\kappa(m-1)]A(n+1, m-1)M(m-1) + \gamma(n+1)A(n+1|m)M(m) - \{\nu + [\lambda + \mu n](1 + \kappa m) + \sigma n(1 - \kappa m) + \gamma n\}A(n, m)M(m). \quad (3.8)$$

Summing this equation over n provides a still exact description of the distribution of bed elevations $M(m)$ in terms of the conditional mean particle activity $\langle n|m\rangle = \sum_n nA(n|m)$:

$$0 = [\lambda + \mu\langle n|m + 1\rangle][1 + \kappa(m + 1)]M(m + 1) + \sigma\langle n|m - 1\rangle[1 - \kappa(m - 1)]M(m - 1) - \{[\lambda + \mu\langle n|m\rangle](1 + \kappa m) + \sigma\langle n|m\rangle(1 - \kappa m)\}M(m). \quad (3.9)$$

Unforunately, these two equations are no easier to solve than the original master equation, since the coupling between n and m is not reduced in equation (3.8).

The simplest approximation to these equations holds that κ is so small that the dynamics of n are totally independent of m: $A(n|m) = A(n)$. Taking this limit in equation (3.8), summing over m, and using $\langle m\rangle = 0$ reproduces the *Ancey et al.* (2008) particle activity model. As shown by *Ancey et al.* (2008), this has solution

$$A(n) = \frac{\Gamma(r + n)}{\Gamma(r)n!}p^r(1 - p)^n. \quad (3.10)$$

which is a negative binomial distribution for the particle activity with parameters $r = (\nu+\lambda)/\mu$ and $p = 1-\mu/(\sigma+\gamma)$. This result implies $\langle n|m\rangle = \langle n\rangle$, so with the definitions of E and D and the equilibrium condition $E = D$, equation (3.9) provides

$$0 \approx [1 + \kappa(m + 1)]M(m + 1) + [1 - \kappa(m - 1)]M(m - 1) - 2M(m). \quad (3.11)$$

This mean field equation matches the discrete Ornstein-Uhlenbeck model of bed elevation changes developed by *Martin et al.* (2014). We summarize that the independent bed elevation and particle activity models of *Martin et al.* (2014) and *Ancey et al.* (2008) derive from the model we present in a mean field approximation when κ is insignificant.

In the supplementary information we show the Fokker-Planck approximation (*Gardiner*, 1983) formed by expanding $M(m \pm 1)$ to second order in m within equation (3.11) provides the solution $M(m) \propto \exp(-\kappa m^2)$: this is a normal distribution of bed elevations with variance $\sigma_m^2 \propto \frac{1}{2\kappa}$. As we will demonstrate in section 5.3, and as we have already suggested with equation (3.6), this is a poor approximation to the bed elevation variance. Nevertheless, this approximation does capture the Gaussian shape of the bed elevation distribution. The essential issue with this mean field approach is that the conditional mean particle activity $\langle n|m\rangle$ varies significantly with m in actuality, especially when collective entrainment contributes to the mean entrainment rate E. We will discuss these points subsequently when developing more refined approximations and presenting numerical results.

A more careful approximate solution to equation (3.9) can be obtained by prescribing a phenomenological equation for $\langle n|m\rangle$ into equation (3.9) in order to close the equation for m without solving equation (3.8). From numerical simulations we determine that

$$\langle n|m\rangle \approx \langle n\rangle \Big(1 - \frac{2\kappa m}{1-\mu/\sigma}\Big) \tag{3.12}$$

captures the general features of the conditional mean particle activity. As we show in the supplementary information, introducing this closure equation to (3.9), making the Fokker-Planck approximation, and neglecting terms of $O(\kappa^2)$ provides

$$M(m) \approx M_0 e^{-2\kappa m^2}, \tag{3.13}$$

representing a Gaussian distribution with variance $\sigma_m^2 = \frac{1}{4\kappa}$ – smaller than the former mean field theory by a factor of two and in agreement with the result posited in equation (3.6). M_0 is a normalization constant. As we will demonstrate, this closure equation approach shows good coorespondence with numerical solutions of equation (5.4), at least for the flow parameters in table 3.1.

3.3 Results

From the initial conditions, all simulations show a rapid attainment of steady-state stochastic dynamics of n and m which support a time-independent joint distribution $P(n, m)$. We show an elevation time-series in the bottom panel of figure 3.1. In order to describe the implications of coupling bedload transport to bed elevation changes, we present the numerical and analytical results for the probability distributions of bedload transport and bed elevations in section 3.3.1 and the statistical moments of these quantities in section 3.3.2. We isolate the effects of collective entrainment on bed elevation changes in section 3.3.3, and we present the resting times of sediment undergoing burial in section 3.3.4.

3.3.1 Probability distributions of bedload transport and bed elevations

We compute this joint distribution by counting occurrences of the states (n, m) in the simulated time series. From this joint distribution we compute marginal distributions $P(n)$ and $P(m)$ by summing over m and n respectively. A representative subset of these marginal distributions is displayed in figure 4.1 alongside the approximate results of equations (3.10) and (3.13). The mean field equation (3.10) for the particle activity n closely represents the numerical results, and while there are small differences between numerical and analytical results for the relative number m of resting particles, the numerical solutions approximately match equation (3.13), having Gaussian profiles consistent with our assumption of a symmetric scaling of erosion and deposition rates with bed elevation changes.

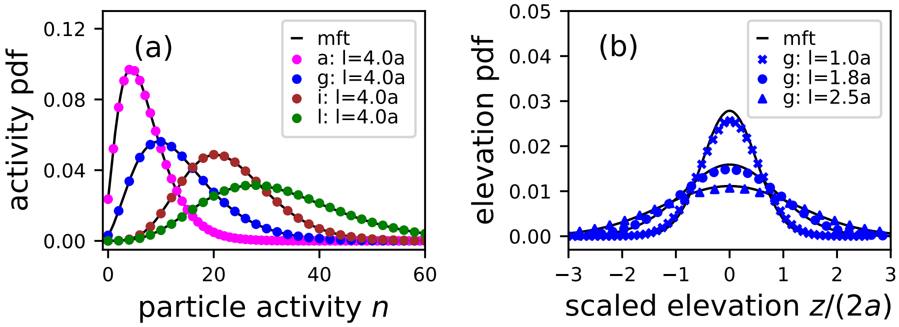

Figure 3.2: Panel (a) presents the probability distribution of particle activity n and panel (b) presents the probability distribution of the relative number of particles m for a representative subset of simulations. These distributions represent different flows from table 3.1, distinguished by color, and different values of the active layer depth l (equivalently the coupling constant κ), distinguished by the marker style. The mean field theories (mft) of equations (3.10) and (3.13) are displayed as solid black lines.

3.3.2 Statistical moments of bed elevation and the particle activity

We calculate the moments of n and m by summing over $P(n,m)$. The jth order unconditional moment of the particle activity n derives from

$$\langle n^j \rangle = \sum_n n^j P(n), \tag{3.14}$$

while the jth order moment of n held conditional on m is

$$\langle n^j | m \rangle = \sum_n n^j P(n,m). \tag{3.15}$$

We observe no dependence of the moments of m on the value of n. The mean elevation is always $\langle m \rangle = 0$ due to our initial assumption of

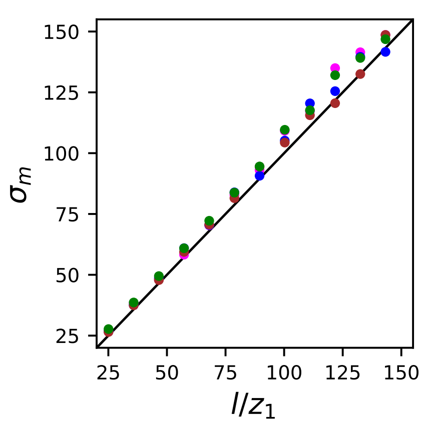

symmetry in the entrainment and deposition rate scaling with m. Figure 4.2 demonstrates that the variance of bed elevations is approximately $\sigma_z^2 = z_1^2 \sigma_m^2 = \frac{1}{4\kappa} = l^2$, agreeing with the approximation in equation (3.13); this result supports our earlier assertion that l is a characteristic length scale of bed elevation fluctuations. The close correspondence between the mean field approximation and the numerical simulations in figure (4.1a) suggests the unconditional moments of n correspond closely with the *Ancey et al.* (2008) result. We find them to be identical within numerical uncertainty.

The coupling between bed elevation changes and the erosion and deposition rates develop a strong dependence of the particle activity on m. Figure (3.4) displays the mean shift $[\langle n|m\rangle - \langle n\rangle]/\langle n\rangle$ and the variance shift $[\mathrm{var}(n|m) - \mathrm{var}(n)]/\mathrm{var}(n)$ of the particle activity due to departures of the bed elevation from its mean position. Figure (3.4a) demonstrates that the *Ancey et al.* (2008) flow conditions support departures of the mean particle activity by as much as 60% from the overall mean value when the bed is in a degraded state $z \approx -3l$, and the activity can be decreased by 20% when the bed is in an aggraded state. The closure model (3.12) used to derive the approximate bed elevation distribution (3.13) is plotted behind the conditional mean profiles in figure (3.4a), where it appears to be crude approximation, as it does not capture the asymmetry in this quantity. Nevertheless, figure 4.2 demonstrates the variance $1/(4\kappa)$ derived from this closure equation is representative of the numerical relationship. For the parameters of the *Ancey et al.* (2008) experiments, figure (3.4b) displays a variance shift with bed elevation changes that is less severe than the mean shift but is nevertheless appreciable, with bed elevations changing the magnitude of bedload activity

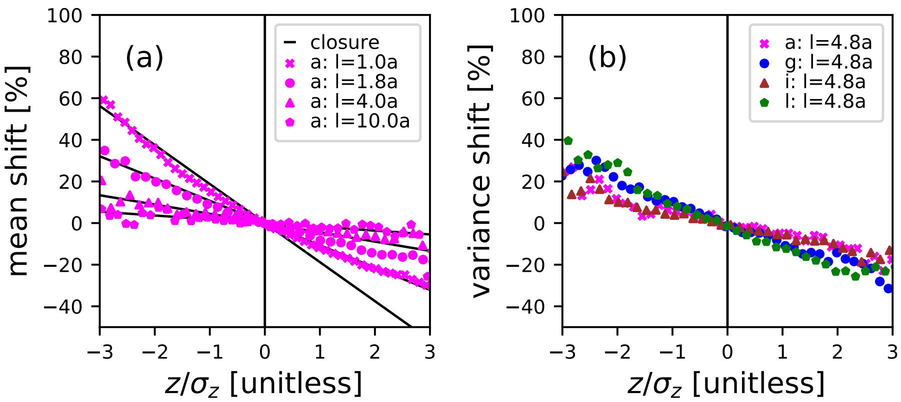

Figure 3.4: The shifts between particle activity moments conditioned on instantaneous elevations and their over-all mean values. Panel (a) indicates the mean particle activity shift versus the bed elevation measured in units of $\sigma_z = l$. This shift displays asymmetric dependence on m at the flow conditions of the *Ancey et al.* (2008) experiements, and departures of the bedload transport mean can be as much as 60% when the bed is in a severely degraded state with $z \approx -3l$. The closure equation (3.12) is plotted in panel (a) Panel (b) demonstrates a more symmetrical variance shift with some dependence on flow conditions displaying shifts of up to 20% with bed elevations. These results indicate that bedload statistics measurements on short timesclaes could be severely biased by departures from the mean bed elevation.

fluctuations by as much as 20%. We summarize that bed elevation changes regulate the particle activity moments, with a moment suppression effect when the bed is aggraded, and a moment enhancement effect when the bed is degraded.

3.3.3 Collective entrainment and bedload activity fluctuations

Noting that bed elevations regulate the particle activity moments, we now study the influence of collective entrainment on this effect by modifying the relative proportion of the individual to collective contributions in the mean entrainment rate $E = \lambda + \sigma\langle n\rangle$. Using the equilibrium condition $E = D$, we determine the fraction of entrainment due to the collective process is $f = \mu\langle n\rangle/E = \mu/\sigma$. Using this fraction, we can hold E constant and modify the prevalence of the collective entrainment process by setting $\lambda = E(1-f)$ and $\mu = \sigma f$. As we interpolate f between zero and one, the particle activity component of the master equation 5.4 interpolates from a purely Poissonian model (*Ancey et al.*, 2006) to a negative binomial model (*Ancey et al.*, 2008), isolating the imprint of collective entrainment on particle activity statistics over a dynamic sedimentary bed. Figure 3.5 depicts the modification of the

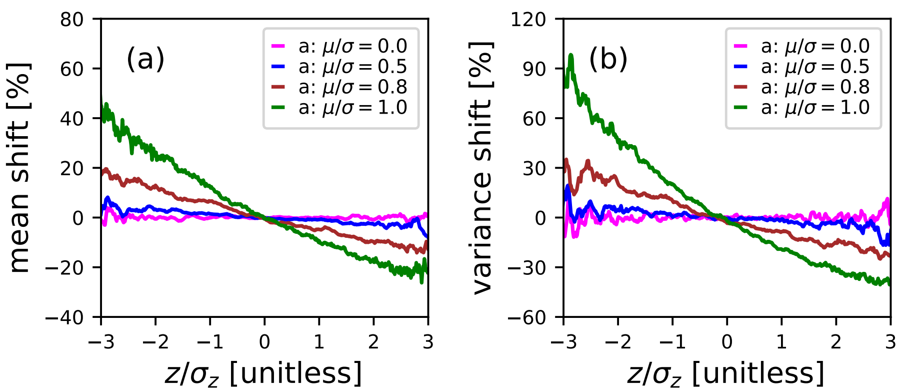

Figure 3.5: The shift of the mean particle activity in panel (a) and its fluctuations in panel (b) with departures of the bed elevation from its mean. All simulations are at flow condition (g) from table 3.1 except λ and μ are modified to shift the fraction $f = \mu/\sigma$ of the over-all entrainment rate E due to collective entrainment. Clearly, collective entrainment drives strong departures of the bedload statistics away from the mean field model (3.10) at large departures from the mean bed elevation. Panel (b) shows particle activity fluctuations suppressed by 90% when $z \approx -3l$ and collective entrainment is the dominant process. When collective entrainment is absent, meaning $\mu/\sigma = 0$, this moment regulation effect vanishes: it is a consequence of collective entrainment.

particle activity mean and variance as the importance of collective entrainment is tuned (through λ and μ) with all other parameters fixed. When $f = 0$, the bed elevation ceases to influence the particle activity mean or variance, while larger fractions increasingly enable the moment regulation effect we introduced in section 3.3.2.

3.3.4 Resting times of sediment undergoing burial

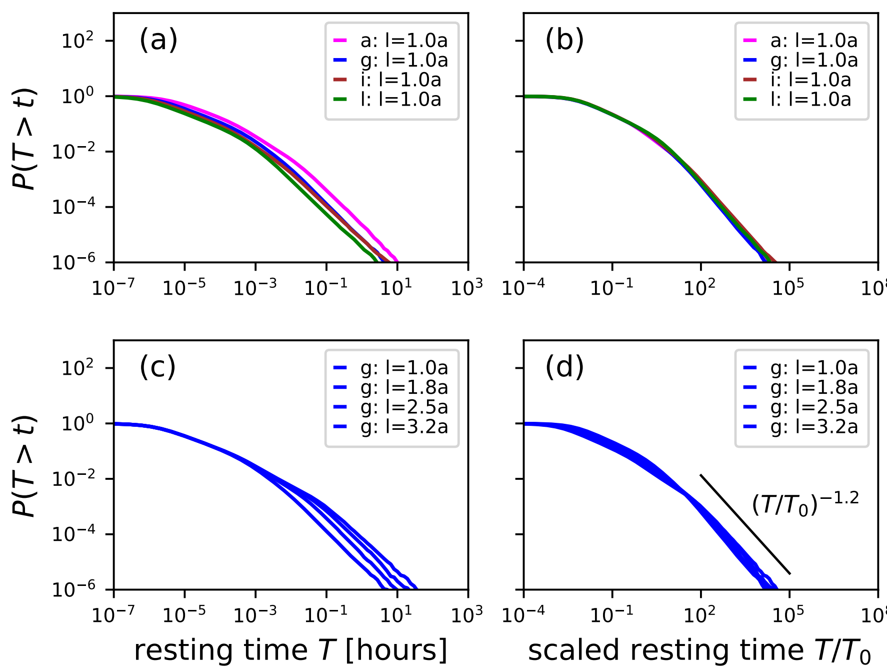

Figure 3.6: Resting time statistics scale differently with transport conditions and the bed elevation variance. Panel (a) shows differing flow conditions at a fixed l value, while panel (c) shows fixed flow conditions at differing l. When scaled by T_0 (3.17), both types of difference collapse in the tails of the distributions, as shown in panels (b) and (d). In panels (b) and (d), the black dotted lines indicate a power law decay of the collapsed tails having parameter $\alpha \approx 1.18$.

Resting times for sediment undergoing burial are obtained from analyzing the return times from above in the time-series of m (e.g., *Redner and Dorfman*, 2002). Following *Voepel et al.* (2013) and *Martin et al.* (2014), we concentrate on a particular bed elevation m', and find all time intervals separating deposition events at $m = m'$ from erosion events at $m = m'+1$. These are the return times from above of the sedimentary bed conditional to the elevation m'. Binning these conditional return times (using logarithmically-spaced bins to reduce computational load) and counting the occurrences in each bin, we obtain an exceedance distribution of return times t_r held conditional to the elevation m': $P(T > t_r|m')$. Using the marginal probability distribution of bed elevations $P(m)$ (figure 4.1(b)), we derive the unconditional exceedance distribution of resting times as a sum over all elevations (*Martin et al.*, 2014; *Voepel et al.*, 2013; *Yang and Sayre*, 1971; **?**):

$$P(T > t_r) = \sum_{m'} P(m')P(T > t_r|m'). \tag{3.16}$$

A representative subset of these results are displayed in figure 3.6. Comparing panels 3.6(a) and 3.6(c) shows two separate variations with input parameters: first, the distributions vary with the flow conditions, and second, they vary with the standard deviation of bed elevations (l). However, as shown in panels 3.6(b) and 3.6(d), a characteristic timescale T_0 is found to collapse away both variations. We obtained this T_0 heuristically by considering the characteristic speed of bed elevation change. This is the mean number of grains leaving the bed per unit time is E, and the removal of a single grain changes the bed elevation by z_1 (3.1). Therefore, bed elevations change with a characteristic speed $v = z_1E$. Since the range of elevation deviations is l (figure 4.2), the time required for the bed to shift through this characteristic distance is l/v, or equivalently

$$T_0 = \frac{l}{z_1E}. \tag{3.17}$$

When scaling the resting time by this T_0, we obtain the collapse shown in figure 3.6. Using the log-likelihood estimation technique described by

Newman (2005), we estimate the scaled resting time non-exceedance distributions decay as a heavy tailed power law with parameter $\alpha = 1.18 \pm 0.32$ for all return times satisfying $T/T_0 > 10^3$. These distributions are sufficiently heavy tailed to violate the central limit theorem and drive anomalous super-diffusion of bedload, a result which supports the earlier conclusions of *Voepel et al.* (2013) and *Martin et al.* (2014).

3.4 Discussion

3.4.1 Context of the research

Einstein developed the first stochastic models of bedload tracer diffusion (*Einstein*, 1937) and the bedload flux (*Einstein*, 1950), and his ideas can be viewed as the nexus of an entire paradigm of research that extends into the present day (e.g., *Ancey et al.*, 2008; *Hassan et al.*, 1991; *Hubbell and Sayre*, 1964; *Nakagawa and Tsujimoto 9 Kyoto*, 1977; *Wu et al.*, 2019a). These models aim to predict bedload transport characteristics from stochastic concepts of individual particle motions. With some exceptions (*Shi and Wang*, 2014; *Wu et al.*, 2019a,b; *Yang and Sayre*, 1971; **?**), existing descriptions are spatially one-dimensional, concentrating on the motion of grains in the downstream direction without including the vertical dimension wherein local bed elevation changes imply sediment burial (*Martin et al.*, 2014; *Voepel et al.*, 2013) and change the mobility of surface grains (*Yang and Sayre*, 1971; **?**).

3.4.2 New contributions

In this paper, we have built on earlier works (*Ancey et al.*, 2008; *Martin et al.*, 2014) to include the vertical dimension of bed elevation dynamics, study the interplay between bedload transport and bed elevation fluctuations, and investigate resting time distributions of sediment undergoing burial. To our knowledge, this model is the first description of bedload transport and bed elevations as a coupled stochastic population model based on individual grains. Numerical solutions and analytical approximations provided negative binomial distributions of bedload activity and normal distributions of bed elevations. Although experiments under more natural conditions with segregation processes, migrating bedforms, or sediment supply perturbations have shown particle activity distributions with heavier tails (*Dhont and Ancey*, 2018; **?**) and non-Gaussian bed elevations (*Aberle and Nikora*, 2006; *Singh et al.*, 2012), our results reproduce the key features of the most controlled bed elevation (*Martin et al.*, 2014; *Wong et al.*, 2007) and bedload transport (*Ancey et al.*, 2008; *Heyman et al.*, 2016) experiments in the literature.

Our inclusion of coupling between the bed elevation and entrainment and deposition rates revealed a novel dependence of particle activity on bed elevation changes, highlighting a new consequence of the collective entrainment process (*Ancey et al.*, 2008; *Lee and Jerolmack*, 2018). This coupling develops a significant variation of the particle activity moments with deviations of the bed from its mean elevation. We isolated the role of collective entrainment in this bedload activity regulation, and pointed out that particle activity variations with bed elevations dissapear in the absence of collective entrainment. Finally, we obtained resting times for sediment undergoing burial within the sedimentary bed by analyzing return times from above in the bed elevation time-series. We found heavy-tailed power law resting times with tail parameters sufficient to drive anomalous diffusion of bedload at long timescales. The distribution tails were found to collapse across flow conditions using a timescale formed from the mean erosion rate and the active layer depth.

As our model builds on earlier works describing particle activity and bed elevation changes independently, it also reduces to these works in simplified limits when the coupling between the particle activity and bed elevation vanishes. With the mean field approach in section 3.2.2, we derived the *Martin et al.* (2014) Ornstein-Uhlenbeck model for bed elevations and the *Ancey et al.* (2008) birth-death model for the particle activity as simplified limits of our coupled model. While the mean field description of bed elevations over-predicts the bed elevation variance by approximately a factor of two, it does capture the Gaussian shape of the bed elevation distribution, and its conclusions on the tail characteristics of resting time distributions for sediment undergoing burial are identical to ours within the numerical uncertainty: *Martin et al.* (2014) described a power-law distribution with tail parameter $\alpha \approx 1$ which falls neatly within our estimation $\alpha = 1.18 \pm 0.32$. In addition to our original contributions, we have corroborated the models of *Ancey et al.* (2008) and *Martin et al.* (2014) from an alternate perspective, showing their results to be mostly robust when accounting for bed elevation changes.

3.4.3 Next steps for research

The model we have presented computes statistical characteristics of the bedload particle activity and bed elevation within a control volume by assuming all particles on the bed surface have similar mobility characteristics while sediment transport and bed topography are in equilibrium. In actuality, particles span a range of sizes, and spatial organization occurs both in the forces imparted to particles by the flow (*Amir et al.*, 2014; *Shih et al.*, 2017) and in the mobility characteristics of particles on the bed surface (*Charru et al.*, 2004; *Hassan et al.*, 2007; *Nelson et al.*, 2014). Together, these factors may generate spatial correlations in particle activities that models concentrating on a single control volume will be unable to capture. Models chaining multiple control volumes together have shown spatial correlations in the particle activity as a result of collective entrainment (*Ancey et al.*, 2015; *Heyman et al.*, 2014), and similar approaches have also been applied to study correlations in turbulent flows (*Gardiner*, 1983). In light of this work, we consider the model we have presented as a preliminary step toward a multiple-cell model of particle activities and bed elevation changes with potential to express spatial correlations between longitudinal profile and particle activity statistics.

Like *Martin et al.* (2014), we obtained heavy-tailed power-law resting times for sediment undergoing burial by treating bed elevation changes as an unbounded random walk with a mean reverting tendency. This result suggests sediment burial can explain the heavy-tailed rests seen in field data

(*Bradley*, 2017; *Olinde and Johnson*, 2015; **?**). Our resting time distributions show a divergent variance and possibily a divergent mean, since this occurs for $\alpha < 1$ (**?**) which is within range of our results. Divergent mean resting time distributions present a paradox, since they imply all particles should eventually be immobile, violating the equilibrium transport assumption. *Voepel et al.* (2013) demonstrated that a bounded random walk for bed elevations provides a power-law distribution that eventually transitions to a faster thin-tailed decay, allowing for power-law scaling like our result and *Martin et al.* (2014) without this divergent mean paradox. One resolution to this issue could come from a spatially distributed model with multiple cells. Neighboring locations might bound excessive local elevation changes through granular relaxations from gradients above the angle of repose. In this interpretation, divergent mean power law resting time distributions may be relics of single cell models for bed elevation changes. We should always expect a maximum depth to which the bed can degrade relative to neighboring locations; this could temper the power law tail without required the reflecting boundaries used by *Voepel et al.* (2013).

Finally, we studied probability distribution functions and first and second moments of the particle activity and bed elevation, making novel conclusions about coordination between the statistical characteristics of these quantites which deserve experimental testing. In the last decade, particle tracking experiments have emerged (*Fathel et al.*, 2015; *Heyman et al.*, 2016; *Lajeunesse et al.*, 2010; *Liu et al.*, 2019; *Martin et al.*, 2014; *Roseberry et al.*, 2012), that allow joint resolution of bed elevations and bedload transport. A suitably designed experiment could test our prediction that bed elevations regulate particle activity statistics, as essentially represented in figures 3.4 and 3.5. However, we have left many other statistical characteristics of bedload transport for future studies. For example, the dependence of bedload transport (*Singh et al.*, 2009; **?**) and bed elevation statistics (*Aberle and Nikora*, 2006; *Singh et al.*, 2009, 2012) on the spatial and temporal scales over which they are observed is an emerging research topic. Statistical quantities can either be monoscaling or multiscaling across the observation scale (**?**), and we currently lack physical understanding and general conclusions about the scale dependence of particle activity and bed elevation signals. The model we have presented shows statistical monoscaling for both quantites (e.g. **?**), whereas other experiments indicate statistical multiscaling (*Aberle and Nikora*, 2006; *Singh et al.*, 2009, 2012). We consider this topic to go beyond the scope of the present work, and we have focused on statistical characteristics at the highest temporal resolutions, with no averaging over the observation scale.

3.5 Summary and conclusion

We developed a stochastic model for particle activity and local bed elevations including feedbacks between elevation changes and the erosion and deposition rates. This model includes collective entrainment, whereby moving particles tend to destabilize stationary ones. We analyzed this model using a mixture of numerical and analytical methods and provided two key results:

1. Resting times for sediment undergoing burial lie on a heavy-tailed power law distributions with tail parameter $\alpha \approx 1.2$;

2. Collective entrainment generates a statistical regulation effect, whereby bed elevation changes modify the mean and variance of the particle activity by as much as 90%: this effect vanishes when collective entrainment is absent.

These results imply measurements of bedload transport statistics could be severely biased at observation timescales smaller than adjustments of the bed elevation timeseries when collective entrainment occurs. Next steps are to generalize our model to a multi-cell framework and to study spatial correlations in bed elevation and particle activity statistics.

Chapter 4

Burial-induced three-range diffusion in sediment transport

Many environmental problems including channel morphology (*Hassan and Bradley*, 2017), contaminant transport (*Macklin et al.*, 2006), and aquatic habitat restoration (*Gaeuman et al.*, 2017) rely on our ability to predict the diffusion characteristics of coarse sediment tracers in river channels. Diffusion is quantified by the time dependence of the positional variance σ_x^2 of a group of tracers. With the scaling $\sigma_x^2 \propto t$, the diffusion is said to be normal, since this is found in the classic problems (*Philip*, 1968). However, with the scaling $\sigma_x^2 \propto t^\gamma$ with $\gamma \neq 1$, the diffusion is said to be anomalous (*Sokolov*, 2012), with $\gamma > 1$ defining super-diffusion and $\gamma < 1$ defining sub-diffusion (*Metzler and Klafter*, 2000). *Einstein* (1937) developed one of the earliest models of bedload diffusion to describe a series of flume experiments (**?**). Interpreting individual bedload trajectories as a sequence of random steps and rests, Einstein originally concluded that a group of bedload tracers undergoes normal diffusion.

More recently, Nikora et al. realized coarse sediment tracers can show either normal or anomalous diffusion depending on the length of time they have been tracked (*Nikora et al.*, 2001b, 2002). From numerical simulations and experimental data, Nikora et al. discerned "at least three" scaling ranges $\sigma_x^2 \propto t^\gamma$ as the observation time increased. They associated the first range with "local" timescales less than the interval between subsequent collisions of moving grains with the bed, the second with "intermediate" timescales less than the interval between successive resting periods of grains, and the third with "global" timescales composed of many intermediate timescales. Nikora et al. proposed super-diffusion in the local range, anomalous or normal diffusion in the intermediate range, and sub-diffusion in the global range. They attributed these ranges to "differences in the physical processes which govern the local, intermediate, and global trajectories" of grains (*Nikora et al.*, 2001b), and they called for a physically based model to explain the diffusion characteristics (*Nikora et al.*, 2002).

Experiments support the Nikora et al. conclusion of multiple scaling ranges (*Fathel et al.*, 2016; *Martin et al.*, 2012), but they do not provide consensus on the expected number of ranges or their scaling properties. This lack of consensus probably stems from resolution issues. For example, experiments have tracked only moving grains, resolving the local range (*Fathel et al.*, 2016; *Furbish et al.*, 2012a, 2017); grains resting on the bed surface between movements, resolving the intermediate range (*Einstein*, 1937; *Nakagawa and Tsujimoto 9 Kyoto*, 1977; *Yano*, 1969); grains either moving or resting on the bed surface, likely resolving local and intermediate ranges (*Martin et al.*, 2012); or grains resting on the surface after floods, likely resolving the global range (*Bradley*, 2017; *Phillips et al.*, 2013). At long timescales, a significant fraction of tracers bury under the bed surface (*Ferguson et al.*, 2002; *Haschenburger*, 2013; *Hassan et al.*, 1991, 2013; *Papangelakis and Hassan*, 2016), meaning burial dominates long term diffusion characteristics (*Bradley*, 2017; *Martin et al.*, 2014; *Voepel et al.*, 2013), possibly at global or even longer "geomorphic" timescales (*Hassan and Bradley*, 2017) than Nikora et al. originally considered. As a result, three diffusion ranges can be identified by patching together multiple datasets (*Nikora et al.*, 2002; *Zhang et al.*, 2012), but they are not resolved by any one dataset.

Newtonian bedload trajectory models also show multiple diffusion ranges, although they also do not provide consensus on the expected number of ranges or their scaling properties. The majority of these models predict two ranges of diffusion (local and intermediate) without predicting a global range. Among these, *Nikora et al.* (2001b) used synthetic turbulence (*Kraichnan*, 1970) with a discrete element method for the granular phase (**?**); *Bialik et al.* (2012) used synthetic turbulence with a random collision model (*Sekine and Kikkawa*, 1992); and *Fowler* (2016) used a Langevin equation with probabilistic rests. To our knowledge, only *Bialik et al.* (2015) have claimed to capture all three ranges from a Newtonian approach. They incorporated a second resting mechanism into their earlier model (*Bialik et al.*, 2012), implicitly suggesting that three diffusion ranges could result from two distinct timescales of sediment rest. However, Newtonian approaches have not evaluated the effect of sediment burial on tracer diffusion, probably due to the long simulation timescales required.

Random walk bedload diffusion models constructed in the spirit of *Einstein* (1937) provide an alternative to the Newtonian approach and can include a second timescale of rest by incorporating sediment burial. Einstein originally modeled bedload trajectories as instantaneous steps interrupted by durations of rest lying on statistical distributions (*Hassan et al.*, 1991), but this generates only one range of normal diffusion (*Einstein*, 1937; *Hubbell and Sayre*, 1964; *Nakagawa and Tsujimoto 9 Kyoto*, 1977). Recently, researchers have generalized Einstein's model in a few different ways to describe multiple diffusion ranges. *Lisle et al.* (1998) and **?** promoted Einstein's instantaneous steps to motion intervals with random durations and a constant velocity, providing two diffusion ranges – local and intermediate. *Wu et al.* (2019a) retained Einstein's instantaneous steps but included the possibility that grains can become permanently buried as they rest on the bed, also providing two diffusion ranges – intermediate and global. These earlier works suggest the minimal required components to model three bedload diffusion ranges: (1) exchange between motion and rest intervals and (2) the sediment burial process.

In this study, we incorporate these two components into Einstein's original approach to describe three diffusion ranges with a physically based model, as called for by *Nikora et al.* (2002). Einstein was a giant in river geophysics and fostered an entire paradigm of research leveraging and generalizing his stochastic methods (*Gordon et al.*, 1972; *Hubbell and Sayre*, 1964; *Nakagawa and Tsujimoto 9 Kyoto*, 1977; *Paintal*, 1971; *Yang and Sayre*, 1971; *Yano*, 1969). Einstein's model can be viewed as a pioneering application of the continuous time random walk (CTRW) developed by *Montroll* (1964) in condensed matter physics to describe the diffusion of charge carriers in solids. To incorporate motion intervals and sediment burial, we utilize the multi-state CTRW developed by *Weiss* (1976, 1994) that extends the CTRW of *Montroll* (1964). Below, we develop and solve the model in section 5.2. Then, we discuss the predictions of our model, present its implications for local, intermediate, and global ranges of bedload diffusion, and suggest next steps for bedload diffusion research in sections 5.4 and 5.5.

4.1 Bedload trajectories as a multi-state random walk

4.1.1 Assumptions of the burial model

We construct a three-state random walk where the states are motion, surface rest, and burial, and we label these states as $i = 2$ (motion), $i = 1$ (rest), and $i = 0$ (burial). Our target is the probability distribution $p(x, t)$ to find a grain at position x and time t if we know it started with the initial distribution $p(x, 0) = \delta(x)$. We characterize times spent moving or resting on the surface by exponential distributions $\psi_2(t) = k_2 e^{-k_2 t}$ and $\psi_1(t) = k_1 e^{-k_1 t}$, since numerous experiments show thin-tailed distributions for these quantities (*Ancey et al.*, 2006; *Einstein*, 1937; *Fathel et al.*, 2015; *Martin et al.*, 2012; *Roseberry et al.*, 2012). We expect our conclusions will not be contingent on the specific distributions chosen, since all thin-tailed distributions provide similar diffusion characteristics in random walks (*Weeks and Swinney*, 1998; *Weiss*, 1994). We consider grains in motion to have characteristic velocity v (*Lisle et al.*, 1998; **?**), and we model burial as long lasting enough to be effectively permanent (*Wu et al.*, 2019a), with grains resting on the surface having a probability per unit time κ to become buried, meaning

$\Phi(t) = e^{-\kappa t}$ represents the probability that a grain is not buried after resting for a time t, while $1 - \Phi(t)$ represents the probability that it is buried. We specify the initial conditions with probabilities θ_1 and θ_2 to be in rest and motion at $t = 0$, and we require $\theta_1 + \theta_2 = 1$ for normalization.

4.1.2 Governing equations

Using these assumptions, we derive the governing equations for the set of probabilities $\omega_{ij}(x,t)$ that a transition occurs from state i to state j at position x and time t using the statistical physics approach to multi-state random walks (*Schmidt et al.*, 2007; *Weeks and Swinney*, 1998; *Weiss*, 1994). Denoting by $g_{ij}(x,t)$ the probability for a particle to displace by x in a time t within the state i before it transitions to the state j, the transition probabilities $\omega_{ij}(x,t)$ sum over all possible paths to the state i from previous locations and times:

$$\omega_{ij}(x,t) = \theta_i g_{ij}(x,t) + \sum_{k=0}^{2} \int_0^x dx' \int_0^t dt' \omega_{ki}(x',t') g_{ij}(x-x', t-t'). \quad (4.1)$$

Defining another set of probabilities $G_i(x,t)$ that a particle displaces by a distance x in a time t within the state i and possibly remains within the state, we perform a similar sums over paths for the probabilities to be in the state i at x, t:

$$p_i(x,t) = \theta_i G_i(x,t) + \sum_{k=0}^{2} \int_0^x dx' \int_0^t dt' \omega_{ki}(x',t') G_i(x-x', t-t'). \quad (4.2)$$

Finally, the overall probability to be at position x at time t is

$$p(x,t) = \sum_{k=0}^{2} p_k(x,t) \quad (4.3)$$

This joint density is completely determined from the solutions of equations (4.1-4.2). We only need to specify the distributions g_{ij} and G_i.

4.1.3 Joint probability distribution of particle position with burial

We construct these distributions from the assumptions described in section 4.1.1. Since particles resting on the bed surface bury in a time t with probability $\Phi(t)$, and resting times are distributed as $\psi_1(t)$, we obtain $g_{12}(x,t) = \delta(x)k_1e^{-k_1t}e^{-\kappa t}$ and $g_{10}(x,t) = \delta(x)k_1e^{-k_1t}(1-e^{-\kappa t})$. Since motions have velocity v for times distributed as $\psi_2(t)$, we have $g_{21}(x,t) = \delta(x-vt)k_2e^{-k_2t}$. Since burial is quasi-permanent, all other $g_{ij} = 0$. The G_i are constructed in the same way except using the cumulative probabilities $\int_t^\infty dt'\psi_i(t) = e^{-k_it}$, since these characterize motions and rests that are ongoing (*Weiss*, 1994). We obtain $G_1(x,t) = \delta(x)e^{-k_1t}$ and $G_2(x,t) = \delta(x-vt)e^{-k_2t}$.

To solve equations (4.1-4.2) with these g_{ij} and G_i, we take Laplace transforms in space and time ($x, t \to \eta, s$) using a method similar to *Weeks and Swinney* (1998) to unravel the convolution structure of these equations, eventually obtaining

$$\tilde{p}(\eta,s) = \frac{1}{s}\frac{(s+\kappa+k')s + \theta_1(s+\kappa)\eta v + \kappa k_2}{(s+\kappa+k_1)\eta v + (s+\kappa+k')s + \kappa k_2}, \tag{4.4}$$

where $k' = k_1 + k_2$. Inverting this result using known Laplace transforms (*Arfken*, 1985; *Prudnikov et al.*, 1988) obtains

$$\begin{aligned} p(x,t) = {} & \theta_1\Big[1 - \frac{k_1}{\kappa+k_1}\Big(1-e^{-(\kappa+k_1)t}\Big)\Big]\delta(x) \\ & + \frac{1}{v}e^{-\Omega\tau-\xi}\Big(\theta_1\Big[k_1\mathcal{I}_0\big(2\sqrt{\xi\tau}\big) + k_2\sqrt{\frac{\tau}{\xi}}\mathcal{I}_1\big(2\sqrt{\xi\tau}\big)\Big] \\ & + \theta_2\Big[k_1\delta(\tau) + k_2\mathcal{I}_0\big(2\sqrt{\xi\tau}\big) + k_1\sqrt{\frac{\xi}{\tau}}\mathcal{I}_1\big(2\sqrt{\xi\tau}\big)\Big]\Big) \\ & + \frac{1}{v}\frac{\kappa k_2}{\kappa+k_1}e^{-\kappa\xi/(\kappa+k_1)}\Big[(\theta_1/\Omega)\mathcal{Q}_2(\xi/\Omega,\Omega\tau) + \theta_2\mathcal{Q}_1(\xi/\Omega,\Omega\tau)\Big] \end{aligned} \tag{4.5}$$

for the joint distribution that a tracer is found at position x at time t. This result generalizes the earlier results of *Lisle et al.* (1998) and *Einstein* (1937) to include sediment burial. In this equation, we used the shorthand notations $\xi = k_2x/v$, $\tau = k_1(t - x/v)$, and $\Omega = (\kappa + k_1)/k_1$ (*Lisle et al.*, 1998). The $\mathcal{I}_\nu$ are modified Bessel functions of the first kind and the $\mathcal{Q}_\mu$ are generalized Marcum Q-functions defined by $\mathcal{Q}_\mu(x, y) = \int_0^y e^{-z-x}(z/x)^{(\mu-1)/2}\mathcal{I}_{\mu-1}(2\sqrt{xz})dz$ and originally devised for radar detection theory (*Marcum*, 1960; *Temme and Zwillinger*, 1997). The Marcum Q-functions derive from the burial process. Since we assumed resting grains could bury with an exponential probability while the resting probability follows a modified Bessel distribution (*Einstein*, 1937; *Lisle et al.*, 1998), burial develops the Q-function convolution structure.

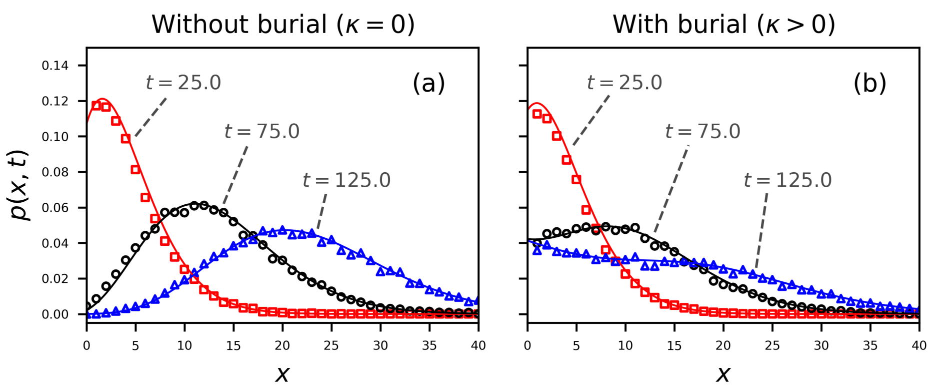

Figure 4.1: Joint distributions for a grain to be at position x at time t are displayed for the choice $k_1 = 0.1$, $k_2 = 1.0$, $v = 2.0$. Grains are considered initially at rest ($\theta_1 = 1$, $\theta_2 = 0$). The solid lines are the analytical distribution in equation (4.5), while the points are numerically simulated, showing the correctness of our derivations. Colors pertain to different times. Units are unspecified, since we aim to demonstrate the general characteristics of $p(x, t)$. Panel (a) shows the case $\kappa = 0$ – no burial. In this case, the joint distribution tends toward Gaussian at large times (*Einstein*, 1937; *Lisle et al.*, 1998). Panel (b) shows the case when grains have rate $\kappa = 0.01$ to become buried while resting. Because of burial, the joint distribution tends toward a more uniform distribution than Gaussian.

Figure 4.1 depicts the distribution (4.5) alongside simulations generated by a direct method based on evaluating the cumulative transition probabilities between states on a small timestep (*Barik et al.*, 2006). When grains do not become buried, as in panel (a) of figure 4.1, the distribution becomes Gaussian-like at relatively large observation times, exemplifying normal diffusion and satisfying the central limit theorem. When grains become buried, as in panel (b) of figure 4.1, the Q-function terms prevent the distribution from approaching a Gaussian at large timescales, exemplifying anomalous diffusion (*Weeks and Swinney*, 1998) and violating the central limit theorem (*Metzler and Klafter*, 2000; *Schumer et al.*, 2009).

4.1.4 Downstream diffusion

To obtain an analytical formula for tracers diffusing downstream while they gradually become buried, we derive the first two moments of position by taking derivatives with respect to η of the Laplace space distribution (B.13) using an approach similar to *Shlesinger* (1974) and *Weeks and Swinney* (1998), and we use these to calculate the positional variance $\sigma_x^2 = \langle x^2 \rangle - \langle x \rangle^2$. The first two moments are

$$\langle x(t) \rangle = A_1 e^{(b-a)t} + B_1 e^{-(a+b)t} + C_1, \tag{4.6}$$

$$\langle x^2(t) \rangle = A_2(t) e^{(b-a)t} + B_2(t) e^{-(a+b)t} + C_2, \tag{4.7}$$

so the variance is

$$\sigma_x^2(t) = A(t) e^{(b-a)t} + B(t) e^{-(a+b)t} + C(t). \tag{4.8}$$

In these equations, $a = (\kappa + k_1 + k_2)/2$ and $b = \sqrt{a^2 - \kappa k_2}$ are effective rates having dimensions of inverse time, while the A, B, and C factors are provided in table 4.1.

The positional variance (4.8) is plotted in figure 4.2 for conditions $\theta_1 = 1$ and $k_2 \gg k_1 \gg \kappa$. We interpret "$\gg$" to mean "of at least an order of magnitude greater". These conditions are most relevant to tracers in gravel-bed rivers, since they represent that grains are initially at rest (*Hassan et al.*, 1991; *Wu et al.*, 2019a), motions are typically much shorter than rests (*Einstein*, 1937; *Hubbell and Sayre*, 1964), and burial requires a much

Table 4.1: Abbreviations used in the expressions of the mean (4.6), second moment (4.7) and variance (4.8) of bedload tracers.

$$A_1 = \frac{v}{2b}\big[\theta_2 + \frac{k_1+\theta_2\kappa}{b-a}\big]$$
$$B_1 = -\frac{v}{2b}\big[\theta_2 - \frac{k_1+\theta_2\kappa}{a+b}\big]$$
$$C_1 = -\frac{v}{2b}\big[\frac{k_1+\theta_2\kappa}{b-a} + \frac{k_1+\theta_2\kappa}{a+b}\big]$$
$$A_2(t) = \frac{v^2}{2b^3}\Big[(bt-1)[k_1+\theta_2(2\kappa+k_1+b-a)] + \theta_2 b + \frac{(\kappa+k_1)(\theta_2\kappa+k_1)}{(b-a)^2}[(bt-1)(b-a)-b]\Big]$$
$$B_2(t) = \frac{v^2}{2b^3}\Big[(bt+1)[k_1+\theta_2(2\kappa+k_1-a-b)] + \theta_2 b - \frac{(\kappa+k_1)(\theta_2\kappa+k_1)}{(a+b)^2}[(bt+1)(a+b)+b]\Big]$$
$$C_2 = \frac{v^2}{2b^3}(\kappa+k_1)(\theta_2\kappa+k_1)\Big[\frac{2b-a}{(b-a)^2} + \frac{a+2b}{(a+b)^2}\Big]$$
$$A(t) = A_2(t) - 2A_1C_1 - A_1^2\exp[(b-a)t]$$
$$B(t) = B_2(t) - 2B_1C_1 - B_1^2\exp[-(a+b)t]$$
$$C(t) = C_2 - C_1^2 - 2A_1B_1\exp[-2at]$$

longer time than typical rests (*Ferguson and Hoey*, 2002; *Haschenburger*, 2013; *Hassan and Church*, 1994). Figure 4.2 demonstrates that under these conditions the variance (4.8) shows three diffusion ranges with approximate power law scaling ($\sigma_x^2 \propto t^\gamma$) that we identify as the local, intermediate, and global ranges proposed by Nikora et al., followed by a fourth range of no diffusion ($\sigma_x^2 = \text{const}$) stemming from the burial of all tracers. We suggest to call the fourth range geomorphic, since any further transport in this range can occur only if scour re-exposes buried grains to the flow (*Martin et al.*, 2014; *Voepel et al.*, 2013; *Wu et al.*, 2019b; **?**).

4.1.5 Diffusion exponents and three range scaling

Two limiting cases of equation (4.8) provide the scaling exponents γ of the diffusion $\sigma_x^2 \propto t^\gamma$ in each range. Limit (1) represents times so short a negligible amount of sediment burial has occurred, $t \ll 1/\kappa$, while limit (2) represents times so long motion intervals appear as instantaneous steps of mean length $l = v/k_2$, $1/k_2 \to 0$ while $v/k_2 = \text{constant}$. Limit (1) provides local exponent $2 \leq \gamma \leq 3$ depending on the initial conditions θ_i, and

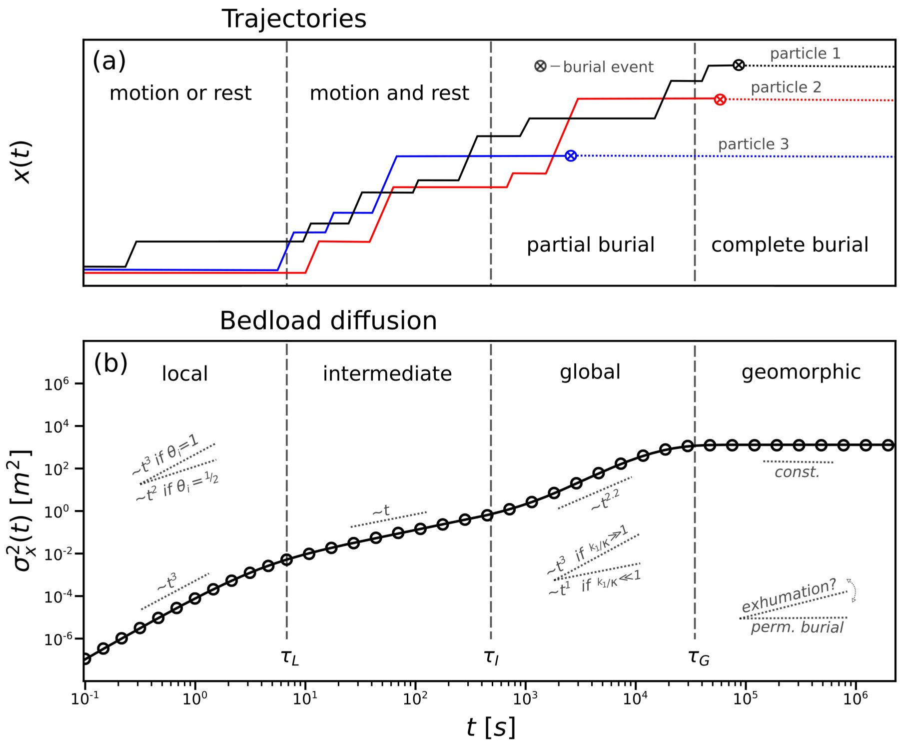

Figure 4.2: Panel (a) sketches conceptual trajectories of three grains, while panel (b) depicts the variance (4.8) with mean motion time 1.5 s, resting time 30.0 s, and movement velocity 0.1 m/s – values comparable to laboratory experiments transporting small (5 mm) gravels (*Lajeunesse et al.*, 2010; *Martin et al.*, 2012). The burial timescale is 7200.0s (two hours), and grains start from rest ($\theta_1 = 1$). The solid line is equation (4.8), and the points are numerically simulated. Panel (b) demonstrates four distinct scaling ranges of σ_x^2: local, intermediate, global, and geomorphic. The first three are diffusive. Three crossover times τ_L, τ_I, and τ_G divide the ranges. Within each range, a slope key demonstrates the scaling $\sigma_x^2 \propto t^\gamma$. Panel (a) demonstrates that different mixtures of motion, rest, and burial states generate the ranges. At local timescales, grains usually either rest or move; at intermediate timescales, they transition between rest and motion; at global timescales, they transition between rest, motion, and burial; and at geomorphic timescales, all grains bury. Additional slope keys in the local and global ranges of panel (b) illustrate the effect of initial conditions and rest/burial timescales on the diffusion, while the additional slope key within the geomorphic range demonstrates the expected scaling when burial is not permanent, as we discuss in section 5.4.

intermediate exponent $\gamma = 1$. If grains start in motion or rest exclusively, meaning one $\theta_i = 0$, the local exponent is $\gamma = 3$, while if grains start in a mixture of motion and rest states, meaning neither θ_i is zero, the local exponent is $\gamma = 2$. Limit (2) provides global exponent $1 \leq \gamma \leq 3$ depending on the relative importance of κ and k_1. In the extreme $k_1/\kappa \ll 1$, we find $\gamma = 1$ in the global range, while in the opposite extreme $k_1/\kappa \to \infty$ we find $\gamma = 3$. We summarize when $k_2 \gg k_1 \gg \kappa$ so all three diffusion ranges exist, equation (4.8) implies:

1. local range super-diffusion with $2 < \gamma < 3$ depending on whether grains start from purely motion or rest ($\gamma = 3$) or from a mixture of both states ($\gamma = 2$),

2. intermediate range normal diffusion $\gamma = 1$ independent of model parameters, and

3. global range super-diffusion $1 < \gamma < 3$ depending on whether burial happens relatively slowly ($\gamma \to 1$) or quickly ($\gamma \to 3$) compared to surface resting times.

Finally, the burial of all tracers generates a geomorphic range of no diffusion.

4.2 Discussion

4.2.1 Local and intermediate ranges with comparison to earlier work

We extended *Einstein* (1937) by including motion and burial processes in a multi-state random walk (*Weeks and Swinney*, 1998; *Weiss*, 1994) to demonstrate that a group of bedload tracers moving downstream while gradually becoming buried will generate a super-diffusive local range (*Fathel et al.*, 2016; *Martin et al.*, 2012; *Witz et al.*, 2019), a normal-diffusive intermediate range (*Nakagawa and Tsujimoto 9 Kyoto*, 1977; *Yano*, 1969), and a super-diffusive global range (*Bradley*, 2017; *Bradley et al.*, 2010), before the diffusion eventually terminates in a geomorphic range (*Hassan and Bradley*, 2017). *Nikora et al.* (2002) highlighted the need for such a physical description, although they suggested to use a two-state random walk between motion and rest states with heavy-tailed resting times, and they did not discuss sediment burial. However, other works have demonstrated that a two-state walk with heavy-tailed rests provides two diffusion ranges – not three (*Fowler*, 2016; *Weeks et al.*, 1996), and although heavy-tailed resting times have been documented for surface particles (*Fraccarollo and Hassan*, 2019; *Liu et al.*, 2019), they are more often associated with buried particles (*Martin et al.*, 2012, 2014; *Olinde and Johnson*, 2015; *Shi and Wang*, 2014; *Voepel et al.*, 2013; **?**), while surface particles retain light-tailed resting times (*Ancey et al.*, 2006; *Einstein*, 1937; *Nakagawa and Tsujimoto 9 Kyoto*, 1977; *Yano*, 1969). Accordingly, we developed a random walk model of bedload trajectories with light-tailed surface resting times that incorporates sediment burial.

The local and intermediate range diffusion characteristics resulting from our model correspond closely to the original Nikora et al. concepts, while our global range has a different origin than Nikora et al. envisioned. *Nikora et al.* (2001b) explained that local diffusion results from the non-fractal (smooth) characteristics of bedload trajectories between subsequent interactions with the bed, while intermediate diffusion results from the fractal (rough) characteristics of bedload trajectories after many interactions with the bed. Our model represents these conclusions: non-fractal (and super-diffusive) bedload trajectories exist on timescales short enough that each grain is either resting or moving, while fractal (and normal-diffusive) bedload trajectories exist on timescales when grains are actively switching between motion and rest states. We conclude that local and intermediate ranges stem from the interplay between motion and rest timescales, as demonstrated by earlier two-state random walk models (*Lajeunesse et al.*, 2018; *Lisle et al.*, 1998) and by all Newtonian models that develop sequences of motions and rests (*Bialik et al.*, 2012; *Nikora et al.*, 2001b), even those including heavy-tailed rests (*Fowler*, 2016).

4.2.2 Global and geomorphic ranges with next steps for research

Nikora et al. explained that divergent resting times generate a sub-diffusive global range. However, studies have demonstrated that divergent resting times can generate super-diffusion in asymmetric random walks (*Weeks and Swinney*, 1998; *Weeks et al.*, 1996), and both experiments (*Bradley*, 2017; *Bradley et al.*, 2010) and models (*Shi and Wang*, 2014; *Wu et al.*, 2019a,b) of bedload tracers undergoing burial have demonstrated global range super-diffusion. While our results also show global range super-diffusion, they do not necessarily refute the Nikora et al. conclusion of sub-diffusion at long timescales. We assumed sediment burial was a permanent condition which developed a non-diffusive geomorphic range. In actuality, burial is a temporary condition, because bed scour can exhume buried sediment back into transport (*Wu et al.*, 2019b), probably after heavy-tailed intervals (*Martin et al.*, 2014; *Voepel et al.*, 2013; **?**). We anticipate that a generalization of our model to include heavy-tailed timescales between burial and exhumation would develop four ranges of diffusion, where the long-time decay of the exhumation time distribution would dictate the geomorphic range diffusion characteristics as depicted in figure 4.2. If cumulative exhumation times decay faster than $T^{-1/2}$, as suggested by equilibrium transport models (*Martin et al.*, 2014; *Voepel et al.*, 2013; **?**) and laboratory experiments (*Martin et al.*, 2012, 2014), we expect a super-diffusive geomorphic range (*Weeks and Swinney*, 1998). However, if they decay slower than $T^{-1/2}$, as implicitly suggested by the data of *Olinde and Johnson* (2015), we expect a genuinely sub-diffusive geomorphic range (*Weeks and Swinney*, 1998), leaving Nikora et al. with the final word on long-time sub-diffusion.

The analytical solution of bedload diffusion in equation (4.8) reduces exactly to the analytical solutions of the *Lisle et al.* (1998) and *Lajeunesse et al.* (2018) models in the limit without burial ($\kappa \to 0$), the *Wu et al.* (2019a) model in the limit of instantaneous steps ($k_2 \to \infty$ and $l = v/k_2$), and the original *Einstein* (1937) model in the limit of instantaneous steps without burial. These reductions demonstrate that the majority of recent bedload diffusion models, whether developed from Exner-type equations (*Pelosi and*

Parker, 2014; *Shi and Wang*, 2014; *Wu et al.*, 2019a) or advection-diffusion equations (*Lajeunesse et al.*, 2018; *Lisle et al.*, 1998), can be viewed equivalently as continuous-time random walks applied to individual bedload trajectories. Within random walk theory, sophisticated descriptions of transport with variable velocities (*Masoliver and Weiss*, 1994; *Zaburdaev et al.*, 2008), correlated motions (*Escaff et al.*, 2018; *Vicsek and Zafeiris*, 2012), and anomalous diffusion (*Fa*, 2014; *Masoliver*, 2016; *Metzler et al.*, 2014) have been developed. Meanwhile, in bedload transport research, variable velocities (*Furbish et al.*, 2012a; *Heyman et al.*, 2016; *Lajeunesse et al.*, 2010), correlated motions (*Heyman et al.*, 2014; *Lee and Jerolmack*, 2018; *Saletti and Hassan*, 2020), and anomalous diffusion (*Bradley*, 2017; *Fathel et al.*, 2016; *Schumer et al.*, 2009) constitute open research issues. We believe further developing the linkage between existing bedload models and random walk concepts could rapidly progress our understanding.

4.3 Conclusion

We developed a random walk model to describe sediment tracers transporting through a river channel as they gradually become buried, providing a physical description of the local, intermediate, and global diffusion ranges identified by *Nikora et al.* (2002). Pushing their ideas somewhat further, we proposed a geomorphic range to describe diffusion characteristics at timescales larger than the global range when burial and exhumation both moderate downstream transport. At base level, our model demonstrates that (1) durations of sediment motions, (2) durations of sediment rest, and (3) the sediment burial process are sufficient to develop three diffusion ranges that terminate when all tracers become buried. A next step is to incorporate exhumation to better understand the geomorphic range. Ultimately, we emphasize that the multi-state random walk formalism used in this paper implicitly underlies most existing bedload diffusion models and provides a powerful tool for researchers targeting landscape-scale understanding from statistical concepts of the underlying grain-scale dynamics.

Chapter 5

Collisional Langevin model of the bedload sediment velocity distributions

5.1 Introduction

Bulk bed load transport rates show wide and frequent fluctuations which originate from coupling between the fluid and granular phases. Due to these fluctuations, measured transport rates often show slow convergence through time, and predicted rates often deviate from measured values by several orders of magnitude (*Ancey*, 2020). These challenges limit numerous ecological and engineering applications that rely on sediment transport predictions (). In recent decades, stochastic formulations of the bed load flux have become increasingly popular for their potential to predict the mean transport rates required by applications while also predicting fluctuations (*Ancey et al.*, 2008), quantifying the dependence of measurements on the observation scale (*Turowski*, 2010), and linking bulk transport characteristics to the "microstructural" dynamics of individual grains (*Ancey and Heyman*, 2014). Recent indications that sediment transport fluctuations might explain longstanding and unsolved problems in alluvial channel stability, such as channel width maintenance (*Abramian et al.*, 2019) and bedform initiation (*Bohorquez and Ancey*, 2016; *Jerolmack and Mohrig*, 2005) provide additional motivation to develop these stochastic approaches. One subset of stochastic methods expresses downstream transport rates as a sum over the instantaneous streamwise velocities of all particles in motion within a control volume (*Ancey et al.*, 2008; *Furbish et al.*, 2012a). These approaches rely on the instantaneous velocity distribution of sediment particles (*Lajeunesse et al.*, 2010), but our understanding of these distributions unfortunately remains limited. We have as of yet no consensus on the shape of the bedload velocity distribution (is it Exponential, Gaussian, Gamma, or some other shape?), and although models have described some extreme endmember distributions (e.g. *Ancey and Heyman*, 2014; *Fan et al.*, 2014), we have as of yet no mechanistic models that describe the full range of experimental observations (*Fathel et al.*, 2015; *Heyman et al.*, 2016; *Houssais and Lajeunesse*, 2012; *Lajeunesse et al.*, 2010; *Liu et al.*, 2019). In this chapter, I develop a stochastic model of particle velocities which addresses this shortcoming.

Particle trajectories are a compromise between turbulent drag and particle-bed collision (*Wiberg and Smith*, 1985). We therefore anticipate that the Stokes number, which is known to characterize colliding bodies within a viscous fluid (), is an important dimensionless parameter of the bedload velocity distribution. The Stokes number is defined as ... where ....

High-speed video experiments have measured different streamwise particle velocity distributions without providing much understanding as to why one distribution or another appears in a given set of hydraulic and sedimentary conditions.One set of studies has shown exponential particle velocity distributions (*Charru et al.*, 2004; *Fathel et al.*, 2016, 2015; *Lajeunesse et al.*, 2010; *Roseberry et al.*, 2012; *Seizilles et al.*, 2014). These experiments involve uniformly-sized small sands or glass beads ($0.05-2$mm) having typical Stokes numbers $St \sim 1-10$. Their flow conditions are generally sub-critical ($Fr < 1$) and turbulent ($Re > 5000$) but not always: flows in *Lajeunesse et al.* (2010) were super-critical ($Fr > 1$), and flows in *Charru et al.* (2004) and **?** were viscous. A second set of studies have shown Gaussian particle velocity distributions (*Ancey and Heyman*, 2014; *Heyman et al.*, 2016;

Martin et al., 2012). In these experiments, particles are typically larger ($2-8$mm) uniformly-sized gravels or glass beads having higher Stokes numbers ($St \sim 10-500$). In all Gaussian cases, flows are turbulent ($Re > 5000$) and super-critical ($Fr > 1$). Two other experiments display velocity distributions that are intermediate between exponential and Gaussian and appear more like a Gamma distribution (*Houssais and Lajeunesse*, 2012; *Liu et al.*, 2019). The *Houssais and Lajeunesse* (2012) experiments involved a binomal distribution of glass beads with diameters 0.7mm and 2.2mm in turbulent and supercritical flow conditions. They resolved the velocity distributions for larger grains only. The *Liu et al.* (2019) experiments used uniformly-graded sand having median diameter 1.1mm. Flows were again turbulent and subcritical. From this experimental record, we can summarize that the shape of the velocity distribution does not consistentely relate to whether a flow is super or sub-critical (Fr), whether sediment grains are natural (sand, gravel) or synthetic (beads), or whether the flow is laminar or turbulent (Re). However, the typical Stokes numbers of particles do seem to increase monotonically from exponential velocity experiments (where $St \sim 1$), to intermediate (Gamma-like) experiments (where $St \sim 10$), and eventually to Gaussian experiments (where $St \sim 10^2$.) Apparently, the shape of streamwise bed load velocity distributions depends on the particle size.

Existing models of streamwise bed load velocities can be divided into computational and statistical physics categories. Computational models numerically integrate some approximate coupled dynamics for individual grains and the fluid, generally modelling particles as spheres interacting through repulsive forces, and the flow using direct simulation of the Navier-Stokes equations or some related approximation (such as large eddy simulation or the St-Venant equations). When streamwise particle velocities have been analyzed in such simulations, they show exponential tails (*Furbish and Schmeeckle*, 2013; *González et al.*, 2017) that agree with only a subset of the experimental data. Statistical physics models have incorporated stochastic driving and resisting terms into the Newtonian dynamics of individual grains to develop a Langevin-like description of bed load particle motions. For the downstream velocity $u(t)$, *Fan et al.* (2014) wrote

$\dot{u} = F - \gamma \mathrm{sgn} u + \xi(t)$ where F represents the steady component of the fluid forcing, the term involving γ is a quasi-static (Coulomb-type) friction term representing momentum dissipation by particle-bed collisions, and $\xi(t)$ is a Gaussian white noise representing variability in these forces. This model provides exponential velocity distributions which agree with one subset of experiments. *Ancey and Heyman* (2014) took a similar approach that includes different forces, solving $\dot{u} = \gamma(\overline{u} - u) + \xi(t)$. Here the term involving γ is similar to a Stokes drag, except it involves the mean sediment velocity $\overline{u}$, not the fluid velocity as for a "real" Stokes drag. $\xi(t)$ is again a Gaussian white noise representing fluctuations, and the model provides Gaussian velocity distributions that agree with another subset of experiments. While these models build insight into grain-scale sediment transport mechanics and provide powerful techniques with which to approach the problem, they have not yet provided a comprehensive explanation for the range of streamwise velocity distributions resolved in experiments.

Here, motivated by the realization that experimental particle velocity distributions vary systematically with the grain size, as summarized above, we hypothesize that the shape of the streamwise velocity distribution is controlled by the momentum dissipation characteristics of particle-bed collisions. It is well-known that the elasticity of granular collisions within viscous fluids depends on the particle size. In addition, the velocity distributions of granular gases are known to develop increasingly heavier tails than the Gaussian (Boltzmann) form of elastic gases as the inelasticity of particle-particle collisions is increased. Taking inspiration from this established knowledge, we develop below a model for sediment grains in transport as they undergo inelastic particle-bed collisions. Our intentions are to test the hypothesis that particle-bed collision characteristics explain the range of experimentally-observed streamwise bed load particle velocity distributions, and to introduce more realistic forces into earlier statistical physics descriptions of individual bed load particle dynamics. We develop the model and explain our assumptions in section 5.2, then we present the analytical solution and major results in 5.3. We finally discuss the implications of these results, summarize our findings, and suggest ideas for further research in sections 5.4 and 5.5.

5.2 Mechanistic description of particle velocities

Figure **??** indicates the configuration we have in mind. Nearly spherical and cohesionless particles of diameter d and mass m moving as bed load down a slope inclined at an angle θ in a steady turbulent shear flow. The flow is just strong enough to drive grains into rarefied transport of a kind typical in gravel-bed rivers: particles saltate along the bed in sequences of collisions between events of erosion and deposition; moving particles collide often with stationary particles, but rarely with other moving particles. Particles respond to turbulent drag forces $F_D(t)$ and episodic particle-bed collision forces. In contrast to the computational physics approach, we do not aim to characterize the exact timeseries of the forces on an individual particle. Instead, we model the ensemble of possible force timeseries that particles could conceivably experience. Each possibility implies a different velocity timeseries $u(t)$ in the downstream direction. Our objective is to calculate the probability distribution $P(u)$ of this downstream velocity by averaging over the ensemble of forces. We include the most realistic article-bed collision and fluid forces we can while still allowing for analytical solutions.

Collision forces dissipate streamwise momentum, partly by converting it to vertical, lateral, or rotational momentum, and partly by deforming particles and generating heat (**?**). The microscopic details of particle-particle collisions have been thoroughly studied (*Brach*, 1989; *Lorenz et al.*, 1997; *Montaine et al.*, 2011). Here, we introduce a restitution-like coefficient ε as indicated in figure **??**. This ranges from $\varepsilon = 0$ for completely inelastic collisions to $\varepsilon = 1$ for completely elastic collisions. If the streamwise velocity just prior to a collision is u, just after the collision it becomes εu. Since this quantity combines effects of particle shape and collision geometry and should vary from one collision to the next, we consider that the fraction of streamwise momentum dissipated per collision ε lies on a statistical distribution $\rho(\varepsilon)$. Similar ideas are available in the granular physics literature

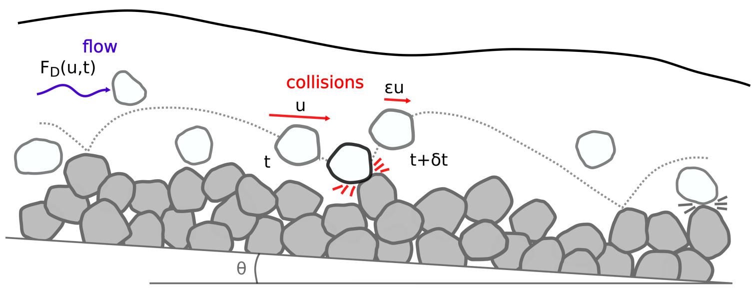

Figure 5.1: Definition sketch of rarefied sediment transport with turbulent fluid drag and particle-bed collision forces. During saltation, pre-collisional streamwise velocities u are transformed to postcollisional velocities $\varepsilon u < u$.

(**?**). Further assuming that the number of collisions per unit time is ν and that the time intervals between subsequent particle-bed collisions are exponentially distributed (*Gordon et al.*, 1972), we write the collision force in the downstream direction as

$$F_C(u,t) = -mu \sum_{k=1}^{N_\nu(t)} (1-\varepsilon_k)\delta(t-\tau_k). \tag{5.1}$$

Here, $N_\nu(t)$ is the number of collisions in time t, the τ_k $(k = 1, 2, \dots)$ are times at which collisions occur, and the ε_k are elasticity coefficients characterizing the amount by which each collision slows the particle down. This collision force is a sequence of random impulses which are proportional to the pre-collisional streamwise momentum. This collision model should be adequate when the contact times between moving and resting particles are small compared to the times between collisions. These conditions are always satisfied for the idealized saltation-type motion depicted in figure **??**.

Fluid forces on a coarse particle in a viscous flow depend on the Reynolds number $\Re_p = dV/\nu$ defined by the particle size d, slip velocity V between particle and fluid, and kinematic viscosity ν. These forces have been calculated analytically from the Navier-Stokes equations for vanishing $\Re_p$ and include acceleration, history, and velocity-dependent drag terms (*Hjelmfelt and Mockros*, 1966; *Maxey and Riley*, 1983; **?**). At realistic $\Re_p$ analytical results are limited, so it is standard practice to turn instead to empirical corrections on the small $\Re_p$ formulas (*Schmeeckle et al.*, 2007; **?**). A dominant contribution to the downstream drag force F_D on nearly spherical particles at large $\Re_p$ can be written $F_D = \frac{\pi}{8}\rho_f d^2 C_D(\Re_p)|V|V$, where ρ_f is the fluid density, d is the particle diameter, $C_D(\Re_p)$ is an empirical drag coefficient, and $V = U - u$ is the slip velocity between the fluid (U) and particle (u) velocities (*Coleman*, 1967; *Dwivedi et al.*, 2012; *Schmeeckle et al.*, 2007). In the present model we set $C_D = \frac{24}{\Re_p}(1 + 0.194\Re_p^{0.631})$ (*Clift et al.*, 1978; *González et al.*, 2017) and we do not involve acceleration and history terms for simplicity, although we acknowledge their potential importance for coarse sediment transport (*Armenio and Fiorotto*, 2001; **?**; **?**).

Drag forces have been argued to fluctuate rapidly compared to the inertial response times of coarse sediment grains (*Fan et al.*, 2014). The magnitude of drag fluctuations has been observed to follow a Gaussian distribution (*Celik et al.*, 2014; *Dwivedi et al.*, 2010; *Hofland and Battjes*, 2006; *Schmeeckle et al.*, 2007). Using these ideas, we make two key simplifications of the drag force above. First, we split the drag F_D into quasi-steady and fluctuating components (*Michaelides*, 1997), and second, we represent drag fluctuations as a Gaussian white noise characterized by a particle diffusivity D (*Ancey and Heyman*, 2014; *Fan et al.*, 2014). Defining $\bar{V}$ as a representative slip velocity which we specify more carefully later, $\bar{C}_D$ as the empirical drag coefficient evaluated at this slip velocity, and $\xi(t)$ as a Gaussian white noise of mean 0 and variance 1 (*Gardiner*, 1983), we express the fluid forces as

$$F_D(t) = \frac{\pi}{8}\rho_f d^2 \bar{C}_D \bar{V}^2 + \sqrt{2D}\eta(t). \tag{5.2}$$

In this drag force **??** and the collision force 5.1, the turbulent fluctuations $\xi(t)$, collision times τ_k, and dissipation coefficients ε_k, can take any values consistent with their distribution and correlation functions. This set of possiblities defines a statistical ensemble.

5.2.1 Langevin equation for collisional transport

With the above forces, we express the Langevin equation $m\dot{u}(t) = F_D(t) + F_C(t)$ for the sediment dynamics as

$$m\dot{u}(t) = \Gamma + \sqrt{2D}\eta(t) - mu(t)\xi_{\nu,\varepsilon}(t). \tag{5.3}$$

This equation replaces the steady friction terms of earlier stocahstic bed load models with an episodic term which provides a more realistic representation of particle-bed collisions during saltation. It represents a jump-diffusion process (*Daly and Porporato*, 2006) with multiplicative Poisson noise (*Denisov et al.*, 2009; *Dubkov et al.*, 2016). Collisions introduce “jumps” in velocity while turbulent generates ”diffusion”. The collision term is ”multiplicative” in the sense that u multiplies the Poisson noise. Equations like 5.3 have long been studied in the stochastic physics literature (*Hanggi*, 1978; **?**), but solving such equations remains extremely challenging (*Daly and Porporato*, 2010; *Dubkov and Kharcheva*, 2019; *Luczka et al.*, 1995; *Mau et al.*, 2014). One issue is that multiplicative white noises imply the prescription dilemma of stochastic calculus (*Gardiner*, 1983; **?**), meaning 5.3 is not defined without further specifying an integration rule (**?**). Here, the Ito interpretation (lower endpoint integration rule) is the physical choice since the energy dissipated by collisions depends strictly on pre-collisional velocities, not post-collisional. Given this integration rule, the remaining issues are to obtain the integro-differential equation characterizing the ensemble of velocities defined by 5.3, and then to solve this equation for the velocity distribution $P(u)$.

5.2.2 Chapman-Komogorov equation and particle-bed collision integral

We derive the equation governing the streamwise velocity distribution $P(u,t)$ from a simple limiting argument in appendix B.1, finding

$$\nu^{-1}\partial_t P(u,t) = -\tilde{\Gamma}\partial_u P(u,t) + \tilde{D}\partial_u^2 P(u,t) + \mathcal{I}_c(u,t). \tag{5.4}$$

In this equation, we introduced the scaled parameters $\tilde{\Gamma} = \Gamma/(\nu m)$ and $\tilde{D} = D/(\nu m)$. The term

$$\mathcal{I}_c(u,t) = -P(u,t) + \int_0^1 \frac{d\varepsilon}{\varepsilon} P\big(\frac{u}{\varepsilon}, t\big)\rho(\varepsilon) \tag{5.5}$$

is a "collision integral" term representing particle-bed collisions. Equation 5.4 is a nonlocal extension of the Fokker-Planck equation used in earlier bed load models (*Ancey and Heyman*, 2014; *Fan et al.*, 2014). Such equations combining are known as Chapman-Komogorov equations (*Gardiner*, 1983). Nonlocality is introduced by the collision integral 5.5 which transfers probability from higher pre-collisional velocities u/ε to lower post-collisional velocities u. This term is analogous to the collision integral of the Boltzmann equation in kinetic theory and granular gases (**??**). Physically, it corresponds to binary collisions between particles having different masses and random resitution coefficients **?** in the limit that the mass of one particle (here, the particle resting on the bed) goes to infinity. Mathematically, it represents the probability distribution of the product between ε and u (c.f. *Feller*, 1967).

Owing to its nonlocality, equation 5.4 does not admit analytical solutions as is, so we make one further approximation. We assume the distribution of dissipation coefficients $\rho(\varepsilon)$ is sharply peaked at some most common (mode) value ε'. This allows for a Kramers-Moyal type expansion of the particle-bed collision integral (*Gardiner*, 1983). Expanding all terms in the integrand except $\rho(\varepsilon)$ provides

$$\mathcal{I}_c(u,t) = -P(u,t) + \frac{1}{\varepsilon'}P\big(\frac{u}{\varepsilon'}, t\big) + \sum_{k=1}^{\infty} \frac{\alpha_k}{k!}(\varepsilon - \varepsilon')^k \Big[\frac{1}{\varepsilon}P\big(\frac{u}{\varepsilon}\big)\Big]^{(k)}\Big|_{\varepsilon=\varepsilon'}, \tag{5.6}$$

where the $\alpha_k = \int_0^1 d\varepsilon \rho(\varepsilon)(\varepsilon - \varepsilon')^k$ are the central moments of ε around the mode elasticity ε' and the superscript (k) denotes the kth derivative. In what follows, we drop all but the first two terms to obtain the leading order contribution of particle-bed collisions to the velocity distribution. Higher orders could always be included later by perturbation theory. We solve the resulting approximate equation in steady-state, when $\partial P(u,t)/\partial t = 0$. Scaling the time in Equation 5.4, we can see this solution will be a good approximation to the time-dependent problem when particle motions generally survive multiple collisions.

5.3 Results

5.3.1 Derivation of the bedload velocity distribution

Hereafter we drop the prime on the most common streamwise restitution coefficient ε'. With the truncation to two terms, equation 5.4 gives

$$0 = -\tilde{\Gamma}\partial_u P(u) + \tilde{D}\partial_u^2 P(u) - P(u) + \frac{1}{\varepsilon}P\left(\frac{u}{\varepsilon}\right), \tag{5.7}$$

which is now a non-local ordinary differential equation. Such equations have seen some attention in the mathematics literature, where they are called pantograph equations (**???**) for their relationship to a current collection device used on electric trains (*Ockendon and Tayler*, 1971). In the appendix we solve equation 5.7 using Laplace transforms, providing

$$P(u) = \frac{\theta(-u)}{K_+}\sum_{l=0}^{\infty}\frac{\varepsilon^{-l}e^{\lambda_+\varepsilon^{-l}u}}{\prod_{m=1}^{l}(-\tilde{D}\lambda_+^2\varepsilon^{-2m} + \tilde{\Gamma}\lambda_+\varepsilon^{-m} + 1)} + \frac{\theta(u)}{K_-}\sum_{l=0}^{\infty}\frac{\varepsilon^{-l}e^{\lambda_-\varepsilon^{-l}u}}{\prod_{m=1}^{l}(-d\lambda_-^2\varepsilon^{-2m} + \gamma\lambda_-\varepsilon^{-m} + 1)}. \tag{5.8}$$

The factors $\lambda_\pm$ are defined in the appendix; they are proportional to $\tilde{\Gamma}/\tilde{D}$. The normalization factors are $K_\pm$ are

$$K_\pm = d(\lambda_+ - \lambda_-)\prod_{l=1}^{\infty}(-d\lambda_\pm^2\varepsilon^{2l} + \gamma\lambda_\pm\varepsilon^l + 1). \tag{5.9}$$

Although this velocity distribution appears quite complicated, one can verify that this is a normalized probability distribution which has very simple limiting behaviors as the most common dissipation coefficient ε approaches fully elastic ($\varepsilon = 1$) and inelastic ($\varepsilon = 0$) values.

It is rather simple to derive the moments of this probability distribution by multiplying 5.7 by u, integrating, and then solving the resulting moment evolution equations (c.f. **?**). The first moment is

$$\langle u \rangle = \frac{\Gamma}{\nu(1-\varepsilon)} = \frac{\gamma}{1-\varepsilon}, \tag{5.10}$$

which is scales weakly with the mean fluid drag and sharply with the rate and typical elasticity of collisions. The second moment is

$$\langle u^2 \rangle = 2\frac{d + \gamma\langle u \rangle}{1-\varepsilon^2}, \tag{5.11}$$

leading to the velocity variance ($\sigma_u^2 = \langle u^2 \rangle - \langle u \rangle^2$)

$$\sigma_u = \sqrt{\frac{2d+\gamma^2}{1-\varepsilon^2}}. \tag{5.12}$$

This equation demonstrates that velocity fluctuations originate from both the steady and fluctuating components of the flow forces, yet the variance is linear in these factors and is therefore relatively insensitive to them. In contrast, velocity fluctuations depend sharply on the parameters representing particle-bed collisions.

Figure 5.2 depicts velocity characteristics for different realizations of the fluid and collisional forces. We can see an apparent transition from exponential-like to Gaussian-like velocity distributions as typical collisions vary from more inelastic ($\varepsilon \to 0$) to more elastic ($\varepsilon \to 1$). In between, the full distribution 5.8 resembles a Gamma distribution, although it is not a Gamma distribution.

5.3.2 Exponential and Gaussian regimes: limits to earlier work

In fact, the apparent transition in figure 5.2 can be made rigorous: despite its complex appearance, simple Gaussian and exponential distributions appear as rigorous mathematical limits of equation 5.8. When particle-bed collisions

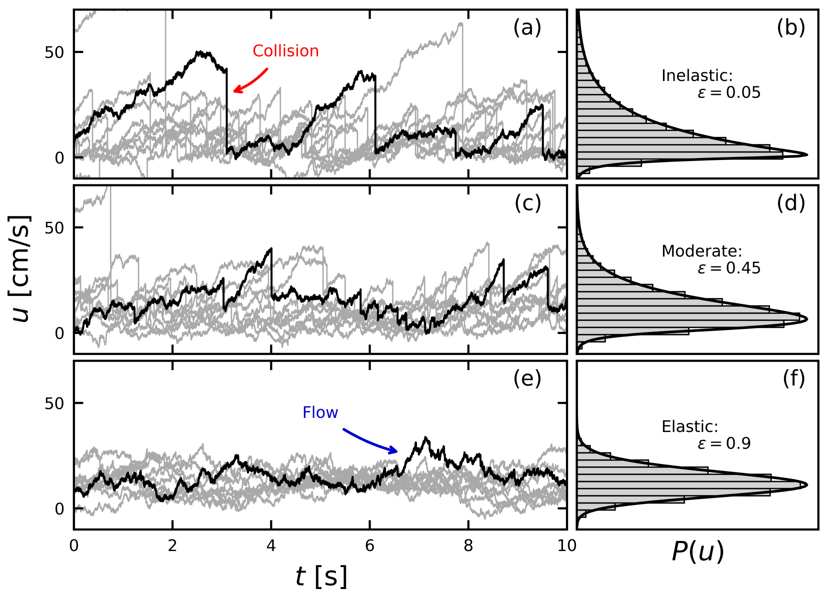

Figure 5.2: Left panels show velocity realizations as gray traces. Velocities are calculated from Monte Carlo simulations. Individual realizations are singled out as black traces. Particle-bed collisions imply sudden downward-velocity jumps. Flow forces generate fluctuating positive accelerations between collisions. Right panels show simulated histograms of particle velocities and exact solutions from equation 5.8.

are completely inelastic, 5.8 becomes an exponential distribution, and when they are completely elastic, 5.8 becomes Gaussian. Figure 5.3 demonstrates more closely the approach of the distribution toward these limits.

The exponential limit of 5.8 as $\varepsilon \to 0$ is rather easy to see. Taking $\varepsilon \to 0$ in 5.8, all terms in the series except for that with $l = 0$ become exponentially small, leaving behind the same two-sided exponential distribution derived by *Fan et al.* (2014) up to notational differences:

$$P(u) = \frac{d}{\sqrt{\gamma^2 + 4d}} e^{\frac{\gamma u}{2d} - \frac{\sqrt{\gamma^2+4d}|u|}{2d}}. \tag{5.13}$$

Thus, for bed load transport conditions with typically very inelastic particle-

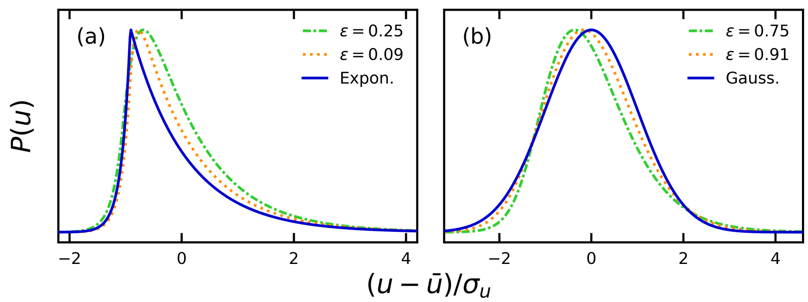

Figure 5.3: The particle velocity distribution approaches an exponential distribution in (a) as particle-bed collisions become extremely elastic ($\varepsilon \to 1$), and it approaches a Gaussian in (b) as they become extremely inelastic ($\varepsilon \to 0$). On the abscissa, the mean sediment velocity is standardized by its mean $\bar{u}$ and standard deviation σ_u.

bed collisions, we can expect exponential-like velocities and large deviations from a Gaussian behavior.

The Gaussian limit as $\varepsilon \to 1$ of 5.8 is more difficult to evaluate. The challenge is that the statistical moments 4.6 and **??** diverge at the same time as the denominator factors of the distribution 5.8. In appendix B.2 we return instead to the original equation 5.7 to evaluate this elastic limit, obtaining

$$P(u) = \frac{1}{\sqrt{2\pi\sigma_u^2}} e^{-\frac{(u-\bar{u})^2}{2\sigma_u^2}}. \tag{5.14}$$

This result is identical to the velocity distribution derived by *Ancey and Heyman* (2014), up to notation.

5.3.3 Comparison with experimental data

Now we compare the analytical distribution 5.8 with the available experimental data. Upfront, we point out that the distribution above has free parameters and this is only a proof of concept that the velocity distribution is capable of fitting the available experimental data; it is not a proof that this is the underlying mechanism for these data blahblahblah that was a

a/d	$M = 4$	$M = 8$	Callan
0.1	1.56905	1.56	1.56904
0.3	1.50484	1.504	1.50484
0.55	1.39128	1.391	1.39131
0.7	1.32281	10.322	1.32288
0.913	1.34479	100.351	1.35185

Table 5.1: Values of kd at which trapped modes occur when $\rho(\theta) = a$.

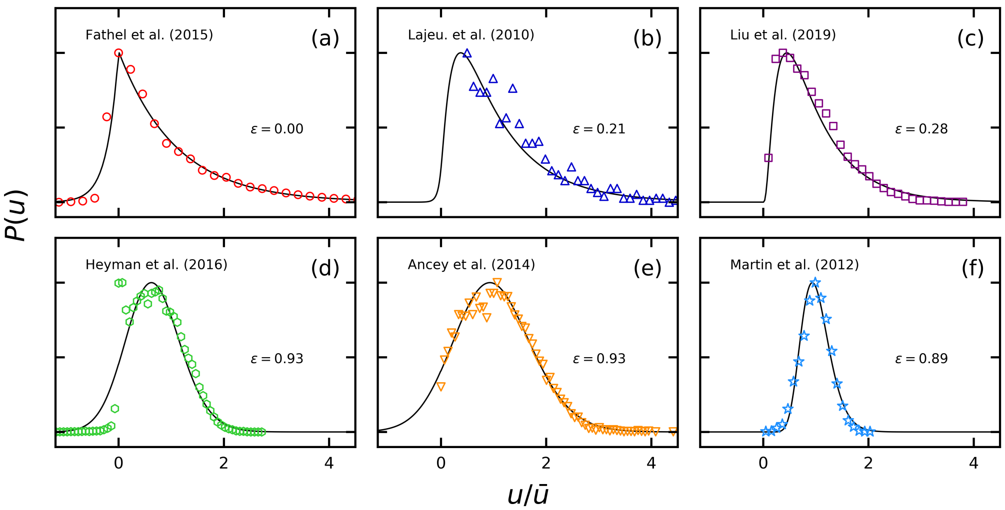

Figure 5.4: The features of the four possible modes corresponding to (a) periodic
and (b) half-periodic solutions.

good writing day.

5.4 Discussion

Here, I developed a Langevin description of bed load sediment transport which includes episodic collisions between particles and the bed. The model relates the shape of the instantaneous streamwise particle velocity distribution to the elasticity of particle-bed collisions, generalizes earlier approaches available in the literature which did not treat episodic collisions (*Ancey and*

Heyman, 2014; *Fan et al.*, 2014), and provides a new physical explanation for the different streamwise sediment velocity distributions resolved in experiments. Although in reality, the turbulent forces on moving sediment particles vary in a complex spatio-temporal way, we have approximated the fluid forces on bed load particles as spatially uniform Gaussian white noise. Even though the non-Gaussian aspects of fluid turbulence certainly do impact sediment entrainment (*Celik et al.*, 2014; **?**), this flow model appears more or less justified since sediment transport experiments provide similar velocity distributions regardless of whether the flow is viscous or turbulent (*Charru et al.*, 2004; *Lajeunesse et al.*, 2010), and since particle relaxation times are typically long compared to the timescales of turbulent fluctuations (*Hofland and Battjes*, 2006; *Schmeeckle et al.*, 2007; **?**). We modelled particle-bed collision forces as a sequence of instantaneous impulses where the intervals between successive collisions were characterized as exponential random variables. The effect of each collision on the streamwise particle velocities was parameterized by a restitution-like coefficient. Although such approximate descriptions of particle-particle collisions are common in the theory of granular gases, the setting here is somewhat different than grains in air. Because particles within a viscous flow in general interact at a distance, we should expect the collision model will become poor when the time between subsequent collisions becomes small. Therefore, although the model seems appropriate for saltation, it should be critically examined for "reptation", when the times between subsequent particle-bed collisions are short. Of course, more realistic flow and collision forces could always be incorporated into Langevin equations for bed load transport, although these might require numerical methods for their solution. The theory of granular gases provides some indication of the types of more nuanced collision models which are possible (**??**).

Sediment transport experiments reveal correlations between particle size and the shape of the bed load velocity distribution. Experiments with smaller particles tend to give exponential distributions, and those with larger particles give Gaussian distributions. In fluid dynamics, the dissipation characteristics of particle-particle collisions in viscous flows are known to depend on the particle size and approach velocity through the Stokes number. In kinetic theory, it is known that gases of ideal elastic particles generate Gaussian (Boltzmann) velocity distributions, while gases of inelastic grains generate non-Gaussian distributions (**??**). Taken together, these ideas suggest that we might relate the shape of the particle velocity distribution to particle size. We can estimate typical Stokes numbers of colliding bed load particles in experiments as ..., using with the flow shear velocity and mean streamwise sediment velocity to calculate V. Estimating in this way, transport experiments with exponential velocities have $St \sim 1-10$, those with neither exponential nor Gaussian velocities have $St \sim 10-100$, and those with Gaussian velocities have $St > 100$. In experiments relating restitution coefficient to Stokes number for idealized collisions, restitution coefficients vary sharply from 0 to 1 as St ranges from 1 to 500 *Joseph et al.* (2001); *Yang and Hunt* (2006); **?**. Although collision geometry and grain shape certainly complicate the narrative, these values of St are consistent with our model conclusion that the shape of the particle velocity depends on the elasticity of collisions.

In real channels, grain sizes often span a wide range. A major implication of the dependence of the shape of the particle velocity distribution on grain size is that different grain sizes in a mixture will impart distinct fluctuation signatures to the overall bulk transport rate. Even in the absence of sorting effects and differential mobility, smaller grains can be expected to carry more control over the largest fluctuations in the overall transport rate, since their velocity distributions have wider tails.

5.4.1 Implications for landscape evolution

Many phenomena of landscape evolution depend on the velocities of individual grains. The erosion rates of bedrock rivers are for example parameterized by the impact velocities of individual sediment grains against the bedrock surface (**???**), on which they have a sensitive nonlinear dependence. It is not much of a stretch to imagine that bedrock erosion could be dominated by the largest impact velocities that originate from the extreme tail of the bedload velocity distribution. Here, we have shown that the weight of this tail depends sensitively on the dissipation characteristics of particle-bed collisions, suggesting that another feedback, that between dissipation and ... may be at play in the evolution of bedrock canyons.

5.4.2 Analogies to hillslope and wind-driven transport

It has long been recognized, probably since *Bagnold* (1941) and certainly today (), that there are deep analogies between tranpsort phenomena in air and water. In an ideal perspective, we might imagine writing the governing equations for transport in water as a function of the fluid viscosity, then tuning the viscosity between air and water to obtain a description applying to both spheres.

For example, in a mixture of small and large grains, neglecting any sorting effects whereby the mobility of small grains is contingent on the mobility of the large grains, small grains will have exponential velocities with relatively wide fluctuations, while large grains will have Gaussian velocities with relatively narrow fluctuations. Considering the over-all flux then as the number of moving particles times their velocities, transport fluctuations

aeolean transport extension maybe particle size distributions - interesting implications connection to computational physics approach connection to the stochastic description of the flux

5.5 Conclusion

We have demonstrated that particle-bed collisions control the shape of the particle velocity distribution.

Chapter 6

Summary and future work

6.1 The overall strategy

6.1.1 Langevin and master equations

6.1.2 Idealized noises and their combinations

6.2 Key contributions

6.2.1 Probability distribution of the sediment flux from micromechanics of particle trajectories

6.2.2 Inclusion of velocity fluctuations into Einstein's model of individual particle trajectories

6.2.3 Quantification of the control of bed elevation fluctuations over sediment transport fluctuations

6.2.4 Predicting how sediment burial affects the downstream spreading of sediment tracer particles

6.3 Models and the real world

6.4 Conclusion and next steps

Bibliography

Aberle, J., and V. Nikora, Statistical properties of armored gravel bed surfaces, *Water Resources Research*, *42*, 1–11, 2006. → pages 65, 67, 68

Abramian, A., O. Devauchelle, G. Seizilles, and E. Lajeunesse, Boltzmann Distribution of Sediment Transport, *Physical Review Letters*, *123*, 14,501, 2019. → page 84

Allen, B., and A. Kudrolli, Granular bed consolidation, creep, and armoring under subcritical fluid flow, *Physical Review Fluids*, *7*, 1–13, 2018. → pages 2, 15

Amir, M., V. I. Nikora, and M. T. Stewart, Pressure forces on sediment particles in turbulent open-channel flow: A laboratory study, *Journal of Fluid Mechanics*, *757*, 458–497, 2014. → pages 2, 66

An, C., X. Fu, G. Wang, and G. Parker, Effect of grain sorting on gravel bed river evolution subject to cycled hydrographs: Bed load sheets and breakdown of the hydrograph boundary layer, *Journal of Geophysical Research: Earth Surface*, *122*, 1513–1533, 2017. → page 43

Ancey, C., Bedload transport: a walk between randomness and determinism. Part 1. The state of the art, *Journal of Hydraulic Research*, *58*, 1–17, 2020. → pages 2, 23, 24, 26, 29, 30, 31, 42, 45, 83

Ancey, C., and J. Heyman, A microstructural approach to bed load transport: Mean behaviour and fluctuations of particle transport rates, *Journal of Fluid Mechanics*, *744*, 129–168, 2014. → pages 11, 12, 23, 27, 28, 30, 31, 34, 42, 43, 83, 84, 86, 89, 91, 95, 96

Ancey, C., and I. Pascal, Estimating Mean Bedload Transport Rates and Their Uncertainty, *Journal of Geophysical Research: Earth Surface*, *125*, 1–29, 2020. → page 2

Ancey, C., T. Böhm, M. Jodeau, and P. Frey, Statistical description of sediment transport experiments, *Physical Review E - Statistical, Nonlinear, and Soft Matter Physics*, *74*, 1–14, 2006. → pages 16, 22, 23, 42, 46, 47, 48, 61, 72, 80

Ancey, C., A. C. Davison, T. Böhm, M. Jodeau, and P. Frey, Entrainment and motion of coarse particles in a shallow water stream down a steep slope, *Journal of Fluid Mechanics*, *595*, 83–114, 2008. → pages xiv, xviii, 15, 22, 23, 27, 30, 31, 42, 47, 48, 49, 50, 51, 52, 53, 54, 55, 56, 59, 60, 61, 64, 65, 66, 83, 84, 136

Ancey, C., P. Bohorquez, and J. Heyman, Stochastic interpretation of the advection-diffusion, *Journal of Geophysical Research : Earth Surface*, *120*, 325–345, 2015. → page 66

Arfken, G., *Mathematical methods for physicists*, Academic Press, Inc., 1985. → pages 7, 74, 126, 128, 129

Armanini, A., *Principles of river hydraulics*, 2017. → page 17

Armanini, A., V. Cavedon, and M. Righetti, A probabilistic/deterministic approach for the prediction of the sediment transport rate, *Advances in Water Resources*, *81*, 10–18, 2015. → page 17

Armenio, V., and V. Fiorotto, The importance of the forces acting on particles in turbulent flows, *Physics of Fluids*, *13*, 2437–2440, 2001. → page 89

Azéma, E., and F. Radjaï, Force chains and contact network topology in sheared packings of elongated particles, *Physical Review E - Statistical, Nonlinear, and Soft Matter Physics*, *85*, 1–12, 2012. → page 11

Bagnold, *Physics of Blown Sand*, 1941. → page 99

Bagnold, R. A., Experiments on a gravity-free dispersion of large solid spheres in a Newtonian fluid under shear, *Proceedings of the Royal Society of London. Series A. Mathematical and Physical Sciences*, *225*, 49–63, 1954. → pages 14, 44

Bagnold, R. A., The flow of cohesionless grains in fluids, *Philosophical Transactions of the Royal Society of London. Series A, Mathematical and Physical Sciences*, *249*, 235–297, 1956. → pages 2, 14

Bagnold, R. A., An Approach to the Sediment Transport Problem from General Physics, *Tech. Rep. 4*, U.S. Geological Survey, Washington, DC, 1966. → page 14

Bagnold, R. A., The nature of saltation and of 'bed-load' transport in water, *Proc. Roy. Soc. London, Series a*, *332*, 473–504, 1973. → page 14

Balakrishnan, V., On a simple derivation of master equations for diffusion processes driven by white noise and dichotomic Markov noise, *Pramana*, *40*, 259–265, 1993. → pages 7, 9, 33

Ballio, F., V. Nikora, and S. E. Coleman, On the definition of solid discharge in hydro-environment research and applications, *Journal of Hydraulic Research*, *52*, 173–184, 2014. → page 14

Ballio, F., D. Pokrajac, A. Radice, and S. A. Hosseini Sadabadi, Lagrangian and Eulerian Description of Bed Load Transport, *Journal of Geophysical Research: Earth Surface*, *123*, 384–408, 2018. → page 14

Banerjee, T., S. N. Majumdar, A. Rosso, and G. Schehr, Current fluctuations in noninteracting run-and-tumble particles in one dimension, *Physical Review E*, *101*, 1–16, 2020. → page 34

Barik, D., P. K. Ghosh, and D. S. Ray, Langevin dynamics with dichotomous noise; Direct simulation and applications, *Journal of Statistical Mechanics: Theory and Experiment*, 2006. → page 76

Barry, J. J., J. M. Buffington, and J. G. King, A general power equation for predicting bed load transport rates in gravel bed rivers, *Water Resources Research*, *40*, 1–22, 2004. → page 2

Bathurst, J. C., Effect of coarse surface layer on bed-load transport, *Journal of Hydraulic Engineering*, *133*, 1192–1205, 2007. → page 2

Bena, I., Dichotomous Markov noise: Exact results for out-of-equilibrium systems, *International Journal of Modern Physics B*, *20*, 2825–2888, 2006. → page 9

Bennett, C. H., Serially deposited amorphous aggregates of hard spheres, *Journal of Applied Physics*, *43*, 2727–2734, 1972. → pages 51, 54

Berezhkovskii, A. M., and G. H. Weiss, Detailed description of a two-state non-Markov system, *Physica A: Statistical Mechanics and its Applications*, *303*, 1–12, 2002. → page 126

Bialik, R. J., V. I. Nikora, and P. M. Rowiński, 3D Lagrangian modelling of saltating particles diffusion in turbulent water flow, *Acta Geophysica*, *60*, 1639–1660, 2012. → pages 71, 80

Bialik, R. J., V. I. Nikora, M. Karpiński, and P. M. Rowiński, Diffusion of bedload particles in open-channel flows: distribution of travel times and second-order statistics of particle trajectories, *Environmental Fluid Mechanics*, *15*, 1281–1292, 2015. → page 71

Bohorquez, P., and C. Ancey, Particle diffusion in non-equilibrium bedload transport simulations, *Applied Mathematical Modelling*, *40*, 7474–7492, 2016. → page 84

Brach, R. M., Rigid body collisions, *American Society of Mechanical Engineers (Paper)*, *56*, 133–138, 1989. → page 87

Bradley, D. N., Direct Observation of Heavy-Tailed Storage Times of Bed Load Tracer Particles Causing Anomalous Superdiffusion, *Geophysical Research Letters*, *44*, 12,227–12,235, 2017. → pages 4, 47, 67, 70, 79, 81, 82

Bradley, D. N., G. E. Tucker, and D. A. Benson, Fractional dispersion in a sand bed river, *Journal of Geophysical Research*, *115*, F00A09, 2010. → pages 79, 81

Cameron, S. M., V. I. Nikora, and M. J. Witz, Entrainment of sediment particles by very large-scale motions, *Journal of Fluid Mechanics*, *888*, 2020. → page 4

Celik, A. O., P. Diplas, C. L. Dancey, and M. Valyrakis, Impulse and particle dislodgement under turbulent flow conditions, *Physics of Fluids*, *22*, 1–13, 2010. → page 46

Celik, A. O., P. Diplas, and C. L. Dancey, Instantaneous pressure measurements on a spherical grain under threshold flow conditions, *Journal of Fluid Mechanics*, *741*, 60–97, 2014. → pages 2, 4, 18, 89, 97

Charru, F., Selection of the ripple length on a granular bed sheared by a liquid flow, *Physics of Fluids*, *18*, 1–9, 2006. → page 18

Charru, F., H. Mouilleron, and O. Eiff, Erosion and deposition of particles on a bed sheared by a viscous flow, *Journal of Fluid Mechanics*, *519*, 55–80, 2004. → pages 2, 4, 18, 29, 50, 66, 84, 97

Cheng, N. S., Analysis of bedload transport in laminar flows, *Advances in Water Resources*, *27*, 937–942, 2004. → page 17

Church, M., Bed material transport and the morphology of alluvial river channels, *Annual Review of Earth and Planetary Sciences*, *34*, 325–354, 2006. → page 2

Church, M., and A. Zimmermann, Form and stability of step-pool channels: Research progress, *Water Resources Research*, *43*, 2007. → page 21

Clark, A. H., M. D. Shattuck, N. T. Ouellette, and C. S. O'Hern, Onset and cessation of motion in hydrodynamically sheared granular beds, *Physical Review E - Statistical, Nonlinear, and Soft Matter Physics*, *92*, 1–28, 2015. → page 11

Clark, A. H., M. D. Shattuck, N. T. Ouellette, and C. S. O'Hern, Role of grain dynamics in determining the onset of sediment transport, *Physical Review Fluids*, *2*, 2017. → pages 11, 15

Clift, R., J. R. Grace, and M. E. Weber, Bubbles, Drops, and Particles, 1978. → page 89

Coleman, N. L., A theoretical and experimental study of drag and lift forces acting on a sphere resting on a hypothetical streambed, in *International Association for Hydraulic Research Congress*, pp. 185–192, Littleton, CO, 1967. → page 89

Coleman, S. E., and V. I. Nikora, Exner equation: A continuum approximation of a discrete granular system, *Water Resources Research*, *45*, 1–8, 2009. → page 21

Correa, A., D. Windhorst, D. Tetzlaff, P. Crespo, R. Célleri, J. Feyen, and L. Breuer, Accelerating advances in continental domain hydrologic modeling, *Water Resources Research*, *53*, 5998–6017, 2017. → page 52

Daly, E., and A. Porporato, Probabilistic dynamics of some jump-diffusion systems, *Physical Review E - Statistical, Nonlinear, and Soft Matter Physics*, *73*, 1–7, 2006. → page 90

Daly, E., and A. Porporato, Effect of different jump distributions on the dynamics of jump processes, *Physical Review E - Statistical, Nonlinear, and Soft Matter Physics*, *81*, 1–10, 2010. → page 90

Denisov, S. I., W. Horsthemke, and P. Hänggi, Generalized Fokker-Planck equation: Derivation and exact solutions, *European Physical Journal B*, *68*, 567–575, 2009. → page 90

Dey, S., and S. Z. Ali, Review Article: Advances in modeling of bed particle entrainment sheared by turbulent flow, *Physics of Fluids*, *30*, 2018. → page 18

Dhont, B., and C. Ancey, Are Bedload Transport Pulses in Gravel Bed Rivers Created by Bar Migration or Sediment Waves?, *Geophysical Research Letters*, *45*, 5501–5508, 2018. → pages 30, 48, 65

Diplas, P., C. L. Dancey, A. O. Celik, M. Valyrakis, K. Greer, and T. Akar, The role of impulse on the initiation of particle movement under turbulent flow conditions, *Science*, *322*, 717–720, 2008. → page 18

Drake, T. G., R. L. Shreve, W. E. Dietrich, P. J. Whiting, and L. B. Leopold, Bedload transport of fine gravel observed by motion-picture photography, *Journal of Fluid Mechanics*, *192*, 193–217, 1988. → page 8

Dubkov, A. A., and A. A. Kharcheva, Steady-state probability characteristics of Verhulst and Hongler models with multiplicative white Poisson noise, *European Physical Journal B*, *92*, 1–6, 2019. → page 90

Dubkov, A. A., O. V. Rudenko, and S. N. Gurbatov, Probability characteristics of nonlinear dynamical systems driven by δ -pulse noise, *Physical Review E*, *93*, 1–7, 2016. → page 90

Dwivedi, A., B. Melville, and A. Y. Shamseldin, Hydrodynamic forces generated on a spherical sediment particle during entrainment, *Journal of Hydraulic Engineering*, *136*, 756–769, 2010. → page 89

Dwivedi, A., B. W. Melville, A. Y. Shamseldin, and T. K. Guha, Analysis of hydrodynamic lift on a bed sediment particle, *Journal of Geophysical Research: Earth Surface*, *116*, 2011. → page 46

Dwivedi, A., B. Melville, A. J. Raudkivi, A. Y. Shamseldin, and Y. M. Chiew, Role of turbulence and particle exposure on entrainment of large spherical particles in flows with low relative submergence, *Journal of Hydraulic Engineering*, *138*, 1022–1030, 2012. → pages 2, 89

Einstein, H. A., Bed load transport as a probability problem, Ph.D. thesis, ETH Zurich, 1937. → pages xx, 5, 7, 8, 16, 26, 30, 37, 41, 45, 46, 47, 64, 69, 70, 71, 72, 74, 75, 76, 79, 80, 81

Einstein, H. A., *The bedload function for sediment transportation in open channel flows*, technical ed., Soil Conservation Service, Washington, DC, 1950. → pages 16, 18, 30, 46, 47, 48, 49, 51, 64

Elghannay, H., and D. Tafti, LES-DEM simulations of sediment transport, *International Journal of Sediment Research*, *33*, 137–148, 2018. → page 11

Engelund, F., and J. Fredsoe, A sediment transport model for straight alluvial channels., *Nordic Hydrology*, *7*, 293–306, 1976. → page 15

Escaff, D., R. Toral, C. Van Den Broeck, and K. Lindenberg, A continuous-time persistent random walk model for flocking, *Chaos*, *28*, 1–11, 2018. → pages 43, 82

Ettema, R., and C. F. Mutel, Hans Albert Einstein: Innovation and compromise in formulating sediment transport by Rivers, *Journal of Hydraulic Engineering*, *130*, 477–487, 2004. → page 5

Fa, K. S., Uncoupled continuous-time random walk model: Analytical and numerical solutions, *Physical Review E - Statistical, Nonlinear, and Soft Matter Physics*, *89*, 1–9, 2014. → page 82

Fan, N., D. Zhong, B. Wu, E. Foufoula-Georgiou, and M. Guala, A mechanistic-stochastic formulation of bed load particle motions: From individual particle forces to the Fokker-Planck equation under low transport rates, *Journal of Geophysical Research: Earth Surface*, *119*, 464–482, 2014. → pages 11, 28, 30, 31, 84, 85, 89, 91, 94, 97

Fathel, S., D. Furbish, and M. Schmeeckle, Parsing anomalous versus normal diffusive behavior of bedload sediment particles, *Earth Surface Processes and Landforms*, *41*, 1797–1803, 2016. → pages 70, 79, 82, 84

Fathel, S. L., D. J. Furbish, and M. W. Schmeeckle, Experimental evidence of statistical ensemble behavior in bed load sediment transport, *Journal of Geophysical Research F: Earth Surface*, *120*, 2298–2317, 2015. → pages 8, 11, 21, 23, 29, 48, 67, 72, 84

Feller, W., *An Introduction to Probability Theory and its Applications*, 3rd ed., Wiley, 1967. → page 91

Ferguson, R. I., and T. B. Hoey, Long-term slowdown of river tracer pebbles: Generic models and implications for interpreting short-term tracer studies, *Water Resources Research*, *38*, 17–1–17–11, 2002. → pages 4, 5, 77

Ferguson, R. I., D. J. Bloomer, T. B. Hoey, and A. Werritty, Mobility of river tracer pebbles over different timescales, *Water Resources Research*, *38*, 3–1–3–8, 2002. → page 70

Fowler, K. J. A., Simulating runoff under changing climatic conditions, *Water Resources Research*, *52*, 1–24, 2016. → pages 71, 80

Fraccarollo, L., and M. A. Hassan, Einstein conjecture and resting-Time statisticsÂ inÂ the bed-load transport of monodispersedÂ particles, *Journal of Fluid Mechanics*, *876*, 1077–1089, 2019. → page 80

Frey, P., Particle velocity and concentration profiles in bedload experiments on a steep slope, *Earth Surface Processes and Landforms*, *39*, 646–655, 2014. → page 4

Frey, P., and M. Church, Bedload: A granular phenomenon, *Earth Surface Processes and Landforms*, *36*, 58–69, 2011. → pages 2, 11

Furbish, D. J., and M. W. Schmeeckle, A probabilistic derivation of the exponential-like distribution of bed load particle velocities, *Water Resources Research*, *49*, 1537–1551, 2013. → page 85

Furbish, D. J., A. E. Ball, and M. W. Schmeeckle, A probabilistic description of the bed load sediment flux: 4. Fickian diffusion at low transport rates, *Journal of Geophysical Research: Earth Surface*, *117*, 1–13, 2012a. → pages 11, 14, 17, 19, 20, 21, 30, 70, 82, 84

Furbish, D. J., P. K. Haff, J. C. Roseberry, and M. W. Schmeeckle, A probabilistic description of the bed load sediment flux: 1. Theory, *Journal of Geophysical Research: Earth Surface*, *117*, 2012b. → pages 47, 48, 50

Furbish, D. J., S. L. Fathel, and M. W. Schmeeckle, Particle motions and bedload theory: The entrainment forms of the flux and the exner equation, in *Gravel-Bed Rivers: Process and Disasters*, edited by D. Tsutsumi and J. B. Laronne, 1 ed., chap. 4, pp. 97–120, John Wiley & Sons Ltd., 2017. → pages 21, 22, 29, 48, 70

Gaeuman, D., R. Stewart, B. Schmandt, and C. Pryor, Geomorphic response to gravel augmentation and high-flow dam release in the Trinity River, California, *Earth Surface Processes and Landforms*, *42*, 2523–2540, 2017. → pages 46, 69

Gardiner, C. W., *Handbook of stochastic methods for physics, chemistry and the natural sciences*, Springer-Verlag, 1983. → pages 12, 33, 53, 56, 66, 89, 90, 91, 137

Gillespie, D. T., Exact stochastic simulation of coupled chemical reactions, *Journal of Physical Chemistry*, *81*, 2340–2361, 1977. → pages 53, 133

Gillespie, D. T., Stochastic simulation of chemical kinetics, *Annual Review of Physical Chemistry*, *58*, 35–55, 2007. → pages 52, 53, 54, 133

Goh, K. I., and A. L. Barabási, Burstiness and memory in complex systems, *Epl*, *81*, 2008. → page 42

Gomez, B., and M. Church, An assessment of bed load sediment transport formulae for gravel bed rivers, *Water Resources Research*, *25*, 1161–1186, 1989. → page 2

González, C., D. H. Richter, D. Bolster, S. Bateman, J. Calantoni, and C. Escauriaza, Characterization of bedload intermittency near the threshold of motion using a Lagrangian sediment transport model, *Environmental Fluid Mechanics*, *17*, 111–137, 2017. → pages 11, 46, 85, 89

Gordon, R., J. B. Carmichael, and F. J. Isackson, Saltation of plastic balls in a 'one-dimensional' flume, *Water Resources Research*, *8*, 444–459, 1972. → pages 3, 8, 26, 29, 72, 88

Grass, A., Initial Instability of Fine Bed Sand, *Journal of the Hydraulics Division*, *96*, 619–632, 1970. → page 18

Greenbaum, N., A. P. Schick, and V. R. Baker, Re-examination of Bagnold's empirical bedload formulae, *Earth Surface Processes and Landforms*, *25*, 1011–1024, 2000. → page 15

Guala, M., A. Singh, N. Badheartbull, and E. Foufoula-georgiou, Journal of Geophysical Research : Earth Surface Spectral description of migrating bed forms and sediment transport, *Journal of Geophysical Research: Earth Surface*, *119*, 123–137, 2014. → pages 22, 30

Hanggi, P., Correlation Functions and Masterequations of Generalized (Non-Markovian) Langevin Equations, *Z. Physik B*, *31*, 407–416, 1978. → pages 7, 33, 90

Hänggi, P., The functional derivative and its use in the description of noisy dynamical systems, in *Stochastic processes applied to physics*, edited by L. Pesquera and M. A. Rodriguez, p. 69, Santander, Spain, 1985. → page 7

Haschenburger, J. K., Tracing river gravels: Insights into dispersion from a long-term field experiment, *Geomorphology*, *200*, 121–131, 2013. → pages 70, 77

Hassan, M. A. ., and D. N. Bradley, Geomorphic controls on tracer particle dispersion in gravel-bed rivers, in *Gravel-Bed Rivers: Process and Disasters*, edited by D. Tsutsumi and J. B. Laronne, 1st ed., pp. 159–184, John Wiley & Sons Ltd., 2017. → pages 4, 5, 27, 46, 69, 70, 79

Hassan, M. A., and M. Church, Vertical mixing of coarse particles in gravel bed rivers: A kinematic model, *Water Resources Research*, *30*, 1173–1185, 1994. → page 77

Hassan, M. A., M. Church, and A. P. Schick, Distance of movement of coarse particles in gravel bed streams, *Water Resources Research*, *27*, 503–511, 1991. → pages 64, 70, 71, 76

Hassan, M. A., B. J. Smith, D. L. Hogan, D. S. Luzi, A. E. Zimmermann, and B. C. Eaton, 18 Sediment storage and transport in coarse bed streams: scale considerations, in *Developments in Earth Surface Processes*, edited by H. Habersack, H. Piegay, and M. Rinaldi, vol. 11, chap. 18, pp. 473–496, Elsevier B.V, 2007. → pages 2, 21, 66

Hassan, M. A., H. Voepel, R. Schumer, G. Parker, and L. Fraccarollo, Displacement characteristics of coarse fluvial bed sediment, *Journal of Geophysical Research: Earth Surface*, *118*, 155–165, 2013. → page 70

Heyman, J., A study of the spatio-temporal behaviour of bed load transport rate fluctuations, *PhD Dissertation*, *6256*, 116, 2014. → page 48

Heyman, J., F. Mettra, H. B. Ma, and C. Ancey, Statistics of bedload transport over steep slopes: Separation of time scales and collective motion, *Geophysical Research Letters*, *40*, 128–133, 2013. → pages 22, 27, 42, 48

Heyman, J., H. B. Ma, F. Mettra, and C. Ancey, Spatial correlations in bed load transport : Evidence, importance, and modeling, *Journal of*

Geophysical Research: Earth Surface, *119*, 1751–1767, 2014. → pages 48, 66, 82

Heyman, J., P. Bohórquez, and C. Ancey, Exploring the physics of sediment transport in non-uniform super-critical flows through a large dataset of particle trajectories, *J. Geophys. Res:Earth Surf.*, *submitted*, 2015. → page 42

Heyman, J., P. Bohorquez, and C. Ancey, Entrainment, motion, and deposition of coarse particles transported by water over a sloping mobile bed, *Journal of Geophysical Research: Earth Surface*, *121*, 1931–1952, 2016. → pages 11, 14, 23, 29, 48, 65, 67, 82, 84

Hjelmfelt, A. T., and L. F. Mockros, Motion of discrete particles in a turbulent fluid, *Applied Scientific Research*, *16*, 149–161, 1966. → page 89

Hoey, T. B., Temporal variations in bedload transport in rates and sediment storage, *Progress in Physical Geography*, *16*, 319–338, 1992. → page 30

Hofland, B., and J. A. Battjes, Probability density function of instantaneous drag forces and shear stresses on a bed, *Journal of Hydraulic Engineering*, *132*, 1169–1175, 2006. → pages 89, 97

Horsthemke, W., and R. Lefever, *Noise-induced transitions: Theory and applications in physics, chemistry and biology*, 1st ed., Springer-Verlag, Berlin, 1984. → page 9

Houssais, M., and E. Lajeunesse, Bedload transport of a bimodal sediment bed, *Journal of Geophysical Research F: Earth Surface*, *117*, 1–13, 2012. → pages 84, 85

Houssais, M., C. P. Ortiz, D. J. Durian, and D. J. Jerolmack, Onset of sediment transport is a continuous transition driven by fluid shear and granular creep, *Nature Communications*, *6*, 1–8, 2015. → page 15

Houssais, M., C. P. Ortiz, D. J. Durian, and D. J. Jerolmack, Rheology of sediment transported by a laminar flow, *Physical Review E*, *94*, 1–10, 2016. → page 4

Hubbell, D., and W. Sayre, Sand Transport Studies with Radioactive Tracers, *Journal of the Hydraulics Division*, *90*, 39–68, 1964. → pages 47, 64, 71, 72, 76

Jerolmack, D., and D. Mohrig, Interactions between bed forms: Topography, turbulence, and transport, *Journal of Geophysical Research: Earth Surface*, *110*, 2005. → pages 2, 44, 84

Ji, C., A. Munjiza, E. Avital, J. Ma, and J. J. Williams, Direct numerical simulation of sediment entrainment in turbulent channel flow, *Physics of Fluids*, *25*, 2013. → page 11

Jiang, Z., and P. K. Haff, Multiparticle simulation methods applied to the micromechanics of bed load transport, *Water Resources Research*, *29*, 399–412, 1993. → page 11

Joseph, G. G., R. Zenit, M. L. Hunt, and A. M. Rosenwinkel, Particle-wall collisions in a viscous fluid, *Journal of Fluid Mechanics*, *433*, 329–346, 2001. → page 98

Kalinske, A. A., Movement of sediment as bed load in rivers, *Eos, Transactions American Geophysical Union*, *28*, 615–620, 1947. → page 2

KIRCHNER, J. W., W. E. DIETRICH, F. ISEYA, and H. IKEDA, The variability of critical shear stress, friction angle, and grain protrusion in water-worked sediments, *Sedimentology*, *37*, 647–672, 1990. → pages 2, 15

Kraichnan, R. H., Diffusion by a random velocity field, *Physics of Fluids*, *13*, 22–31, 1970. → page 71

Lajeunesse, E., L. Malverti, and F. Charru, Bed load transport in turbulent flow at the grain scale: Experiments and modeling, *Journal of Geophysical Research: Earth Surface*, *115*, 2010. → pages xxi, 8, 11, 18, 67, 78, 82, 84, 97

Lajeunesse, E., O. Devauchelle, F. Lachaussée, and P. Claudin, Bedload transport in laboratory rivers: The erosion-deposition model, in *Gravel-Bed Rivers: Process and Disasters*, pp. 415–438, Kyoto and Takyama, Japan, 2017. → page 18

Lajeunesse, E., O. Devauchelle, and F. James, Advection and dispersion of bed load tracers, *Earth Surface Dynamics*, *6*, 389–399, 2018. → pages 8, 30, 31, 33, 34, 47, 80, 81, 82

Lee, D. B., and D. Jerolmack, Determining the scales of collective entrainment in collision-driven bed load, *Earth Surface Dynamics*, *6*, 1089–1099, 2018. → pages 43, 48, 65, 82

Lisle, I. G., C. W. Rose, W. L. Hogarth, P. B. Hairsine, G. C. Sander, and J. Y. Parlange, Stochastic sediment transport in soil erosion, *Journal of Hydrology*, *204*, 217–230, 1998. → pages xvii, xx, 8, 9, 26, 27, 30, 31, 33, 34, 37, 41, 42, 45, 71, 72, 74, 75, 80, 81, 82, 130

Liu, D., X. Liu, X. Fu, and G. Wang, Quantification of the bed load effects on turbulent open-channel flows, *Journal of Geophysical Research : Earth Surface*, *121*, 767–789, 2016. → page 2

Liu, M. X., A. Pelosi, and M. Guala, A Statistical Description of Particle Motion and Rest Regimes in Open-Channel Flows Under Low Bedload Transport, *Journal of Geophysical Research: Earth Surface*, *124*, 2666–2688, 2019. → pages 47, 67, 80, 84, 85

Lorenz, A., C. Tuozzolo, and M. Y. Louge, Measurements of impact properties of small, nearly spherical particles, *Experimental Mechanics*, *37*, 292–298, 1997. → page 87

Luczka, J., R. Bartussek, and P. Hanggi, White-noise-induced transport in periodic structures., *Epl*, *31*, 431–436, 1995. → page 90

Luque, R. F., and R. van Beek, Erosion and transport of bed-load sediment, *Journal of Hydraulic Research*, *14*, 127–144, 1976. → page 15

Ma, H., J. Heyman, X. Fu, F. Mettra, C. Ancey, and G. Parker, Bed load transport over a broad range of timescales: Determination of three regimes of fluctuations, *Journal of Geophysical Research: Earth Surface*, *119*, 2653–2673, 2014. → page 48

Macklin, M. G., P. A. Brewer, K. A. Hudson-Edwards, G. Bird, T. J. Coulthard, I. A. Dennis, P. J. Lechler, J. R. Miller, and J. N. Turner, A geomorphological approach to the management of rivers contaminated by metal mining, *Geomorphology*, *79*, 423–447, 2006. → pages 46, 69

Malmon, D. V., S. L. Reneau, T. Dunne, D. Katzman, and P. G. Drakos, Influence of sediment storage on downstream delivery of contaminated sediment, *Water Resources Research*, *41*, 1–17, 2005. → page 46

Marcum, J. I., A Statistical Theory of Target Detection By Pulsed Radar, *IRE Transactions on Information Theory*, *6*, 59–267, 1960. → page 75

Martin, R. L., Transient mechanics of bed load sediment transport, Phd dissertation, University of Pennsylvania, 2013. → page 8

Martin, R. L., D. J. Jerolmack, and R. Schumer, The physical basis for anomalous diffusion in bed load transport, *Journal of Geophysical Research: Earth Surface*, *117*, 1–18, 2012. → pages xxi, 11, 47, 70, 72, 78, 79, 80, 81, 85

Martin, R. L., P. K. Purohit, and D. J. Jerolmack, Sedimentary bed evolution as a mean-reverting random walk: Implications for tracer statistics, *Geophysical Research Letters*, *41*, 6152–6159, 2014. → pages 47, 51, 54, 56, 63, 64, 65, 66, 67, 70, 77, 80, 81, 137

Masoliver, J., Fractional telegrapher's equation from fractional persistent random walks, *Physical Review E*, *93*, 1–10, 2016. → page 82

Masoliver, J., and K. Lindenberg, Continuous time persistent random walk: a review and some generalizations, *European Physical Journal B*, *90*, 2017. → page 9

Masoliver, J., and G. H. Weiss, Transport Equations in Chromatography with a Finite Speed of Signal Propagation, *Separation Science and Technology*, *26*, 279–289, 1991. → page 9

Masoliver, J., and G. H. Weiss, Telegrapher's equations with variable propagation speeds, *Physical Review E*, *49*, 3852–3854, 1994. → page 82

Masoliver, J., G. H. Weiss, E. J. Phys, J. Masoliver, and G. H. Weiss, Finite-velocity diffusion, *European Journal of Physics*, *17*, 1996. → page 9

Mau, Y., X. Feng, and A. Porporato, Multiplicative jump processes and applications to leaching of salt and contaminants in the soil, *Physical Review E - Statistical, Nonlinear, and Soft Matter Physics*, *90*, 1–8, 2014. → page 90

Maurin, R., J. Chauchat, B. Chareyre, and P. Frey, A minimal coupled fluid-discrete element model for bedload transport, *Physics of Fluids*, *27*, 2015. → page 11

Maxey, M. R., and J. J. Riley, Equation of motion for a small rigid sphere in a nonuniform flow, *Physics of Fluids*, *26*, 883–889, 1983. → page 89

McEwan, I., and J. Heald, Discrete particle modeling of entrainment from flat uniformly sized sediment beds, *Journal of Hydraulic Engineering*, *127*, 588–597, 2001. → page 11

Metzler, R., and J. Klafter, The random walk's guide to anomalous diffusion: A fractional dynamics approach, *Physics Report*, *339*, 1–77, 2000. → pages 69, 76

Metzler, R., J. H. Jeon, A. G. Cherstvy, and E. Barkai, Anomalous diffusion models and their properties: Non-stationarity, non-ergodicity, and ageing at the centenary of single particle tracking, *Physical Chemistry Chemical Physics*, *16*, 24,128–24,164, 2014. → page 82

Meyer-Peter, E., and R. Müller, Formulas for Bed-Load Transport, *Proceedings of the 2nd Meeting of the International Association of Hydraulic Research*, pp. 39–64, 1948. → pages 3, 15

Michaelides, E. E., Review—the transient equation of motion for particles, bubbles, and droplets, *Journal of Fluids Engineering, Transactions of the ASME*, *119*, 233–247, 1997. → page 89

MILLER, R. L., and R. J. BYRNE, the Angle of Repose for a Single Grain on a Fixed Rough Bed, *Sedimentology*, *6*, 303–314, 1966. → pages 2, 3

Montaine, M., M. Heckel, C. Kruelle, T. Schwager, and T. Pöschel, Coefficient of restitution as a fluctuating quantity, *Physical Review E - Statistical, Nonlinear, and Soft Matter Physics*, *84*, 1–5, 2011. → page 87

Montroll, E. W., Random walks on lattices, *Journal of Mathematical Physics*, *6*, 193–220, 1964. → pages 6, 30, 72

Moss, F., and M. Peter Vaughan Elsmere, Theory of continuous Fokker-Planck systems, *1*, 1989. → page 7

Nakagawa, H., and T. Tsujimoto 9 Kyoto, On probabilistic characteristics of motion of individual sediment particles on stream beds., in *Hydraulic Problems Solved by Stochastic Methods: Second International IAHR Symposium on Stochastic Hydraulics*, pp. 293–320, Water Resources Publications, Lund, Sweden, 1977. → pages 20, 47, 64, 70, 71, 72, 79, 80

Nelson, P. A., D. Bellugi, and W. E. Dietrich, Delineation of river bed-surface patches by clustering high-resolution spatial grain size data, *Geomorphology*, *205*, 102–119, 2014. → page 66

Newman, M. E., Power laws, Pareto distributions and Zipf's law, *Contemporary Physics*, *46*, 323–351, 2005. → page 64

Nikora, V., D. Goring, I. McEwan, and G. Griffith, Spatially averaged open-channel flow over rough bed, *Journal of Hydraulic Engineering*, *127*, 123–133, 2001a. → pages 4, 27

Nikora, V., J. Heald, D. Goring, and I. McEwan, Diffusion of saltating particles in unidirectional water flow over a rough granular bed, *Journal of Physics A: Mathematical and General*, *34*, 2001b. → pages 69, 70, 71, 80

Nikora, V., H. Habersack, T. Huber, and I. McEwan, On bed particle diffusion in gravel bed flows under weak bed load transport, *Water Resources Research*, *38*, 17–1–17–9, 2002. → pages 4, 27, 69, 70, 71, 80, 82

Niño, Y., and M. García, Using Lagrangian particle saltation observations for bedload sediment transport modelling, *Hydrological Processes*, *12*, 1197–1218, 1998. → page 15

Niño, Y., and M. H. Garcia, Experiments on particle-turbulence interactions in the near-wall region of an open channel flow: Implications for sediment transport, *Journal of Fluid Mechanics*, *326*, 285–319, 1996. → page 15

Ockendon, J. R., and A. B. Tayler, The dynamics of a current collection system for an electric locomotive, *Proceedings of the Royal Society of London. A. Mathematical and Physical Sciences*, *322*, 447–468, 1971. → page 92

Olinde, L., and J. P. L. Johnson, Using RFID and accelerometer-embedded tracers to measure probabilities of bed load transport, step lengths, and rest times in a mountain stream, *Water Resources Research*, *51*, 7525–7589, 2015. → pages 47, 67, 80, 81

Paintal, A. S., A stochastic model of bed load transport, *Journal of Hydraulic Research*, *9*, 527–554, 1971. → pages 2, 15, 17, 18, 46, 51, 72

Papangelakis, E., and M. A. Hassan, The role of channel morphology on the mobility and dispersion of bed sediment in a small gravel-bed stream, *Earth Surface Processes and Landforms*, *41*, 2191–2206, 2016. → page 70

Parker, G., and P. C. Klingeman, On why gravel bed streams are paved, *Water Resources Research*, *18*, 1409–1423, 1982. → page 44

Parker, G., C. Paola, and S. Leclair, Probabilistic exner sediment continuity equation for mixtures with no active layer, *Journal of Hydraulic Engineering*, *128*, 801, 2002. → pages 20, 21

Parker, G., G. Seminara, and L. Solari, Bed load at low Shields stress on arbitrarily sloping beds: Alternative entrainment formulation, *Water Resources Research*, *39*, 1–11, 2003. → page 16

Parker, G., M. Hassan, and P. Wilcock, 10 Adjustment of the bed surface size distribution of gravel-bed rivers in response to cycled hydrographs, in *Developments in Earth Surface Processes*, edited by H. Habersack, H. Piegay, and M. Rinaldi, vol. 11, pp. 241–285, Elsevier B.V, 2007. → page 43

Pelosi, A., and G. Parker, Morphodynamics of river bed variation with variable bedload step length, *Earth Surface Dynamics*, *2*, 243–253, 2014. → page 81

Pender, G., T. B. Hoey, C. Fuller, and I. K. McEwan, Selective bedload transport during the degradation of a well sorted graded sediment bed, *Journal of Hydraulic Research*, *39*, 269–277, 2001. → page 51

Philip, J. R., Diffusion by continuous movements, *Physics of Fluids*, *11*, 38–42, 1968. → page 69

Phillips, C. B., R. L. Martin, and D. J. Jerolmack, Impulse framework for unsteady flows reveals superdiffusive bed load transport, *Geophysical Research Letters*, *40*, 1328–1333, 2013. → page 70

Pielou, E. C., *Mathematical Ecology*, 1 ed., John Wiley & Sons Ltd., New York, NY, 2008. → pages 22, 53

Pierce, J. K., and M. A. Hassan, Back to Einstein: Burial-Induced Three-Range Diffusion in Fluvial Sediment Transport, *Geophysical Research Letters*, *47*, 2020. → pages vi, 30

Prudnikov, A. P., I. A. Brychkov, O. I. Marichev, and G. G. Gould, *Integrals and series: vol. 3*, Gordon and Breach Science Publishers, 1986. → page 7

Prudnikov, A. P., Y. A. Brychkov, O. I. Marichev, and R. H. Romer, *Integrals and Series*, Gordon and Breach, New York, 1988. → page 74

Recking, A., F. Liébault, C. Peteuil, and T. Jolimet, Testing bedload transport equations with consideration of time scales, *Earth Surface Processes and Landforms*, *37*, 774–789, 2012. → pages 2, 30

Recking, A., G. Piton, D. Vazquez-Tarrio, and G. Parker, Quantifying the Morphological Print of Bedload Transport, *Earth Surface Processes and Landforms*, *41*, 809–822, 2016. → page 2

Redner, S., and J. R. Dorfman, *A Guide to First-Passage Processes*, vol. 70, Cambridge University Press, Cambridge, 2002. → pages 47, 63

Roseberry, J. C., M. W. Schmeeckle, and D. J. Furbish, A probabilistic description of the bed load sediment flux: 2. Particle activity and motions, *Journal of Geophysical Research: Earth Surface*, *117*, 2012. → pages 48, 67, 72, 84

Rossetto, V., The one-dimensional asymmetric persistent random walk, *Journal of Statistical Mechanics: Theory and Experiment*, *2018*, 2018. → page 9

Saletti, M., and M. A. Hassan, Width variations control the development of grain structuring in steep step-pool dominated streams: insight from flume experiments, *Earth Surface Processes and Landforms*, *45*, 1430–1440, 2020. → pages 21, 82

Santos, B. O., M. J. Franca, and R. M. Ferreira, Coherent structures in open channel flows with bed load transport over an hydraulically rough bed, in *Proceedings of the International Conference on Fluvial Hydraulics, RIVER FLOW 2014*, EPFL-CONF-202022, pp. 883–890, 2014. → page 2

Schmeeckle, M. W., Numerical simulation of turbulence and sediment transport of medium sand, *Journal of Geophysical Research: Earth Surface*, *119*, 1240–1262, 2014. → page 11

Schmeeckle, M. W., and J. M. Nelson, Direct numerical simulation of bedload transport using a local, dynamic boundary condition, *Sedimentology*, *50*, 279–301, 2003. → page 11

Schmeeckle, M. W., J. M. Nelson, and R. L. Shreve, Forces on stationary particles in near-bed turbulent flows, *Journal of Geophysical Research: Earth Surface*, *112*, 1–21, 2007. → pages 46, 89, 97

Schmidt, M. G., F. Sagués, and I. M. Sokolov, Mesoscopic description of reactions for anomalous diffusion: A case study, *Journal of Physics Condensed Matter*, *19*, 2007. → page 73

Schumer, R., M. M. Meerschaert, and B. Baeumer, Fractional advection-dispersion equations for modeling transport at the Earth surface, *Journal of Geophysical Research: Earth Surface*, *114*, 1–15, 2009. → pages 19, 76, 82

Seizilles, G., E. Lajeunesse, O. Devauchelle, and M. Bak, Cross-stream diffusion in bedload transport, *Physics of Fluids*, *26*, 2014. → pages 18, 84

Sekine, M., and H. Kikkawa, Mechanics of saltating grains. II, *Journal of Hydraulic Engineering*, *118*, 536–558, 1992. → pages 3, 11, 71

Seminara, G., L. Solari, and G. Parker, Bed load at low Shields stress on arbitrarily sloping beds: Failure of the Bagnold hypothesis, *Water Resources Research*, *38*, 31–1–31–16, 2002. → page 15

Shi, Z., and G. Wang, Hydrological response to multiple large distant earthquakes in the Mile well, China, *Journal of Geophysical Research F: Earth Surface*, *119*, 2448–2459, 2014. → pages 64, 80, 81, 82

Shih, W. R., P. Diplas, A. O. Celik, and C. Dancey, Accounting for the role of turbulent flow on particle dislodgement via a coupled quadrant analysis of velocity and pressure sequences, *Advances in Water Resources*, *101*, 37–48, 2017. → pages 2, 66

Shlesinger, M. F., Asymptotic solutions of continuous-time random walks, *Journal of Statistical Physics*, *10*, 421–434, 1974. → page 76

Singh, A., K. Fienberg, D. J. Jerolmack, J. Marr, and E. Foufoula-Georgiou, Experimental evidence for statistical scaling and intermittency in sediment transport rates, *Journal of Geophysical Research: Earth Surface*, *114*, 1–16, 2009. → pages 30, 42, 48, 54, 67, 68

Singh, A., F. Porté-Agel, and E. Foufoula-georgiou, On the influence of gravel bed dynamics on velocity power spectra, *Water Resources Research*, *46*, 1–10, 2010. → page 2

Singh, A., E. Foufoula-Georgiou, F. Porté-Agel, and P. R. Wilcock, Coupled dynamics of the co-evolution of gravel bed topography, flow turbulence and sediment transport in an experimental channel, *Journal of Geophysical Research F: Earth Surface*, *117*, 1–20, 2012. → pages 48, 65, 67, 68

Sokolov, I. M., Models of anomalous diffusion in crowded environments, *Soft Matter*, *8*, 9043–9052, 2012. → page 69

Sumer, B. M., L. H. Chua, N. S. Cheng, and J. Fredsøe, Influence of turbulence on bed load sediment transport, *Journal of Hydraulic Engineering*, *129*, 585–596, 2003. → page 2

Swift, R. J., A Stochastic Predator-Prey Model, *Bulletin of the Irish Mathematical Society*, *48*, 57–63, 2002. → page 53

Temme, N. M., and D. Zwillinger, *Special Functions: An Introduction to the Classical Functions of Mathematical Physics*, vol. 65, John Wiley & Sons Ltd., 1997. → pages 75, 128

Tregnaghi, M., A. Bottacin-Busolin, A. Marion, and S. Tait, Stochastic determination of entrainment risk in uniformly sized sediment beds at low transport stages: 1. Theory, *Journal of Geophysical Research: Earth Surface*, *117*, 1–15, 2012. → page 18

Tsujimoto, T., Japanese title, Ph.D. thesis, Kyoto University, 1978. → page 21

Turowski, J. M., Probability distributions of bed load transport rates: A new derivation and comparison with field data, *Water Resources Research*, *46*, 2010. → pages 24, 26, 30, 31, 42, 83

Valyrakis, M., P. Diplas, C. L. Dancey, K. Greer, and A. O. Celik, Role of instantaneous force magnitude and duration on particle entrainment, *Journal of Geophysical Research: Earth Surface*, *115*, 2010. → page 2

Van Den Broeck, C., On the relation between white shot noise, Gaussian white noise, and the dichotomic Markov process, *Journal of Statistical Physics*, *31*, 467–483, 1983. → pages 6, 7

Van Kampen, N. G., *Stochastic Processes in Physics and Chemistry*, 3rd ed., Elsevier B.V., 2007. → pages 12, 25

van Rijn, L. C., Sediment transport, part I: Bed load transport, *Journal of Hydraulic Engineering*, *110*, 1431–1456, 1984. → pages 8, 10

Venditti, J. G., P. A. Nelson, R. W. Bradley, D. Haught, and A. B. Gitto, Bedforms, structures, patches, and sediment supply in gravel-bed rivers, *Gravel-Bed Rivers: Process and Disasters*, pp. 439–466, 2017. → pages 2, 21

Vicsek, T., and A. Zafeiris, Collective motion, *Physics Reports*, *517*, 71–140, 2012. → page 82

Voepel, H., R. Schumer, and M. A. Hassan, Sediment residence time distributions: Theory and application from bed elevation measurements, *Journal of Geophysical Research: Earth Surface*, *118*, 2557–2567, 2013. → pages 47, 63, 64, 67, 70, 77, 80, 81

Vowinckel, B., T. Kempe, and J. Fröhlich, Fluid-particle interaction in turbulent open channel flow with fully-resolved mobile beds, *Advances in Water Resources*, *72*, 32–44, 2014. → page 46

Wachs, A., Particle-scale computational approaches to model dry and saturated granular flows of non-Brownian, non-cohesive, and non-spherical rigid bodies, *Acta Mechanica*, *230*, 1919–1980, 2019. → page 11

Weeks, E. R., and H. L. Swinney, Anomalous diffusion resulting from strongly asymmetric random walks, *Physical Review E - Statistical Physics, Plasmas, Fluids, and Related Interdisciplinary Topics*, *57*, 4915–4920, 1998. → pages 47, 72, 73, 74, 76, 79, 81, 131

Weeks, E. R., J. S. Urbach, and H. L. Swinney, Anomalous diffusion in asymmetric random walks with a quasi-geostrophic flow example, *Physica D: Nonlinear Phenomena*, *97*, 291–310, 1996. → pages 80, 81

Weiss, G. H., The two-state random walk, *Journal of Statistical Physics*, *15*, 157–165, 1976. → page 72

Weiss, G. H., *Aspects and Applications of the Random Walk.*, North Holland, Amsterdam, 1994. → pages 72, 73, 74, 79, 131

Weiss, G. H., Some applications of persistent random walks and the telegrapher's equation, *Physica A: Statistical Mechanics and its Applications*, *311*, 381–410, 2002a. → page 38

Weiss, G. H., Some applications of persistent random walks and the telegrapher's equation, *Physica A: Statistical Mechanics and its Applications*, *311*, 381–410, 2002b. → page 9

Wiberg, P. L., and J. D. Smith, A theoretical model for saltating grains in water., *Journal of Geophysical Research*, *90*, 7341–7354, 1985. → pages 8, 11, 46, 84

Wilcock, P. R., Toward a practical method for estimating sediment-transport rates in gravel-bed rivers, *Earth Surface Processes and Landforms*, *26*, 1395–1408, 2001. → page 3

Wilcock, P. R., and J. C. Crowe, Surface-based transport model for mixed-size sediment, *Journal of Hydraulic Engineering*, *129*, 120–128, 2003. → page 15

Witz, M. J., S. Cameron, and V. Nikora, Bed particle dynamics at entrainment, *Journal of Hydraulic Research*, *57*, 464–474, 2019. → page 79

Wong, M., G. Parker, P. DeVries, T. M. Brown, and S. J. Burges, Experiments on dispersion of tracer stones under lower-regime plane-bed equilibrium bed load transport, *Water Resources Research*, *43*, 1–23, 2007. → pages 48, 49, 51, 52, 54, 65

Wu, Z., E. Foufoula-Georgiou, G. Parker, A. Singh, X. Fu, and G. Wang, Analytical Solution for Anomalous Diffusion of Bedload Tracers Gradually Undergoing Burial, *Journal of Geophysical Research: Earth Surface*, *124*, 21–37, 2019a. → pages 47, 64, 71, 72, 76, 81, 82, 131, 132

Wu, Z., A. Singh, X. Fu, and G. Wang, Transient Anomalous Diffusion and Advective Slowdown of Bedload Tracers by Particle Burial and Exhumation, *Water Resources Research*, *55*, 7964–7982, 2019b. → pages 64, 77, 81

Yalin, M. S., *Mechanics of Sediment Transport.*, (1972), Pergamon Press, 1972. → pages xvi, 15, 16, 17

Yang, C. T., and W. Sayre, Stochastic Model for Sand Dispersion, *Journal of the Hydraulics Division*, *97*, 265–288, 1971. → pages 63, 64, 72

Yang, F. L., and M. L. Hunt, Dynamics of particle-particle collisions in a viscous liquid, 2006. → page 98

Yano, K., Tracer Studies on the Movement of Sand and Gravel, in *Proceedings of the 12th Congress IAHR, Vol 2.*, pp. 121–129, Kyoto, Japan, 1969. → pages 47, 70, 72, 79, 80

Youse, A., P. Costa, and L. Brandt, Single sediment dynamics in turbulent flow over a porous bed - Insights from interface-resolved simulations, *Journal of Fluid Mechanics*, *893*, 1–28, 2020. → page 11

Zaburdaev, V., M. Schmiedeberg, and H. Stark, Random walks with random velocities, *Physical Review E - Statistical, Nonlinear, and Soft Matter Physics*, *78*, 1–5, 2008. → page 82

Zee, C. H., and R. Zee, Formulas for the transportation of bed load, *Journal of Hydraulic Engineering*, *143*, 1–11, 2017. → page 16

Zhang, Y., M. M. Meerschaert, and A. I. Packman, Linking fluvial bed sediment transport across scales, *Geophysical Research Letters*, *39*, 1–6, 2012. → page 70

Appendix A

Ch. 2 calculations

A.1 Derivation of the master equation

A.2 Solution for the position probability distribution

A.3 Moments of position

A.4 Calculation of the flux rate constant

Appendix B

Ch. 4 calculations

B.1 Calculation of the distribution function

Owing to the convolution structure of manuscript equations (1-3), their solution is a formidable problem. Luckily, we have the device of Laplace transforms. These project integro-differential equations into an alternate space in which convolutions are unraveled (e.g., *Arfken*, 1985). The double Laplace transform of a joint probability distribution $p(x,t)$ is defined by

$$\tilde{p}(\eta, s) = \int_0^\infty dx e^{-\eta x} \int_0^\infty dt e^{-st} p(x,t). \tag{B.1}$$

The Laplace-transformed moments of x are linked to derivatives of the double transformed distribution (B.1) (cf., *Berezhkovskii and Weiss*, 2002). Equation (B.1) implies

$$\langle \tilde{x}(s)^k \rangle = (-)^k \partial_\eta^k \tilde{p}(\eta, s)\Big|_{\eta=0}. \tag{B.2}$$

The operator $\langle \circ \rangle$ denotes the ensemble average (e.g., **?**). This means we can compute the variance of position as $\sigma_x^2(t) = \langle x^2 \rangle - \langle x \rangle^2 = \mathcal{L}^{-1}\{\langle \tilde{x}^2 \rangle; t\} - \mathcal{L}^{-1}\{\langle \tilde{x} \rangle; t\}^2$, where $\mathcal{L}^{-1}$ denotes the inverse Laplace transform (e.g., *Arfken*, 1985). This is a powerful tool, since we can use it to derive the positional variance without integrating the distribution in equation (7) of the manuscript.

Double transforming manuscript equations (1-3) using the definition (B.1) gives

$$\begin{aligned}
\tilde{\omega}_{1T}(\eta,s) &= \theta_1\tilde{g}_1(\eta,s)+\tilde{\omega}_2(\eta,s)\tilde{g}_1(\eta,s)-\tilde{\omega}_{1F}(\eta,s), && \text{(B.3)}\\
\tilde{\omega}_{1F}(\eta,s) &= \theta_1\tilde{g}_1(\eta,s+\kappa)+\tilde{\omega}_2(\eta,s)\tilde{g}_1(\eta,s+\kappa), && \text{(B.4)}\\
\tilde{\omega}_2(\eta,s) &= \theta_2\tilde{g}_2(\eta,s)+\tilde{\omega}_{1F}(\eta,s)\tilde{g}_2(\eta,s). && \text{(B.5)}
\end{aligned}$$

This algebraic system solves for

$$\begin{aligned}
\tilde{\omega}_{1T}(\eta,s) &= \frac{\theta_1+\theta_2\tilde{g}_2(\eta,s)}{1-\tilde{g}_1(\eta,s+\kappa)\tilde{g}_2(\eta,s)}\big\{\tilde{g}_1(\eta,s)-\tilde{g}_1(\eta,s+\kappa)\big\}, && \text{(B.6)}\\
\tilde{\omega}_{1F}(\eta,s) &= \frac{\theta_1+\theta_2\tilde{g}_2(\eta,s)}{1-\tilde{g}_1(\eta,s+\kappa)\tilde{g}_2(\eta,s)}\tilde{g}_1(\eta,s+\kappa), && \text{(B.7)}\\
\tilde{\omega}_2(\eta,s) &= \frac{\theta_2+\theta_1\tilde{g}_1(\eta,s+\kappa)}{1-\tilde{g}_1(\eta,s+\kappa)\tilde{g}_2(\eta,s)}\tilde{g}_2(\eta,s). && \text{(B.8)}
\end{aligned}$$

Double transforming manuscript equations (4-6) gives

$$\begin{aligned}
\tilde{p}_0(\eta,s) &= \frac{1}{s}\tilde{\omega}_{1T}(\eta,s), && \text{(B.9)}\\
\tilde{p}_1(\eta,s) &= \theta_1\tilde{G}_1(\eta,s)+\tilde{\omega}_2(\eta,s)\tilde{G}_1(\eta,s), && \text{(B.10)}\\
\tilde{p}_2(\eta,s) &= \theta_2\tilde{G}_2(\eta,s)+\tilde{\omega}_{1F}(\eta,s)\tilde{G}_2(\eta,s). && \text{(B.11)}
\end{aligned}$$

The total probability is $p(x,t)=p_0(x,t)+p_1(x,t)+p_2(x,t)$. Using equations (B.6-B.11) this becomes, in the double Laplace representation,

$$\begin{aligned}
\tilde{p}(\eta,s) = {} & \frac{1}{s}\frac{\theta_1+\theta_2\tilde{g}_2(\eta,s)}{1-\tilde{g}_1(\eta,s+\kappa)\tilde{g}_2(\eta,s)}\big\{\tilde{g}_1(\eta,s)-\tilde{g}_1(\eta,s+\kappa)\big\}\\
&+\frac{\theta_1\big[\tilde{G}_1(\eta,s)+\tilde{g}_1(\eta,s+\kappa)\tilde{G}_2(\eta,s)\big]+\theta_2\big[\tilde{G}_2(\eta,s)+\tilde{g}_2(\eta,s)\tilde{G}_1(\eta,s)\big]}{1-\tilde{g}_1(\eta,s+\kappa)\tilde{g}_2(\eta,s)}.
\end{aligned} \tag{B.12}$$

Plugging the propagators outlined in manuscript equations (8-9) into equation (B.12) gives

$$\tilde{p}(\eta, s) = \frac{1}{s}\frac{(s+\kappa+k')s + \theta_1(s+\kappa)\eta v + \kappa k_2}{(s+\kappa+k_1)\eta v + (s+\kappa+k')s + \kappa k_2}. \tag{B.13}$$

In this equation, $k' = k_1 + k_2$, and we have used the normalization requirement of the initial probabilities: $\theta_1 + \theta_2 = 1$. The double inverse transform of this equation provides the distribution $p(x, t)$. We invert the transform over η first. Using the results 15.103 (transform of exponential), 15.123 (transform of derivative), and 15.141 (transform of Dirac delta function) from *Arfken* (1985) provides

$$\tilde{p}(x, s) = \theta_1 \frac{s+\kappa}{s(s+\kappa+k_1)}\delta(x) + \frac{1}{v}\Big(\frac{(s+\kappa+k')s+\kappa k_2}{s(s+\kappa+k_1)} - \frac{\theta_1(s+\kappa)[s(s+\kappa+k_1)+\kappa k_2]}{s(s+\kappa+k_1)^2}\Big)\exp\Big[-\frac{(s+\kappa+k')s+\kappa k_2}{s+\kappa+k_1}\frac{x}{v}\Big]. \tag{B.14}$$

Inverting the remaining transform over s, applying results 15.152 (substitution), 15.164 (translation), and 15.175 (transform of te^{kt}) from *Arfken* (1985), and defining the shorthand notations $\tau = k_1(t - x/v)$, $\xi = k_2 x/v$, and $\Omega = (\kappa + k_1)/k_1$, gives the simpler form

$$p(x, t) = \theta_1\Big[1 - \frac{k_1}{\kappa+k_1}\big(1 - e^{-(\kappa+k_1)t}\big)\Big]\delta(x) + \frac{1}{v}\exp[\Omega\tau - \xi] \times \mathcal{L}^{-1}\Big\{\Big(\theta_2 + \frac{\theta_1 k_1 + \theta_2 k_2}{s} + \frac{\theta_1 k_1 k_2}{s^2} + \frac{\theta_2 \kappa k_2}{s(s-\kappa-k_1)} + \frac{\theta_1 \kappa k_1 k_2}{s^2(s-\kappa-k_1)}\Big) \times \exp\big[\frac{k_1\xi}{s}\big]; \tau/k_1\Big\}. \tag{B.15}$$

Using entries 2.2.2.1, 2.2.2.8, and 1.1.1.13 from **?** in conjunction with the definition of the Marcum Q-function $\mathcal{P}_\mu(x, t)$ (e.g., *Temme and Zwillinger*, 1997), and inserting the Heaviside functions to account for the fact that grains can neither travel backwards nor at speeds exceeding v, we finally arrive at manuscript equation (10) for the joint distribution $p(x, t)$.

B.2 Calculation of the moments

We compute the first two moments of position x and ultimately its variance using equation (B.2). The first two derivatives of the double Laplace transformed distribution (B.13) are

$$\partial_\eta \tilde{p}(\eta, s) = -v\frac{1}{s}\frac{[(s+\kappa+k')s+\kappa k_2][\theta_2(s+\kappa)+k_1]}{[\eta v(s+\kappa+k_1)+(s+\kappa+k')s+\kappa k_2]^2}, \tag{B.16}$$

$$\partial_\eta^2 \tilde{p}(\eta, s) = 2v^2\frac{1}{s}\frac{(s+\kappa+k_1)[(s+\kappa+k')s+\kappa k_2][\theta_2(s+\kappa)+k_1]}{[\eta v(s+\kappa+k_1)+(s+\kappa+k')s+\kappa k_2]^3}. \tag{B.17}$$

Evaluating these at $\eta = 0$ and applying equation (B.2) provides the Laplace transformed moments

$$\frac{\langle \tilde{x}(s)\rangle}{v} = \frac{1}{s}\frac{\theta_2(s+\kappa)+k_1}{(s+\kappa+k')s+\kappa k_2} = \frac{1}{s}\frac{\theta_2(s+\kappa)+k_1}{(s+a+b)(s+a-b)}, \tag{B.18}$$

$$\frac{\langle \tilde{x}^2(s)\rangle}{2v^2} = \frac{1}{s}\frac{(s+\kappa+k_1)(\theta_2(s+\kappa)+k_1)}{[(s+\kappa+k')s+\kappa k_2]^2} = \frac{1}{s}\frac{(s+\kappa+k_1)(\theta_2(s+\kappa)+k_1)}{(s+a+b)^2(s+a-b)^2}. \tag{B.19}$$

The parameters $a = (\kappa + k')/2$ and $b^2 = a^2 - \kappa k_2$ were introduced to factorize the denominators. These equations can be inverted using the properties 15.164 (translation), 15.11.1 (integration), and 15.123 (differentiation) from *Arfken* (1985) after expansion in partial fractions. For the mean, the calculation is

$$\frac{2b}{v}\langle x\rangle = \left[\theta_2 + (k_1+\theta_2\kappa)\int_0^t dt\right]\mathcal{L}^{-1}\left\{\frac{1}{s+a-b} - \frac{1}{s+a+b}; t\right\} \tag{B.20}$$

$$= \left[\theta_2 + \frac{k_1+\theta_2\kappa}{b-a}\right]e^{(b-a)t} - \left[\theta_2 - \frac{k_1+\theta_2\kappa}{a+b}\right]e^{-(a+b)t} - \left[\frac{k_1+\theta_2\kappa}{b-a} + \frac{k_1+\theta_2\kappa}{a+b}\right]. \tag{B.21}$$

This equation rearranges to manuscript equation (11). The second moment (B.19) is

$$\frac{2b^2}{v^2}\langle x^2\rangle = \Big[\theta_2(\delta(t)+\partial_t) + (\theta_2(2\kappa+k_1)+k_1) + (\kappa+k_1)(\theta_2\kappa+k_1)\int_0^t dt\Big] \times \mathcal{L}^{-1}\Big\{\frac{1}{(s+a-b)^2} + \frac{1}{(s+a+b)^2} - \frac{1}{b(s+a-b)} + \frac{1}{b(s+a+b)}; t\Big\}. \tag{B.22}$$

This becomes

$$\frac{2b^3}{v^2}\langle x^2\rangle = \Big[\theta_2\partial_t + [\theta_2(2\kappa+k_1)+k_1] + (\kappa+k_1)(\theta_2\kappa+k_1)\int_0^t dt\Big] \times \Big((bt-1)e^{(b-a)t} + (bt+1)e^{-(a+b)t}\Big) \tag{B.23}$$

which evaluates to manuscript equation (12). Finally, $\sigma_x^2 = \langle x^2\rangle - \langle x\rangle^2$ derives the variance in manuscript equation (13).

B.3 Limiting behavior of the moments

We determine the diffusion exponents γ in the local, intermediate, and global ranges using the two limiting cases described in the discussion of the manuscript. Limit (1) is $\kappa \to 0$. We take this limit in equations (B.18) and (B.19) with initial condition $\theta_1 = 1$ to obtain

$$\langle \tilde{x}\rangle = vk_1\frac{1}{s^2(s+k')}, \tag{B.24}$$

$$\langle \tilde{x}^2\rangle = 2v^2k_1\frac{s+k_1}{s^3(s+k')^2}. \tag{B.25}$$

Inverting these equations provides the variance

$$\sigma_x^2 = 2v^2\frac{k_1}{k'^4}\Big(k_1\big[\frac{1}{2} - k'te^{-k't} - \frac{1}{2}e^{-2k't}\big] + k_2\big[-2 + k't + (2+k't)e^{-k't}\big]\Big). \tag{B.26}$$

This result encodes two ranges of diffusion and can also be derived from the governing equations of the *Lisle et al.* (1998) and **?** models. Expanding for small t provides $\sigma_x^2(t) = v^2 k_1 t^3/3$ – local range super-diffusion. Expanding for large t provides $\sigma_x^2(t) = 2v^2 k_1 k_2 t/k'^3$ – intermediate range normal diffusion.

We further investigate limit (1) for arbitrary initial conditions. By applying Tauberian theorems, we assert the $t \to 0$ variance is determined by the $s \to \infty$ limits of (B.18) and (B.19) (e.g., *Weeks and Swinney*, 1998; *Weiss*, 1994). Expanding these equations in powers of $1/s$ and inverting the resulting transforms gives

$$\langle x \rangle = v\theta_2 t + \frac{1}{2}v(\theta_1 k_1 - \theta_2 k_2)t^2 + O(t^3), \tag{B.27}$$

$$\langle x^2 \rangle = v^2\theta_2 t^2 + \frac{1}{3}v^2(\theta_1 k_1 - 2\theta_2 k_2)t^3 + O(t^4). \tag{B.28}$$

This equation highlights the effect of initial conditions on the diffusion characteristics of the local range:

$$\sigma_x^2(t) \sim v^2\theta_1\theta_2 t^2 + \frac{1}{3}v^2(\theta_1 k_1 + \theta_2 k_2)t^3. \tag{B.29}$$

We have taken only leading order terms for any option of θ_1 and θ_2. Equation (B.29) shows local range exponent $\gamma = 2$ when initial conditions are mixed (both are non-zero) and $\gamma = 3$ when initial conditions are pure (one is zero).

Limit (2) is $1/k_2 \to 0$ and $v \to \infty$ while $v/k_2 = l$. Under this limit, equations (B.18) and (B.19) provide

$$\langle \tilde{x} \rangle = k_1 l \frac{1}{s(s+\kappa)}, \tag{B.30}$$

$$\langle \tilde{x}^2 \rangle = 2l^2 k_1 \frac{s+\kappa+k_1}{s(s+\kappa)^2}. \tag{B.31}$$

Inverting these equations and introducing the variables $c = lk_1$ (an effective velocity) and $D_d = l^2 k_1$ (a diffusivity) provides positional variance

$$\sigma_x^2(t) = \frac{2D_d(1-e^{-\kappa t})}{\kappa} + \frac{(1-e^{-2\kappa t} - 2e^{-\kappa t}\kappa t)c^2}{\kappa^2}. \tag{B.32}$$

This is mathematically identical to the key result of *Wu et al.* (2019a).

Expanding for small t provides $\sigma_x^2(t) = 2D_d t$ – intermediate range normal diffusion, while sending $t \to \infty$ provides $\sigma_x^2 = (2D_d\kappa + c^2)/\kappa^2$ – a constant variance in the geomorphic range. The global range is characterized by competition between terms in equation (B.32), and shows $2 \leq \gamma \leq 3$ depending on the ratio k_1/κ (cf., *Wu et al.*, 2019a). Finally, both equations (B.26) and (B.32) reduce to the Einstein result $\sigma_x^2(t) = 2D_d t$ in further simplified limits.

Appendix C

Ch. 3 calculations

C.1 Numerical simulation algorithm

The Gillespie Stochastic Simulation Algorithm (SSA) generates exact realizations of a Markov random process from a sequence of random numbers. It was originally developed for chemical physics by *Gillespie* (1977) and is reviewed in **?** and *Gillespie* (2007). The SSA hinges on the defining property of a Markov process. When the transition rates from one state to another are not dependent on the distant past, the process is Markov (e.g., **?**). In the following sections, we begin by demonstrating the time intervals τ between subsequent transitions (i.e., the intervals between transition times) are exponentially distributed within the model we develop in the main text. Then we describe the SSA as a consequence of this property.

C.1.1 Times between transitions of any kind

Our joint stochastic description of bedload and bed elevation changes is characterized by a set of states (n, m) where n and m are positive integers. Our description involves four possible transitions (migration in, entrainment, deposition, migration out) with rates given in equations (2-5) in the main text. From the state (n, m), the rate (probability per unit time) for any transition to occur is the sum over all possibilities:

$$A(n,m) = R_{MI}(n+1,m|n,m) + R_E(n+1,m-1|n,m) \\ + R_D(n-1,m+1|n,m) + R_{MO}(n-1,m|n,m). \quad \text{(C.1)}$$

Using this, the probability that no transition occurs from the state (n,m) in a small time interval $\delta\tau$ is $1 - A(n,m)\delta\tau$. If we denote by $Q(\tau|n,m)$ the probability density that a transition of any kind occurs from the state (n,m) after a time τ, we can express the probability density that a transition happens after a slightly larger time $\tau + \delta\tau$ as

$$Q(\tau + \delta\tau|n,m) = \big[1 - A(n,m)\delta\tau\big]Q(\tau|n,m). \quad \text{(C.2)}$$

This equation invokes the Markov property, since it does not involve the past history of states (n,m). Taking $\delta\tau \to 0$ we find the master equation $\frac{d}{d\tau}Q(\tau|n,m) = -A(n,m)Q(\tau|n,m)$, from which we conclude the time τ between subsequent transitions is distributed as

$$Q(\tau|n,m) = A(n,m)e^{-A(n,m)\tau}. \quad \text{(C.3)}$$

Therefore we have shown the time τ to the next transition from a state (n,m) is exponentially distributed with mean value $\bar{\tau} = 1/A(n,m)$. In deriving this result, we used the normalization condition $1 = \int_0^\infty Q(\tau|n,m)d\tau$.

This result implies if the stochastic process transitioned to the state (n,m) at a time t, the next transition will occur at a time $t + \tau$ with τ a random variable drawn from the exponential distribution C.3. Therefore, we can determine the times between subsequent transitions by drawing exponentially distributed random numbers.

C.1.2 Selection of transitions that occur

So far, we have determined how to step the time from one transition to the next, but we have not specified how to step the state variables n and m at each transition time. That is, we have not specified the type of transitions that occur at each time step. Intuitively, this will depend on the relative magnitudes of the rates from equations (2-5) in the main text: the transition with the highest rate is most likely to occur. This is formalized by generating the ratios

$$S = \left\{ \frac{R_{MI}(n+1, m|n, m)}{A(n, m)}, \frac{R_E(n+1, m-1|n, m)}{A(n, m)}, \frac{R_D(n-1, m+1|n, m)}{A(n, m)}, \frac{R_{MO}(n-1, m|n, m)}{A(n, m)} \right\}. \tag{C.4}$$

By construction, sum$\{S\} = 1$. By forming cumulative sums of the four ratios, we partition the unit interval $[0, 1]$ into four chunks, each associated with a transition – either migration in, entrainment, deposition, or migration out. The transitions with the highest rates have the largest associated chunks. To randomly select the transition that occurs at a transition time, we draw a random number on $[0, 1]$ and find which chunk it falls in.

In summary, to step the process through a single transition, we draw the time interval to the next transition from the distribution (C.3), then draw a uniform random from $[0, 1]$ and use it to select the transition that occurs from the cumulative sum of the ratios in (C.4). The SSA simply iterates this random number generation/selection process to generate exact realizations of the stochastic process: these are series of n and m through time from which we can calculate any statistics of interest.

C.1.3 Pseudo code for the Gillespie SSA

To initialize a simulation, we specify the initial conditions n_0 and m_0, the model parameters for use in equations (2-7) in the main paper, and the desired simulation duration $t_{\max}$. The SSA uses these inputs to generate time series of n and m as follows:

$t = 0$ $n = n_0$Set the initial state (n_0, m_0) $m = m_0$

$t < t_{\max}$; Simulation will go until t surpasses $t_{\max}$ record (n, m, t) Build time series of n and m draw τ from eq. (C.3) Select time to next transition $tt + \tau$ draw a random number r in $[0, 1]$ Select type of transition that occurs compute the ratios r_1, r_2, r_3, r_4 in eq. (C.4) form the cumulative sums $r_i =$

$\sum_{1 \leq j \leq i} r_j$ Now enact the transition $0 \leq r < r_1$ Migration in $nn+1$ $r_1 \leq r < r_2$ Entrainment $nn+1$ $mm-1$ $r_2 \leq r < r_3$ Deposition $nn-1$ $mm+1$ $r_3 \leq r \leq 1$ Migration out $nn-1$

C.2 Approximate solutions of the Master equation

C.2.1 Mean field solution of particle activity

By assuming the dynamics of the particle activity are totally independent of the bed elevation and summing equation (8) of the manuscript over all values of m, we obtain the mean field equation for the particle activity:

$$0 = \nu A(n-1)+[\lambda+\mu(n-1)]A(n-1)+\sigma(n+1)A(n+1)+\gamma(n+1)A(n+1)-(\nu+\lambda+\mu n+\sigma n+\gamma n)A(n). \tag{C.5}$$

This can be solved by introducing the generating function (**?**) $G(x) = \sum_n x^n A(n)$, providing

$$0 = (\nu+\lambda)(x-1)G + [\mu x^2 + \sigma + \gamma - (\mu + \sigma + \gamma)x]\frac{\partial G}{\partial x}, \tag{C.6}$$

which is separable and integrates for

$$G(x) = \left(\frac{\gamma + \sigma - \mu}{\gamma + \sigma - \mu x}\right)^{\frac{\nu+\lambda}{\mu}} \tag{C.7}$$

after applying the normalization condition $G(1) = 1$. From the definition of G we can determine $A(n) = \frac{1}{n!}\frac{d^n G}{dx^n}|_{x=0}$, giving the negative binomial distribution of particle activity demonstrated by *Ancey et al.* (2008) and stated in equation (10) of the manuscript.

C.2.2 Mean field solution of bed elevations

From the negative binomial distribution we have $\langle n|m\rangle = \langle n\rangle$, so equation (9) provides

$$0 = [\lambda + \mu\langle n\rangle][1 + \kappa(m+1)]M(m+1) + \sigma\langle n\rangle[1 - \kappa(m-1)]M(m-1) \\ - \{[\lambda + \mu\langle n\rangle](1 + \kappa m) + \sigma\langle n\rangle(1 - \kappa m)\}M(m). \quad \text{(C.8)}$$

Identifying $E = \lambda + \mu\langle n\rangle$ and $D = \sigma\langle n\rangle$ and incorporating $E = D$ gives equation (11) of the manuscript

$$0 = [1 + \kappa(m+1)]M(m+1) + [1 - \kappa(m-1)]M(m-1) - 2M(m). \quad \text{(C.9)}$$

The *Martin et al.* (2014) Ornstein-Uhlenbeck model.

We solve this using the Fokker-Planck expansion (*Gardiner*, 1983) that effectively converts this discrete Master equation for m into a diffusion equation for the quasi-continuous variable $z = z_1 m$ This works since z_1 is small. Introducing z and writing $\overline{\kappa} = \kappa/z_1$ gives

$$0 = [1 + \overline{\kappa}(z + z_1)]M(z + z_1) + [1 - \overline{\kappa}(z - z_1)]M(z - z_1) - 2M(z). \quad \text{(C.10)}$$

$\overline{\kappa}$ should not depend on z_1 since the magnitude of the feedbacks between bed elevations and entrainment and deposition rates depends on elevation changes, and not on the size of grains or the length of the control volume. Expanding the entire first and second terms to second order z_1 provides the Fokker-Planck equation

$$0 = -2\overline{\kappa}z_1[zM(z)]' + z_1^2 M''(z). \quad \text{(C.11)}$$

Taking into account that this distribution should be normalizable, $\lim_{z\to\pm\infty} M(z) = 0$, we find

$$M = M_0 e^{-\kappa(z/z_1)^2} \quad \text{(C.12)}$$

as stated in the manuscript.

C.2.3 Closure equation approach for bed elevations

We set out to determine an approximate relationship to close $\langle n|m\rangle$ in terms of m valid to first order in κ.

$$\langle n|m\rangle \approx \langle n\rangle - \kappa c m, \tag{C.13}$$

for the mean particle activity conditional to the elevation m into into manuscript equation (9), noting $E = D$, and neglecting terms of $O(\kappa^2)$ provides

$$0 \approx \Big[1+\kappa(m+1)\Big\{1-\frac{\mu c}{E}\Big\}\Big]M(m+1)+\Big[1-\kappa(m-1)\Big\{1+\frac{\sigma c}{E}\Big\}\Big]-\Big[2-\kappa m\Big\{\frac{(\sigma+\mu)c}{E}\Big\}\Big]M(m) \tag{C.14}$$

At this point, we consider c an undetermined positive constant that may depend on the entrainment, migration, and deposition rates. Taking the Fokker-Planck expansion and requiring the distribution $M(m)$ to vanish at infinity for normalization yields

$$0 = 2\kappa m\Big(2 + \frac{(\sigma-\mu)c}{E}\Big)M(m) + \Big\{\Big[2 - \kappa m\frac{(\sigma+\mu)c}{E}\Big]M(m)\Big\}'. \tag{C.15}$$

Finally, integrating, expanding to first order in κ, and exponentiating to solve for M, we find

$$M(m) = M_0 \exp\Big\{-\kappa m^2\Big[1 + \frac{(\sigma-\mu)c}{2E}\Big]\Big\}. \tag{C.16}$$

Since the numerical solutions show $\sigma_m^2 = \frac{1}{4\kappa}$, we determine the closure relation

$$\langle n|m\rangle = \langle n\rangle\Big(1 - \frac{2\kappa m}{1-\mu/\sigma}\Big) \tag{C.17}$$

corresponding to $c = 2E/(\sigma-\mu)$. This is the closure relationship provided in equation (12) of the manuscript that is plotted with the numerical simulations in manuscript figure (4a).

Appendix D

Ch. 5 calculations

D.1 Derivation of Master Equation

To derive the master equation from 5.3, we temporarily consider the Gaussian white noise (GWN) $\xi(t)$ as a Poisson jump process having rate r and jumps $\sqrt{2d}h$ with h distributed as $f(h)$. We will later take a GWN limit on this noise. With this assumption, integrating 5.3 over a small time interval δt considering the Ito interpretation for the collision term provides

$$u(t+\delta t) = \begin{cases} u(t)+\gamma\delta t & \text{with probability } 1-r\delta t-\nu\delta t \\ u(t)+\sqrt{2d}h & \text{with probability } r\delta t \\ \varepsilon u(t) & \text{with probability } \nu\delta t \end{cases} \tag{D.1}$$

Considering the probability $P(u, t+\delta)$ as sum over possible paths from $P(u,t)$ develops

$$P(u, t+\delta t) = (1-r\delta t-\nu\delta t)\int_{-\infty}^{\infty} dw\delta(u-w-\gamma\delta t)P(w,t) \tag{D.2}$$

$$+r\delta t\int_{-\infty}^{\infty} dw\int_{-\infty}^{\infty} dhf(h)\delta(u-w-\sqrt{2d}h)P(w,t) \tag{D.3}$$

$$+\nu\delta t\int_{-\infty}^{\infty} dw\int_{0}^{1} d\varepsilon\rho(\varepsilon)\delta(u-w\varepsilon)P(w,t). \tag{D.4}$$

Evaluating all integrals over δ-functions provides

$$P(u,t+\delta t) = (1 - r\delta t - \nu\delta t)P(u - \gamma\delta t, t) \tag{D.5}$$

$$+r\delta t \int_{-\infty}^{\infty} dh f(h) P(u + \sqrt{2d}h) \tag{D.6}$$

$$+\nu\delta t \int_{0}^{1} \frac{d\varepsilon}{\varepsilon}\rho(\varepsilon)P(\frac{u}{\varepsilon}). \tag{D.7}$$

Finally, we take $\delta t \to 0$ and limit the Poisson noise involving $\sqrt{2d}$ to a Gaussian white noise by taking $r \to \infty$ as $h \to 0$ such that $h^2 r = 1$ **?**. This process finally obtains the master equation (5.4).

D.2 Derivation of Steady-state solution

Defining $\tilde{P}(s) = \int_{-\infty}^{\infty} du e^{ius} P(u)$ as the Fourier transform (FT) of $P(u)$ and taking the FT of **??** develops the recursion relation

$$\tilde{P}(s) = \frac{\tilde{P}(s\varepsilon)}{q(s)}. \tag{D.8}$$

where

$$q(z) = dz^2 - i\gamma z + 1. \tag{D.9}$$

Recursing $N+1$ times provides

$$\tilde{P}(s) = \frac{\tilde{P}(s\varepsilon^{N+1})}{q(s\varepsilon^0)q(s\varepsilon^1)\dots q(s\varepsilon^N)}. \tag{D.10}$$

The polynomials $q(z)$ can always be factored as $q(z) = d(z - i\lambda_-)(z - i\lambda_+)$ where

$$\lambda_\pm = \frac{\gamma}{2d}\Big[1 \pm \sqrt{1 + 4d/\gamma^2}\Big]. \tag{D.11}$$

Using these factors to expand $\tilde{P}(s)$ in partial fractions provides

$$\tilde{P}(s) = \tilde{P}(s\varepsilon^{N+1}) \sum_{l=0}^{N} \Big[\frac{R_l^-}{s\varepsilon^l - i\lambda_-} + \frac{R_l^+}{s\varepsilon^l - i\lambda_+}\Big] \tag{D.12}$$

where the coefficients $R_l^{\pm}$ are the residues of the product $[q(s\varepsilon^0)\dots q(s\varepsilon^N)]^{-1}$:

$$R_l^{\pm} = \frac{s\varepsilon^l - i\lambda_{\pm}}{q(s\varepsilon^0)\dots q(s\varepsilon^N)}\Big|_{s=i\lambda_{\pm}\varepsilon^{-l}}. \tag{D.13}$$

The Fourier transform (D.10) has a beautiful feature as $N \to \infty$: since $0 < \varepsilon < 1$, the prefactor $\tilde{P}(s\varepsilon^{N+1})$ becomes the normalization condition $\tilde{P}(0) = 1$ for the probability distribution $P(u)$ in the limit. Taking this limit and evaluating the residues provides

$$\begin{aligned}\tilde{P}(s) &= \frac{1}{d(\lambda_+ - \lambda_-)\prod_{m=1}^{\infty} q(i\lambda_-\varepsilon^m)} \sum_{l=0}^{\infty} \frac{i}{(s\varepsilon^l - i\lambda_-)\prod_{m=1}^{l} q(i\lambda_-\varepsilon^{-m})} \\ &+ \frac{1}{d(\lambda_+ - \lambda_-)\prod_{m=1}^{\infty} q(i\lambda_+\varepsilon^m)} \sum_{l=0}^{\infty} \frac{-i}{(s\varepsilon^l - i\lambda_+)\prod_{m=1}^{l} q(i\lambda_+\varepsilon^{-m})}\end{aligned} \tag{D.14}$$

Finally, inverting the Fourier transforms term by term with contour integration and incorporating (D.9) provides the steady-state solution (5.8).

D.3 Calculation of the moments

Taking (5.4), multiplying by u^k, integrating over all space, and taking account of normalization of $P(u)$ provides a recursion relation for the moments:

$$0 = Dk(k-1)\langle u^{k-2}\rangle + \Gamma k\langle u^{k-1}\rangle + \nu(\varepsilon^k - 1)\langle u^k\rangle. \tag{D.15}$$

$k = 1$ provides the mean

$$\langle u\rangle = \frac{\Gamma}{\nu(1-\varepsilon)} = \frac{\gamma}{1-\varepsilon} \tag{D.16}$$

while $k = 2$ provides the second moment

$$\langle u^2\rangle = 2\frac{d + \gamma\langle u\rangle}{1-\varepsilon^2}, \tag{D.17}$$

leading to the velocity variance

$$\sigma_u = \sqrt{\frac{2d+\gamma^2}{1-\varepsilon^2}}. \tag{D.18}$$

D.4 Weak and strong collision limits

Now we demonstrate that weak collisions imply a Gaussian-like distribution for sediment velocities. The limit is challenging since the steady-state distribution 5.8 and the moments above all diverge as $\varepsilon \to 1$. Following **?**, this suggests normalizing the distribution $P(u)$ using

$$z = \frac{u-\bar{u}}{\sigma_u} \tag{D.19}$$

and

$$Q(z) = \sigma_u P(u) \tag{D.20}$$

to seek a differential equation for $Q(z)$ with manageable behavior as $\varepsilon \to 1$. Incorporating this transformation into (5.4) provides a "normalized" Master equation

$$(1-\varepsilon^2)\frac{d}{2d+\gamma}Q''(z) - \frac{\gamma\sqrt{1-\varepsilon^2}}{\sqrt{2d+\gamma^2}}Q'(z) - Q(z) + \frac{1}{\varepsilon}Q\Big(z + \Big[\frac{1-\varepsilon}{\varepsilon}z + \frac{\gamma\sqrt{1-\varepsilon^2}}{\varepsilon\sqrt{2d+\gamma^2}}\Big]\Big) = 0 \tag{D.21}$$

This equation remains exact and is only a change of variables from (5.4). Now we approximate the equation for $\varepsilon \to 1$ by expanding the final term to second order around $z = 0$ before setting $\varepsilon = 1$, obtaining

$$Q''(z) + zQ'(z) + Q(z) = 0, \tag{D.22}$$

which is the classic Ornstein-Uhlenbeck Fokker-Planck equation whose solution is the standard normal distribution for $Q(z)$. This solution provides 5.14 when transformed back to the original variables $P(u)$ and u.

Appendix E

Monte Carlo strategies

This will describe how I conducted all of the monte carlo simulations with some example code.